#339 SPECIAL ISSUE
FEBRUARY 2018

ICES
CIEM

ICES REPORT ON OCEAN CLIMATE 2016

Prepared by the Working Group on Oceanic Hydrography

ICES COOPERATIVE RESEARCH REPORT

RAPPORT
DES RECHERCHES
COLLECTIVES

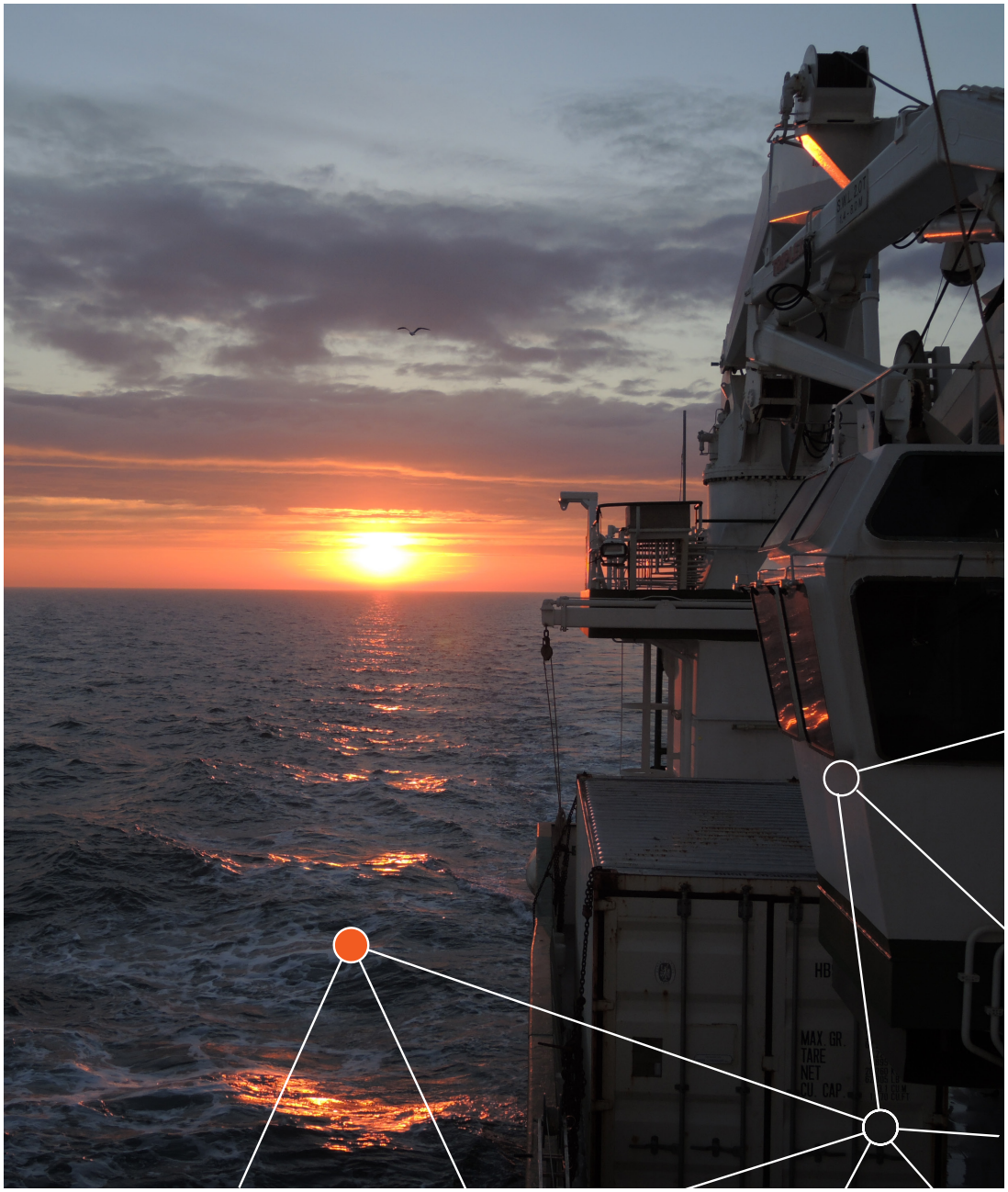

ICES INTERNATIONAL COUNCIL FOR THE EXPLORATION OF THE SEA
CIEM CONSEIL INTERNATIONAL POUR L'EXPLORATION DE LA MER

Members of the ICES Working Group on Oceanic Hydrography (WGOH) at the Faroese Marine Research Institute (Havstovan) Torshavn, Faroes, April 2017.

International Council for the Exploration of the Sea
Conseil International pour l'Exploration de la Mer
H. C. Andersens Boulevard 44–46
DK-1553 Copenhagen V
Denmark
Telephone (+45) 33 38 67 00
Telefax (+45) 33 93 42 15
www.ices.dk
info@ices.dk
Recommended format for purposes of citation:
González-Pola, C., Larsen, K. M. H., Fratantoni, P., Beszczynska-Möller, A., and Hughes, S. L. (Eds). 2018. ICES Report on Ocean Climate 2016. ICES Cooperative Research Report No. 339. 110 pp. https://doi.org/10.17895/ices.pub.4069

Series Editor: Emory D. Anderson

The material in this report may be reused for non-commercial purposes using the recommended citation. ICES may only grant usage rights of information, data, images, graphs, etc. of which it has ownership. For other third-party material cited in this report, you must contact the original copyright holder for permission. For citation of datasets or use of data to be included in other databases, please refer to the latest ICES data policy on ICES website. All extracts must be acknowledged. For other reproduction requests please contact the General Secretary.
This document is the product of an Expert Group under the auspices of the International Council for the Exploration of the Sea and does not necessarily represent the view of the Council.

Cover image: Sun down Celtic Explorer. Photo: Holger Klein, Bundesamt für Seeschifffahrt und Hydrographie, Germany.
https://doi.org/10.17895/ices.pub.4069
ISBN 978-87-7482-210-3
ISSN 2707-7144
© 2018 International Council for the Exploration of the Sea

ICES COOPERATIVE RESEARCH REPORT
RAPPORT DES RECHERCHES COLLECTIVES

ICES REPORT ON OCEAN CLIMATE 2016

#339 SPECIAL ISSUE
FEBRUARY 2018

Prepared by the Working Group on Oceanic Hydrography

DEDICATION TO FABIENNE GAILLARD

ICES Working Group on Oceanic Hydrography (WGOH) would like to dedicate this report to the memory of our colleague Fabienne Gaillard, a researcher from Ifremer based at the Laboratory for Ocean Physics and Satellite remote sensing, Brest, France, who died in 2017 following a battle with illness.

Fabienne organized and directed many oceanographic campaigns in the late 1990s. She served as the scientific secretary of the Multi-Scale Ocean and Atmosphere Program in the early 2000s and was the Assistant Director of the Laboratory of Physical Oceanography, Brest, France from 2008 to 2011. More recently, she was the Director of the newly created French National Ocean Data and Services Cluster (ODATIS).

For many years, Fabienne was a valuable contributor to WGOH, submitting the French contribution to ICES Report on Ocean Climate (IROC). Fabienne and her laboratory hosted the WGOH meeting in Brest in 2010. One of her great contributions was the high quality data product created from Argo data in the North Atlantic; these data are presented in Section 2.3 of this report. For more than a decade, Fabienne worked to develop these tools and products which now form an extremely valuable contribution to the IROC and indeed are widely used across the oceanographic community.

Fabienne was a friend, colleague, and scientist recognized for her scientific rigor and enthusiastic collaboration with others. She will be sadly missed by all in WGOH.

Secchi disk measurement, RV "Celtic Explorer". Photo: Holger Klein, Bundesamt für Seeschifffahrt und Hydrographie, Germany.

1. INTRODUCTION

Long time-series of ocean properties are rare in the surface ocean and even rarer in the deep ocean. The North Atlantic region is unusual in having a relatively large number of locations at which oceanographic data have been collected repeatedly for many years or decades; the longest records go back more than a century.

These valuable data are collated in ICES Report on Ocean Climate (IROC) to provide the very latest information from ICES areas of the North Atlantic and Nordic seas. At locations where the ocean is regularly measured, sea temperature and salinity status are described for 2016. Observed trends over the past decade, and longer where possible, are also included.

In the first section of the report, information is drawn together from the longest time-series in order to give the best possible overview of changes in this area. Although the focus of the report is on temperature and salinity measurements, additional complementary datasets, such as sea level pressure (SLP), air temperature, and ice cover, are provided throughout the report. Also, following its recent publication and recommendations from ICES Working Group on Widely Distributed Stocks (WGWIDE), the Subpolar Gyre index data are included in the IROC for the first time.

The main focus of this report is the observed variability in the upper ocean (the upper 1000 m). The introductory section includes gridded fields constructed by optimal analysis of the Argo float data distributed by the Coriolis Data Center in France. Later in the report, a short section summarizes the variability of the intermediate and deep waters of the North Atlantic.

The data presented here represent an accumulation of knowledge collected by many individuals and institutions through decades of observations. It would be impossible to list them all, but we provide a list of contacts at the end of the report for each dataset, including email addresses for the individuals who provided the information and the data centres at which the full archives of data are held. Much of the data included in this report are available to download via a web tool at http://ocean.ices.dk/iroc, where additional data can also be found.

For readers interested in a more detailed overview in a particular region, a full description of some of the datasets that are used to develop the time-series presented in this report can be found in the annual meeting reports of ICES Working Group on Oceanic Hydrography (WGOH).

1.1 HIGHLIGHTS FOR THE NORTH ATLANTIC 2016

- Air and sea surface temperatures were higher than normal across most of the region, with the exception of the central subpolar North Atlantic (centred on 50°N and including the Irminger and Iceland basins). In Greenland and the Barents Sea, record-high air and sea surface temperatures were observed. North of Iceland, record-high sea surface temperatures were observed.

- A cold anomaly in the surface and upper ocean of the central subpolar North Atlantic persisted in 2016, though it weakened through the year.

- Heat content in the upper layer of the Norwegian Sea reached a record-high value and bottom temperatures across the Northeast US continental shelf were unusually high.

- Salinity in the upper layer of the eastern subpolar North Atlantic and the Norwegian Sea has been decreasing since the late 2000s, and a dramatic freshening and record-low values were observed in the Faroe Bank Channel and Iceland Basin in 2016.

- Ice cover in the Barents Sea reached a record-low, with the first ice-free July on record. For the second

consecutive winter, the Bothnian Bay was not completely ice covered and ice cover elsewhere in the Baltic was lower than normal.

- Experimental forecasts of SLP and surface air temperature are included here for the first time.

1.2 HIGHLIGHTS FOR THE NORTH ATLANTIC ATMOSPHERE IN WINTER 2015/2016

- The winter North Atlantic Oscillation (NAO) index was positive (+0.98) for the third consecutive winter.

- The Azores High was relatively strong, with the high pressure anomaly extending from Newfoundland across southern Europe, while the Iceland Low strengthened at its southern extent. Weaker-than-average winds were evident from southwest of Iceland into the Norwegian Sea, extending to Svalbard and the western Barents Sea.

- Winter air temperatures were only below average (1981–2010) over the Subpolar Gyre; temperatures elsewhere were generally higher than normal, particularly over the Northeast US shelf, Fram Strait, and the Barents Sea.

1.3 BEYOND 2016: INITIAL ASSESSMENT OF THE NORTH ATLANTIC ATMOSPHERE IN WINTER 2016/2017

An initial assessment of the North Atlantic atmosphere at the end of the IROC year is included. Atmospheric conditions during winter are a determining factor of oceanic conditions for the following year; therefore, this outlook offers some predictive capability for spring–autumn 2017.

The SLP pattern for December 2016 to March 2017 indicates that it was the fourth consecutive positive NAO index winter, but again weaker than those preceding it. As expected for a weak NAO index, the SLP anomaly does not reflect a typical NAO pattern, and there was no strong spatial pattern to the windspeed anomaly.

Air temperatures were cold over the Subpolar Gyre, including over the Irminger Sea and Iceland Basin. As in winter 2016, warmer-than-average conditions were evident around the margins of the Subpolar Gyre, but the colder-than-average conditions observed in 2016 remained over the gyre itself.

On board RV "Oceania". Photo: Agnieszka Beszczynska-Möller, Institute of Oceanology, Polish Academy of Sciences, Poland.

NORTH ATLANTIC UPPER OCEAN TEMPERATURE: OVERVIEW

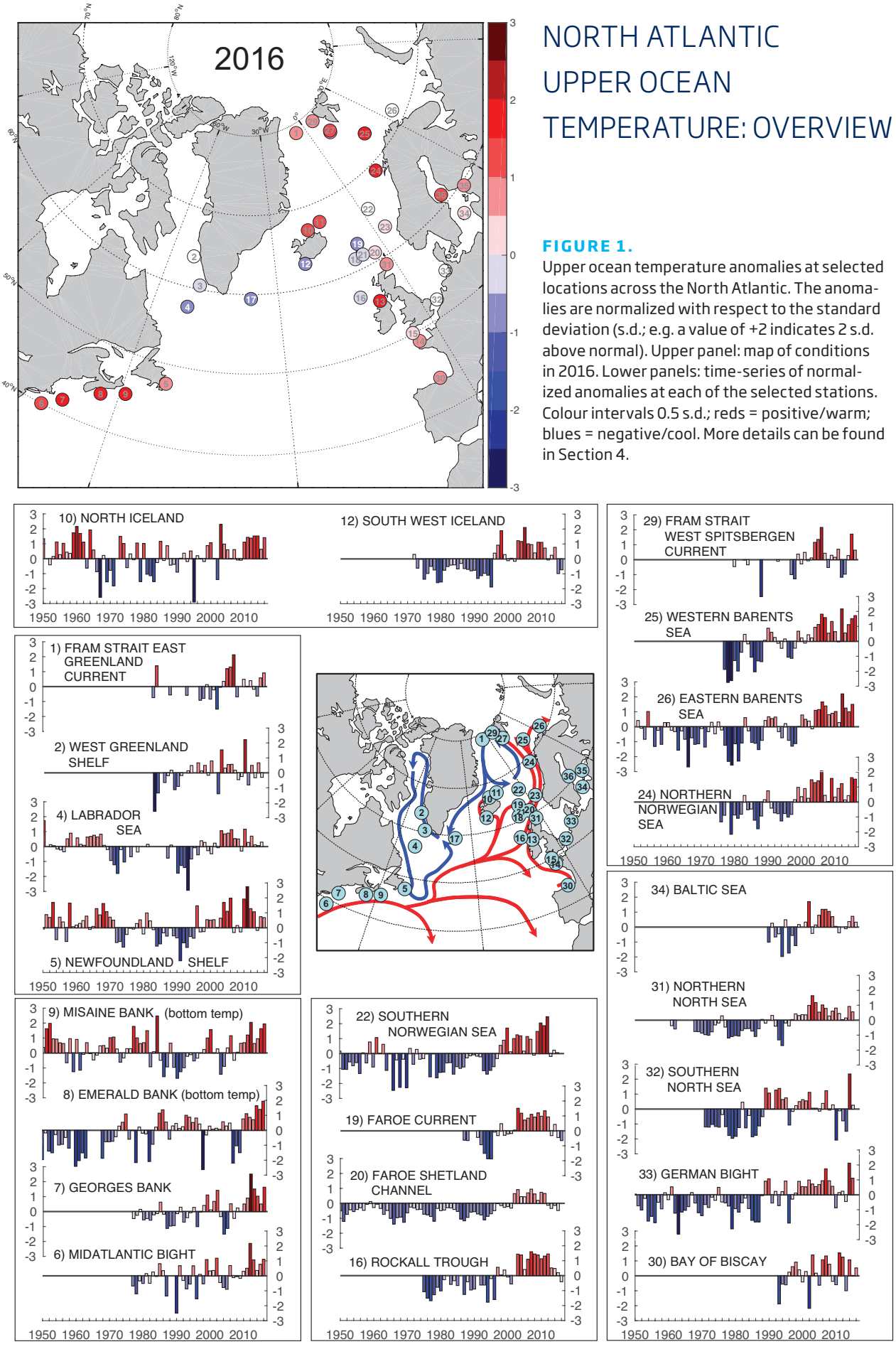

FIGURE 1.
Upper ocean temperature anomalies at selected locations across the North Atlantic. The anomalies are normalized with respect to the standard deviation (s.d.; e.g. a value of +2 indicates 2 s.d. above normal). Upper panel: map of conditions in 2016. Lower panels: time-series of normalized anomalies at each of the selected stations. Colour intervals 0.5 s.d.; reds = positive/warm; blues = negative/cool. More details can be found in Section 4.

NORTH ATLANTIC UPPER OCEAN SALINITY: OVERVIEW

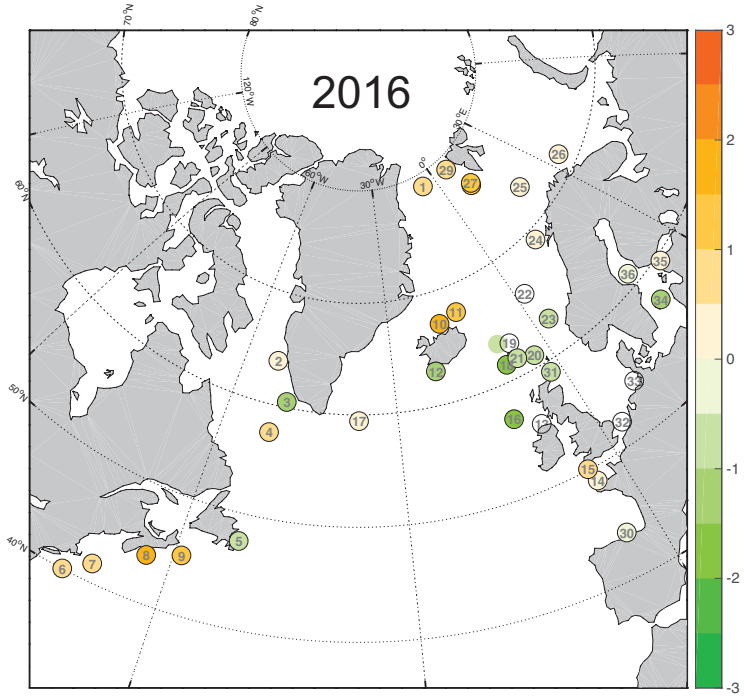

FIGURE 2.
Upper ocean salinity anomalies at selected locations across the North Atlantic. The anomalies are calculated relative to a long-term mean and normalized with respect to the s.d. (e.g. a value of +2 indicates 2 s.d. above normal). Upper panel: map of conditions in 2016. Lower panels: time-series of normalized anomalies at each of the selected stations. Colour intervals 0.5 s.d.; oranges = positive/saline; greens = negative/fresh. More details can be found in Section 4.

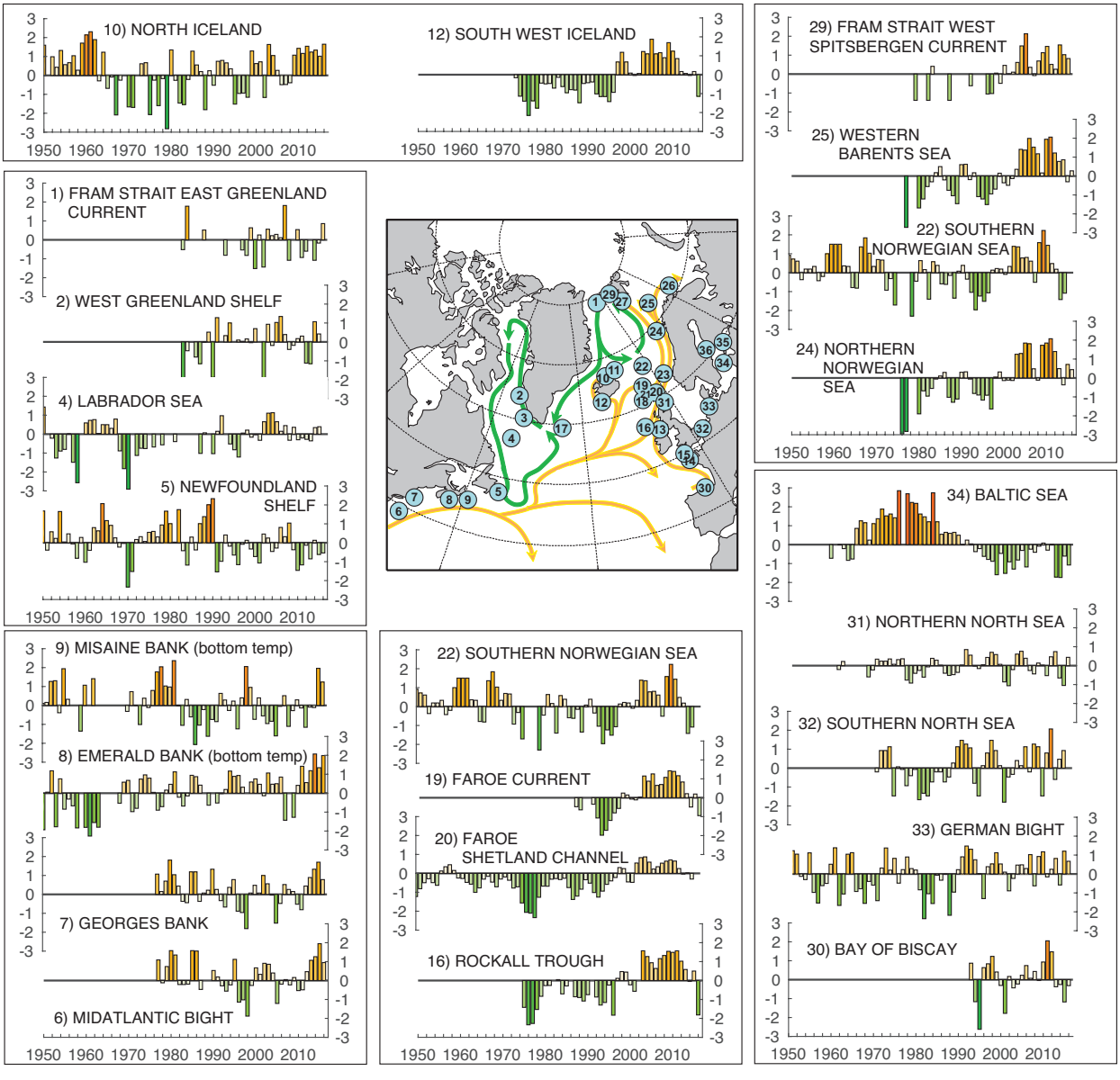

Deploying the CTD in the East Greenland Coastal Current. Photo: Penny Holliday, National Oceanography Centre Southampton, UK.

2. SUMMARY OF UPPER OCEAN CONDITIONS IN 2016

In this section, conditions in the upper layers of the North Atlantic during 2016 are summarized using data from (i) a selected set of sustained observations, (ii) gridded sea surface temperature (SST) data, and (iii) gridded vertical profiles of temperature and salinity from Argo floats.

2.1 *IN SITU* STATIONS AND SECTIONS

Where *in situ* section and station data are presented in the summary tables and figures, normalized anomalies have been provided to allow better comparison of trends in the data from different regions (Figures 1–3; Tables 1 and 2). The anomalies have been normalized by dividing the values by the s.d. of the data during 1981–2010 (or the closest time period available). A value of +2 thus represents data (temperature or salinity) at 2 s.d. higher than normal.

"Sustained observations" or "time-series" are regular measurements of ocean temperature and salinity made over a long period (10–100 years). Most measurements are made 1–4 times a year, but some are made more frequently.

"Anomalies" are the mathematical differences between each individual measurement and the average values of temperature, salinity, or other variables at each location. Positive anomalies in temperature and salinity mean warm or saline conditions; negative anomalies mean cool or fresh conditions.

"Seasonal cycle" describes the short-term changes at the surface of the ocean brought about by the passing of the seasons; the ocean surface is cold in winter and warms through spring and summer. Temperature and salinity changes caused by the seasonal cycle are usually much greater than the prolonged year-to-year changes described here.

	2007	2008	2009	2010	2011	2012	2013	2014	2015	2016
1	2.13	-0.69		0.49	0.01	0.40	-0.18	-0.64	0.58	0.91
2	0.18	-0.46	-0.25	2.22	-0.81	0.50	-0.33	0.67	-0.30	
3	1.04	0.06	0.70	1.15	0.57	1.28	0.18	0.83	-0.47	-0.41
4	-0.19	0.92	-0.32	0.51	-0.21	-0.02	-0.32	-0.39	-1.19	-0.76
5	-0.32	0.15	-0.28	1.92	2.75	1.28	1.07	-0.18	0.74	0.68
6	-0.12	-0.05	-0.17	0.30	0.51	2.17	1.07	0.36	0.77	1.10
7	-0.46	0.24	0.00	0.51	0.90	2.51	1.51	1.03	0.51	1.63
8	-2.20	-1.04	-1.50	0.76	1.12	0.87	0.71	1.64	1.40	1.95
9	-0.49	0.06	0.65	0.69	1.20	2.05	0.64	0.96	1.63	1.95
10	0.61	-0.09	-0.10	1.10	1.43	1.38	1.52	1.52	0.63	1.41
11	-0.65	0.64	0.46	0.30	1.03	0.64	0.79	1.89	0.89	1.15
12	0.96	0.40	1.12	1.11	0.73	-0.07	0.24	0.77	-0.98	-0.73
13			1.45	0.40	1.04	0.62	0.42	1.72	0.71	1.59
14	1.86	0.11	-0.80	-1.95	0.06	0.38	-0.83	1.58	1.04	0.50
15	1.01	0.40	-0.66	0.02	0.05	0.59	-0.26	0.70	0.25	0.19
16	1.60	1.45	1.38	1.13	1.31	1.45	0.52	0.48	0.20	-0.41
17	1.17	-0.56	-0.73	0.55	0.69	-0.29		-0.01	-0.43	-0.75
18	1.10	1.30	1.41	0.73	1.28	-0.03	0.04	0.55	0.13	-0.04
19	1.10	0.92	1.20	0.98	1.34	0.93	-0.32	0.43	-0.45	-0.65
20	0.95	0.63	0.20	0.74	0.66	-0.13	-0.34	-0.14	-0.30	0.23
21	0.71	0.76	0.92	1.36	0.92	0.34	0.45	0.55	0.17	-0.27
22	0.96	-0.11	1.48	2.05	1.87	2.47	-0.19	0.23	0.06	
23	1.89	0.19	1.71	0.86	1.12	0.44	0.55	0.33	0.52	0.35
24	0.45	0.03	1.58	0.33	0.91	1.23	0.14	0.43	1.63	1.53
25	1.59	0.55	1.33	0.65	-0.03	2.17	0.56	1.12	1.52	1.72
26	1.39	0.81	0.90	1.02	0.28	2.20	1.25	1.00	1.50	
27	1.08	-0.23	0.55	0.40	1.02	0.89	0.03	1.11	0.95	1.41
28	0.65	0.22	0.53	-0.01		0.60	-0.23	1.17		0.88
29	1.58	1.28	1.53	1.49	1.66	1.07	1.14	1.53	1.98	0.64
30	1.33	0.77	-0.37	-0.60	1.53	1.25	-1.00	1.07	0.02	0.53
31	0.79	0.28	0.61	0.81	0.45	0.04	0.15	0.86	0.77	0.89
32	1.23	-0.07	0.28	-2.08	-0.12	-0.79	-1.49	2.35	0.26	
33	1.74	0.94	0.57	-0.87	0.15	0.24	-0.45	2.12	1.11	
34	1.19	1.05	0.70	0.05	-0.38		-0.11	0.37	0.72	0.33
35	0.73	1.11	1.61	0.51	-0.51	0.81	1.11	0.03	0.02	0.69
36	1.03	1.39	1.44	-0.50	-1.41	-0.15	0.06	1.58	1.71	1.01

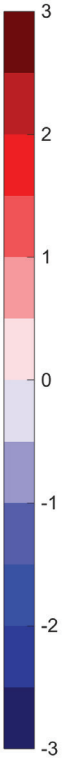

	2007	2008	2009	2010	2011	2012	2013	2014	2015	2016
1	1.81	-1.08		0.54	-0.93	-0.60		-1.08	-0.17	0.86
2	0.39	-0.40	-0.18	0.17	0.31	-1.12	-1.15	1.07	0.42	0.00
3	0.29	0.11	1.24	0.07	1.20	-0.14	0.80	-0.47	0.15	-1.28
4	0.70	-0.91	0.15	0.02	-0.25	-0.46	-0.21	0.31	0.21	0.74
5	0.32	1.04	-0.37	-1.46	-1.17	-0.13	-0.85	0.13	-0.62	-0.54
6	0.05	-0.23	0.16	-0.53	-0.49	0.47	1.07	1.26	1.95	0.95
7	0.52	0.26	0.15	-0.52	-0.81	0.44	0.89	1.33	1.70	0.78
8	-1.43		-1.28	0.42	1.42	0.56	1.19	2.07	1.35	1.99
9	0.51	-1.11	-0.27	0.29	-0.13	-1.16	-0.09	-0.11	1.96	1.24
10	-0.48	-0.39	1.07	1.43	1.16	1.54	1.24	1.34	1.01	1.65
11	0.95	1.07	0.66	0.99	1.13	1.55	1.22	-0.04	0.90	1.06
12	1.16	0.90	1.69	1.24	0.85	0.17	0.06	-0.04	0.17	-1.14
13										
14	1.22	-0.00	-0.02	-0.11	0.87	1.17	0.11	-0.54	0.46	0.38
15	1.09	0.39	0.75	0.46	1.31	0.76	0.79	0.46	1.43	0.85
16	1.16	1.32	1.54	1.49	1.57	1.02	0.58	-0.05	0.50	-1.82
17	0.98	0.00	0.13	1.39	0.85	0.46		0.35	0.71	0.49
18	0.51	1.22	1.61	1.53	1.41	0.31	0.46	-0.08	0.32	-1.53
19	0.70	1.08	1.43	1.39	1.17	0.83	0.22	-0.49	0.20	-0.95
20	0.35	0.54	0.65	0.71	0.66	0.26	-0.04	0.05	-0.29	-0.75
21	0.26	0.58	1.09	1.18	0.75	0.65	0.17	-0.34	-0.37	-0.89
22	0.61	-0.51	1.59	2.23	1.45	0.48	0.18	-1.42	-1.08	
23	0.97	0.51	2.01	1.82	1.53	0.69	0.30	-0.63	0.17	-0.73
24	0.48	-0.12	1.73	1.85	2.07	1.40	0.49	-0.36	0.71	0.44
25	1.53	1.18	0.16	1.95	2.06	1.22	0.77	0.86	-0.30	0.27
26	1.42	0.16	0.52	0.88	1.60	0.34	-0.02	0.16	-0.74	0.00
27	1.25	0.33	0.64	0.95	1.73	1.70	0.97	1.56	0.66	1.02
28	1.45	0.92	0.71	0.82		1.45	1.00	1.74		1.21
29	0.29	-0.16	0.63	1.08	1.42	0.45	0.18	1.50	0.97	0.76
30	0.07	0.43	-0.04	0.93	2.05	1.47	-0.38	-0.26	-1.18	-0.32
31	-0.43	0.14	0.03	-0.52	0.47	0.74	-0.65	-0.75	-0.43	-0.69
32	-0.20	1.27	1.13	-1.47	0.80	2.07	-0.60	0.47	0.93	
33	-0.63	0.93	1.17	-0.15	0.25	0.82	-0.58	1.21	0.67	
34	-0.24	-0.40	-0.08	0.08	-0.29	0.03	-1.71	-1.74	-0.61	-1.08
35	-0.14	0.08	0.82	0.88	-0.76	-0.97	0.81	0.20	-0.26	0.12
36	1.02	0.25	0.64	2.23	2.24	1.20	0.37	1.06	-0.64	-0.05

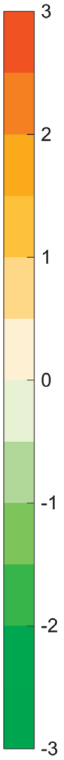

TABLES 1 AND 2.

Changes in temperature (Table 1, top) and salinity (Table 2, bottom) at selected stations in the North Atlantic region during the past decade, 2007–2016. The index numbers on the left can be used to cross-reference each point with information in Figures 1 and 2 and in Table 3. Unless specified, these are upper-layer anomalies. The anomalies are normalized with respect to the s.d. (e.g. a value of +2 indicates that the data (temperature or salinity) for that year were 2 s.d. above normal). Blank boxes indicate that data were unavailable for a particular year at the time of publication. Note that no salinity data are available for Station 13. Colour intervals 0.5 s.d.; red = warm; blue = cold; orange = saline; green = fresh.

Index	Description	Section	Measurement depth	Reference period	Lat.	Lon.	Mean T	s.d. T, °C	Mean S	s.d. S
1	Fram Strait - East Greenland Current	4.22	50-500 m	1983-2010	78.83	−6.00	0.69	0.57	34.650	0.135
2	Fylla section - Station 4 - Greenland Shelf	4.2	0-50 m	1983-2010	63.88	−53.37	2.64	1.10	33.162	0.392
3	Cape Desolation section - Station 3 - Greenland Shelf	4.2	75-200 m	1983-2010	60.47	−50.00	5.72	0.66	34.923	0.062
4	Central Labrador Sea	4.3	15-50 m	1981-2010	57.07	−50.92	4.68	0.69	34.635	0.176
5	Station 27 - Newfoundland Shelf temperature - Canada	4.4	0-175 m	1981-2010	47.55	−52.59	0.33	0.39	31.946	0.166
6	NE US continental shelf - Northern Mid Atlantic Bight	4.6	1-30 m	1981-2010	40.00	−71.00	11.36	0.94	32.710	0.430
7	NE US continental shelf - Northwest Georges Bank	4.6	1-30 m	1981-2010	41.50	−68.30	10.00	0.79	32.580	0.270
8	Emerald Basin - Central Scotian Shelf - Canada	4.5	250 m (near bottom)	1981-2010	44.00	−63.00		0.83		0.151
9	Misaine Bank - Northeast Scotian Shelf - Canada	4.5	250 m (near bottom)	1981-2010	45.00	−59.00		0.63		0.134
10	Siglunes Station 2-4 - North Iceland - North Icelandic Irminger Current - spring	4.7	100 m (near bottom)	1981-2010	67.00	−18.00	3.41	0.98	34.859	0.108
11	Langanes Station 2-6 - Northeast Iceland - East Icelandic Current - spring	4.7	100 m (near bottom)	1981-2010	67.50	−13.50	1.22	0.61	34.729	0.067
12	Selvogsbanki Station 5 - Southwest Iceland - Irminger Current - spring	4.7	50-150 m	1981-2010	63.00	−21.47	7.88	0.47	35.187	0.049
13	Point 33 - Astan	4.11	0-50 m	1998-2010	48.78	−3.94	12.79	0.34	35.206	0.112
14	Western Channel Observatory (WCO) -E1 - UK	4.11	0-200 m	1981-2010	50.03	−4.37	12.43	0.93	35.200	0.100
15	Malin Head Weather Station	4.12	5 m	1981-2010	55.37	−7.34	10.25	0.57		
16	Ellett Line - Rockall Trough - UK (section average)	4.13	0-40 m	1981-2010	56.75	−11.00	9.35	0.28	35.351	0.036
17	Central Irminger Sea subpolar-mode water	4.16	surface	1991-2010	59.40	−36.80	4.35	0.53	34.900	0.031
18	Faroe Bank Channel - West Faroe Islands	4.17	30-800 m	1988-2010	61.40	−8.30	8.80	0.36	35.302	0.043
19	Faroe Current - North Faroe Islands (modified North Atlantic water)	4.17	200-400 m	1987-2010	63.00	−6.00	8.11	0.39	35.249	0.043
20	Faroe Shetland Channel - Shetland Shelf (North Atlantic water)	4.17	upper layer	1981-2010	61.00	−3.00	9.95	0.47	35.398	0.051
21	Faroe Shetland Channel - Faroe Shelf (modified North Atlantic water)	4.17	high salinity core	1981-2010	61.50	−6.00	8.32	0.54	35.256	0.055
22	Ocean Weather Station Mike	4.20	upper layer	1981-2010	66.00	2.00	7.71	0.44	35.176	0.036
23	Southern Norwegian Sea - Svinøy section - Atlantic water	4.20	high salinity core	1981-2010	63.00	3.00	8.04	0.39	35.234	0.039
24	Central Norwegian Sea - Gimsøy section - Atlantic water	4.20	upper layer	1981-2010	69.00	12.00	6.89	0.34	35.154	0.031
25	Fugløya - Bear Island section - Western Barents Sea - Atlantic inflow	4.20	high salinity core	1981-2010	73.00	20.00	5.55	0.46	35.078	0.035
26	Kola section - Eastern Barents Sea	4.21	upper layer	1981-2010	71.50	33.50	4.22	0.52	34.771	0.056
27	Greenland Sea section - West of Spitsbergen 76.5°N	4.20	high salinity core	1996-2010	76.50	10.50	3.19	0.61	35.058	0.043
28	Northern Norwegian Sea - Sørkapp section - Atlantic water	4.20	50 m	1981-2010	76.33	10.00	4.08	0.60	35.073	0.038
29	Fram Strait - West Spitsbergen Current	4.23	50-200 m	1983-2010	78.83	7.00	3.11	0.69	35.027	0.038
30	Santander Station 6 (shelf break) - Bay of Biscay - Spain	4.8	50-200 m	1993-2010	43.71	−3.78	15.74	0.32	35.460	0.160
31	Fair Isle Current water (waters entering North Sea from Atlantic)	4.18	50-200 m	1981-2010	59.00	−2.00	9.93	0.61	34.874	0.132
32	Section average - Felixstowe - Rotterdam - 52°N	4.18	0-200 m	1981-2010	52.00	3.00		0.72		0.212
33	North Sea - Helgoland Roads	4.18	200 m	1981-2010	54.18	7.90	10.26	0.75	32.096	0.568
34	Baltic Proper - east of Gotland - Baltic Sea	4.19	50-200 m	1990-2010	57.50	19.50	9.27	1.03	7.172	0.196
35	Baltic - LL7 - Baltic Sea	4.19	50-500 m	1987-2010	59.51	24.50	3.97	0.73	7.961	0.666
36	Baltic - SR5 - Baltic Sea	4.19	0-30 m	1991-2010	61.05	19.35	3.27	0.58	6.428	0.141

TABLE 3.
Details of the datasets included in Figures 1 and 2 and in Tables 1 and 2. Blank boxes indicate that no information was available for the area at the time of publication. T = temperature, S = salinity. Some data are calculated from an average of more than one station; in such cases, the latitudes and longitudes presented here represent a nominal midpoint along that section.

2.2 SEA SURFACE TEMPERATURE

SSTs across the entire North Atlantic have also been obtained from a combined satellite and *in situ* gridded dataset. Figure 3 shows the seasonal SST anomalies for 2016 (relative to 1981–2010) extracted from the Optimum Interpolation SST dataset version 2 (OISST.v2) provided by the NOAA–CIRES Climate Diagnostics Center in the USA. The 1981–2010 climatology was prepared from a combination of two gridded datasets, namely the Extended Reynolds SST (ERSST) dataset and the OISST. v2 data. At high latitudes, where *in situ* data are sparse and satellite data are hindered by cloud cover, the data may be less reliable. Regions with ice cover for > 50% of the averaging period appear blank.

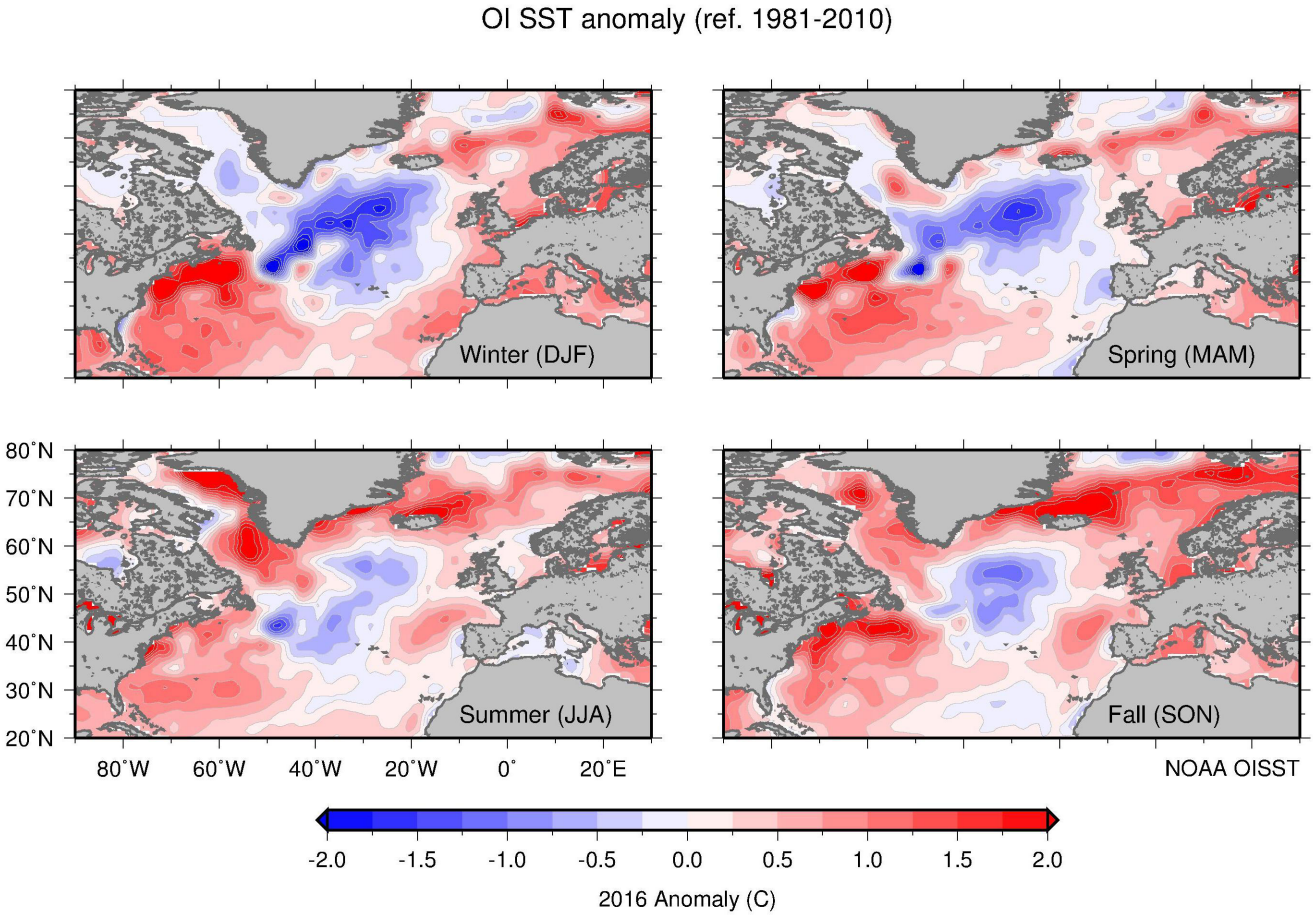

FIGURE 3.
Maps of seasonal sea surface temperature (SST) anomalies (°C) over the North Atlantic for 2016 from the NOAA OISST.v2 dataset provided by the NOAA-CIRES Climate Diagnostics Center, USA. The colour-coded temperature scale is the same in all panels. In this case, the anomaly is calculated with respect to normal conditions for 1981–2010. The data are produced on a 1° grid from a combination of satellite and *in situ* temperature data. Regions with ice cover for > 50% of the averaging period are left blank.

2.3 GRIDDED TEMPERATURE AND SALINITY FIELDS

Argo and the *In Situ* Analysis System (ISAS)

The Argo[1] network of profiling floats has been set up to monitor large-scale global ocean variability. Argo data are transmitted in real-time and are quickly made available by two global data assembly centres. One of the data centres is in Monterrey, USA and the other is the Coriolis Data Center of Ifremer in Brest, France. Delayed-mode data are also available, and these datasets have undergone more detailed quality control and calibration. Depending on the timing of the analysis process, the most recent 1–2 years of data presented in this report may come from a near real-time dataset, and older data will come from the higher-quality delayed-mode datasets.

The dataset presented here was prepared at the Coriolis Data Center[2] . Although the Argo dataset remains the main contribution in the open ocean, Coriolis assembles many types of data transmitted in real-time, merging the Argo dataset with data collected by the Global Telecommunications System relating to mooring, marine animals, gliders, and conductivity, temperature, and depth (CTD) profilers. As the ISAS analysis was designed to produce monthly synthesis over the global ocean, the time and space scales have been adjusted to the most general data availability; overall, this dataset is less skilled at describing conditions in the shallower marginal seas.

In the North Atlantic, the Argo dataset has adequately described temperature and salinity conditions of the upper 2000 m since 2002. This dataset is thus suitable for an overview of the oceanographic conditions in the deeper and more central regions of the North Atlantic basin, complementing the data from the IROC repeat stations and sections that are collected mainly at the periphery of the basin.

Figure 4 shows the 2016 seasonal mean fields of temperature and salinity at 10 m. Temperature and salinity anomalies are calculated relative to monthly climatological averages prepared from a reference climatology World Ocean Atlas 05 (WOA5; Antonov *et al.*, 2006; Loncarnini *et al.*, 2006). Annual mean anomalies of temperature and salinity for recent years at two selected depths, 10 m and 1000 m, are presented in Figures 5 and 6. Finally, in Figure 7, the winter mixed-layer depth (MLD) is shown.

Winter surface temperature and salinity determine the mixed-layer properties. In order to compare all areas over the decade, a simple definition for the mixed-layer depth is adopted, using the level at which density changes by more than 0.03 kg m^{-3} with respect to the 10 m depth. The density definition of the MLD is different to that presented in previous IROCs, where the MLD was calculated using temperature. Using a density criterion is more accurate because it is sensitive to both temperature and salinity stratification and, therefore, will be more relevant in areas of ice melt (e.g. Labrador Sea, Greenland).

Nevertheless, this new method may slightly overestimate the mixed-layer depth in regions of temperature/salinity density compensation. The month of March is selected as the common period for maximum mixed-layer depth. This is not perfectly true as the time of the deepest mixed layer may vary from year to year at a single location and does not occur at the same time over the whole basin (between February and March in the North Atlantic).

Temperature and salinity fields are estimated on a regular half-degree grid using the Coriolis ISAS. For data between 2002 and 2012, the results presented here were produced with delayed-mode data from version 6 (Gaillard, 2012) of the ISAS. For the years 2013–2016, delayed-mode data are not yet available and so the near real-time data from Coriolis are presented.

The ISAS gridded fields are based entirely on *in situ* products, whereas OISST.v2 is prepared using a combination of *in situ* and satellite SSTs. A comparison of Figures 3 and 4 (upper) shows that the pattern of surface temperature anomalies matches reasonably well. The main differences appear in the region east of Newfoundland; this may be caused by undersampling in the Argo dataset of the high variability in this region. One great advantage of the ISAS dataset is the inclusion of both temperature and salinity fields as well as subsurface

1) www.argo.ucsd.edu
2) www.coriolis.eu.org

data; these data, therefore, offer valuable information on conditions in the central North Atlantic where *in situ* sampling from hydrographic surveys is sparse and infrequent.

During winter 2015/2016, the near-surface waters were anomalously cold and fresh in the middle of the Subpolar Gyre and in the Labrador Sea (Figure 4). Farther south, waters were extremely warm and salty in the western basin south of 40°N, indicating a northward shift of the Gulf Stream. A warmer-than-normal Subtropical Gyre is also observed.

The subpolar cold anomaly persisted throughout 2016: although it weakened throughout the beginning of the year, it increased again in autumn (Figure 4). Summer was anomalously warm in the northern subpolar basin, north of 55°N, including the Labrador Sea and the Irminger Basin. South of 55°N, a slight cool anomaly persisted over the northern Subtropical Gyre. North of 40˚N, fresh salinity anomalies intensified throughout the year. Waters were very fresh along the East Greenland coast, while they were saltier in the Labrador Sea along the Canadian coasts and in the Greenland Sea, north of Iceland.

In the eastern North Atlantic, i.e. the Irminger Sea and off the European coast, winter 2015/2016 (as for winter 2014/2015) appears to be one of the extreme coldest for the 2002–2016 period, where temperatures went well below the climatological mean (1° lower in the Irminger Sea). These conditions contrast with the general trend of the warmer-than-normal (WOA5; Antonov *et al*., 2006; Loncarnini *et al*., 2006) conditions observed over the years 2002–2015 in winter and summer in the southwestern part of the basin. One of the warmest summers of the last decade was observed in the Labrador Sea.

The most salient feature of the 2016 annual mean temperature anomaly (using WOA5 as reference climatology; Antonov *et al*., 2006; Loncarnini *et al*., 2006) is an intense cold anomaly, persistent and increasing since 2013 in the subpolar basin from the tip of Greenland to 40°N, along with the persistent and increasing warm anomaly over the Greenland Sea and along the East Greenland coast (Figure 5).

In 2011, a surface salinity anomaly (fresh) was observed in the western North Atlantic basin around 45°N, which then appears to have propagated toward the eastern North Atlantic, entering the Iceland Basin in 2016 (Figure 5). This may have contributed to the abrupt freshening observed in the Iceland Basin (Section 4.14) and over the Faroe Bank Channel (Section 4.16) in 2016; this is yet to be verified. Around the Greenland coast, a strong fresh anomaly has also been observed to increase since 2014. In the Greenland Sea, a persistent warm/salty anomaly has been observed since 2011. In contrast, the Labrador Sea was saltier than usual in 2016, likely favouring convection during winter.

During late winter 2015/2016, in spite of the exceptional winter of 2014/2015, the area covered by a deep mixed layer (deeper than 1000 m), northward from the Labrador Sea to the Irminger Sea, is the second largest within this decade (Figure 7). This deep mixed layer may reflect strong winter convection in both the Labrador and Irminger basins. In the southeastern part, the deep mixed-layer extension stops around 48−50°N such that, in contrast to the 2010/2011, 2013/2014, and 2014/2015 winters, only moderate mixed-layer depths are observed along the shelf in the Bay of Biscay.

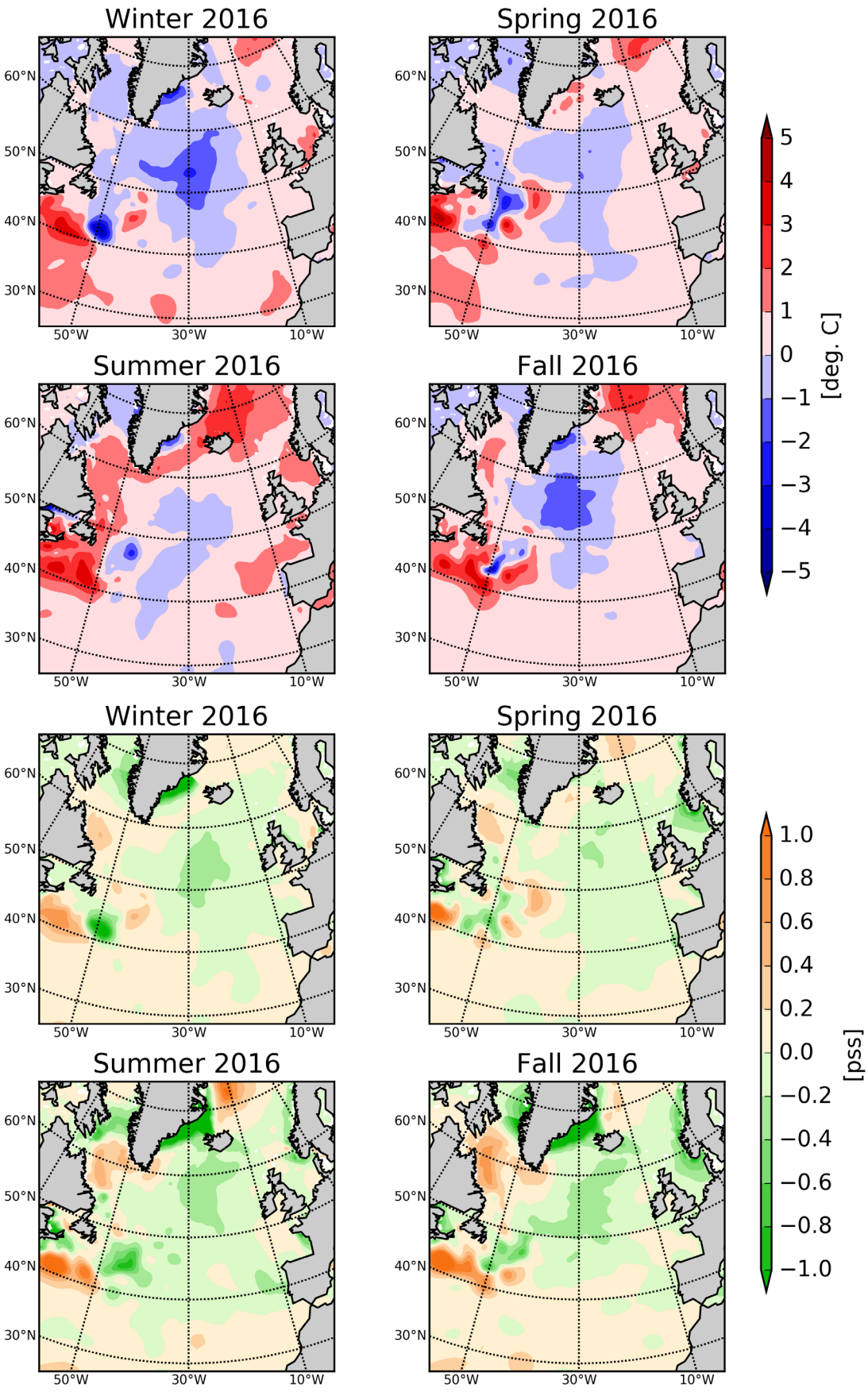

FIGURE 4.
Maps of 2016 seasonal temperature (upper) and salinity (lower) anomalies at 10 m depth in the North Atlantic. Anomalies are the differences between the ISAS monthly mean values and the reference climatology, WOA5. The colour-coded scale is the same in all panels. Data from Coriolis, ISAS monthly analysis of Argo data.

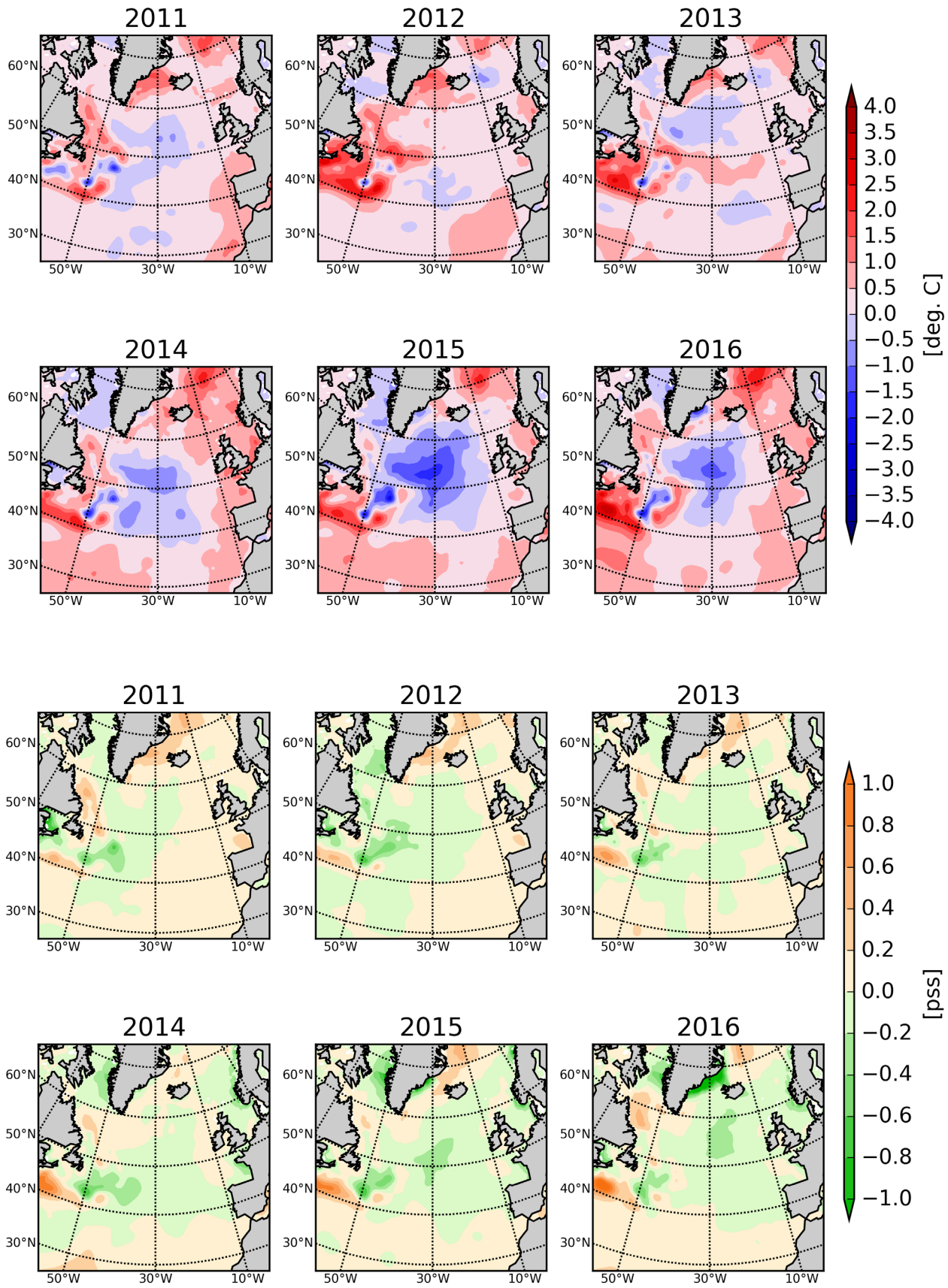

FIGURE 5.
Maps of annual temperature (upper) and salinity (lower) anomalies at 10 m depth in the North Atlantic for the period 2011–2016. Anomalies are the differences between the ISAS monthly mean values and the reference climatology, WOA5. The colour-coded scale is the same in all panels. Data from Coriolis, ISAS monthly analysis of Argo data.

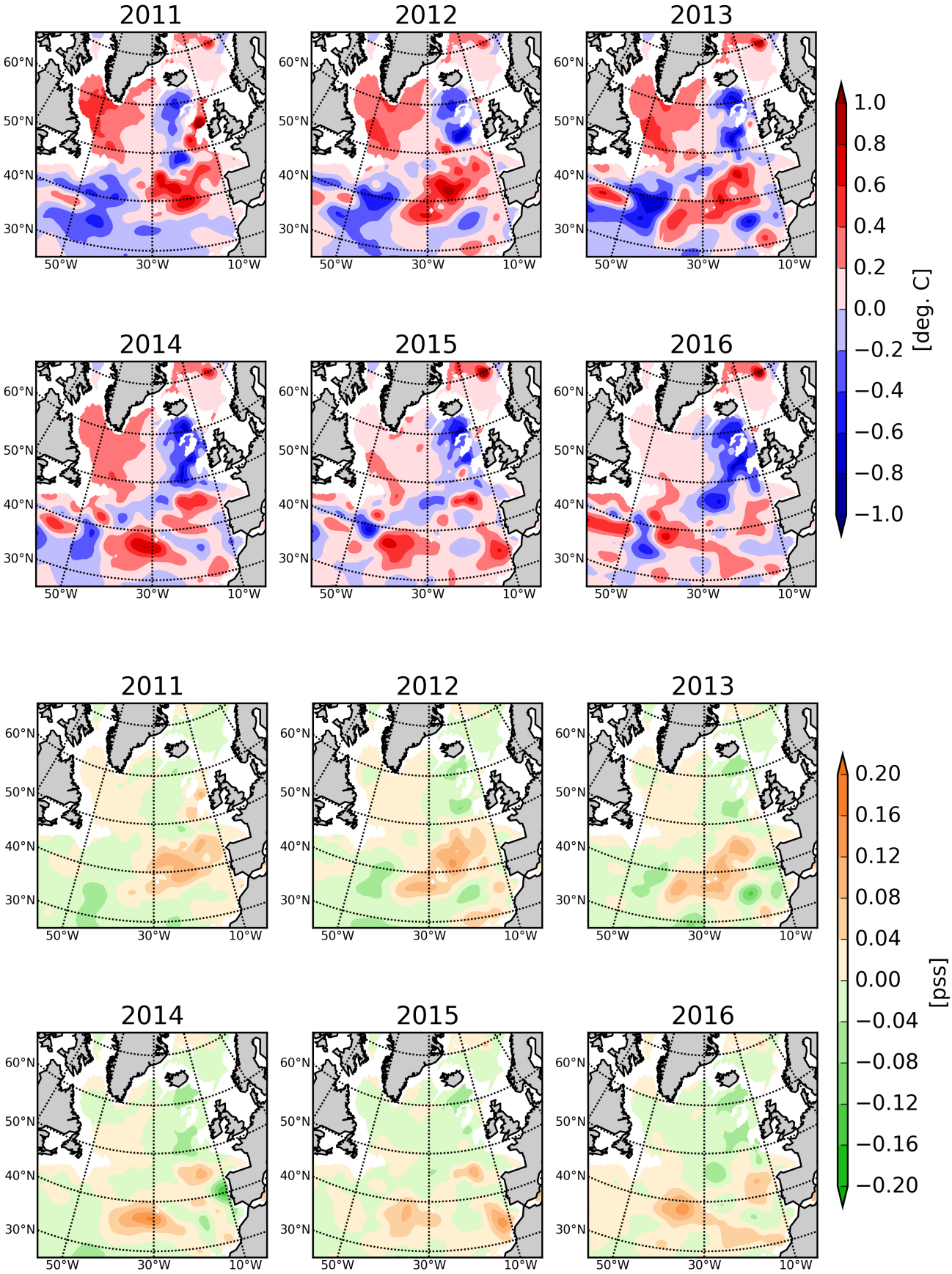

FIGURE 6.
Maps of annual temperature (upper) and salinity (lower) anomalies at 1000 m depth in the North Atlantic for the period 2011–2016. Anomalies are the differences between the ISAS monthly mean values and the reference climatology, WOA5. The colour-coded scale is the same in all panels. Data from Coriolis, ISAS monthly analysis of Argo data.

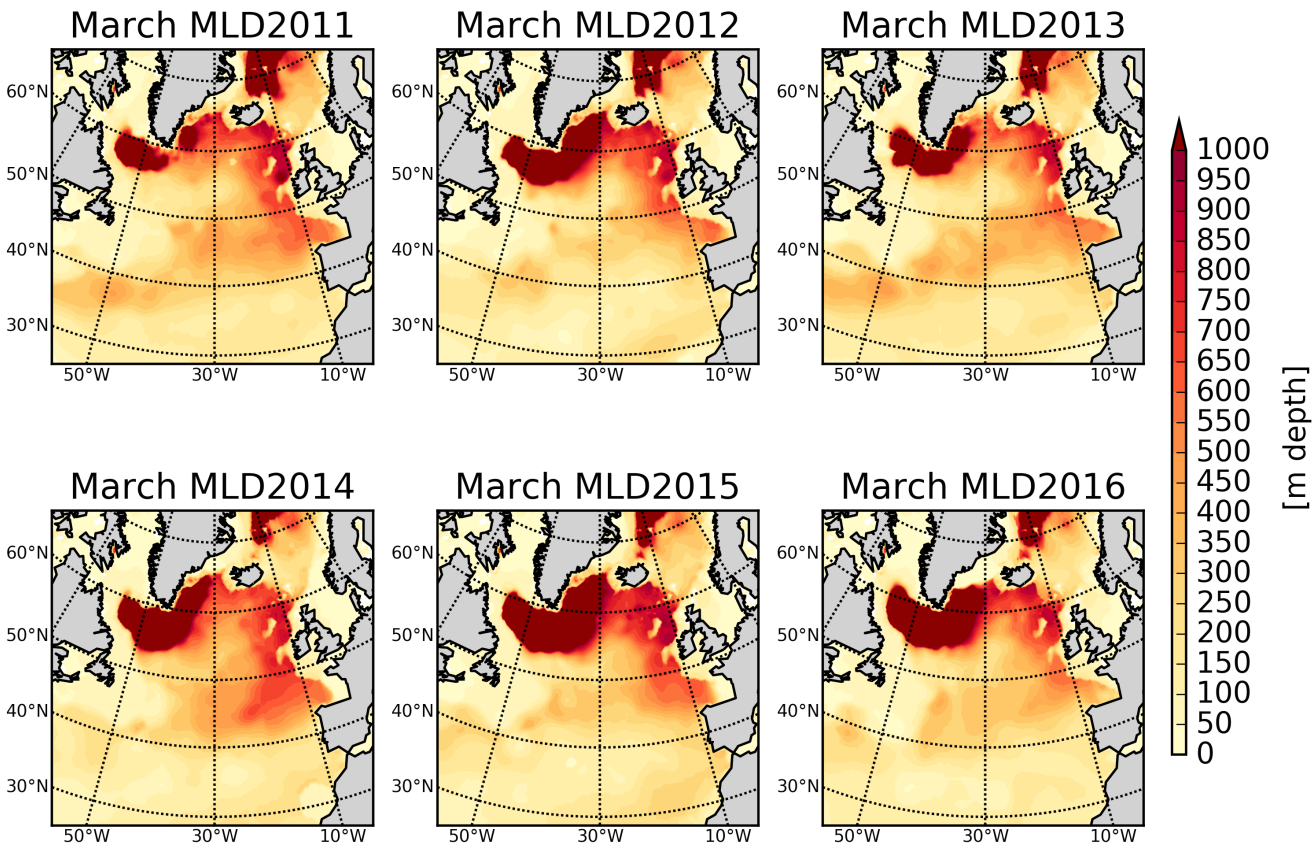

FIGURE 7.
Maps of North Atlantic winter (March) mixed-layer depths for 2011–2016 from the ISAS monthly analysis of Argo data. Note that from 2016, the mixed-layer depth is defined as the depth at which the density has increased by more than 0.03 kg m^{-3} from the density at 10 m depth. This criterion represents MLD in areas that are affected by both temperature and salinity (ice melting).

2.4 SUBPOLAR GYRE INDEX

The surface circulation of the North Atlantic is dominated by two gyres, one that circulates warmer water in a clockwise direction, known as the Subtropical Gyre, and another that circulates cooler waters in the opposite direction, known as the Subpolar Gyre (Figure 14). The Subpolar Gyre encompasses the North Atlantic, East Greenland, and Labrador currents. Both the Subtropical and Subpolar gyres are driven by a combination of processes; the most important for the Subpolar Gyre being the strength and direction of surface winds, the input of heat from atmosphere to ocean, and the large-scale circulation in the world ocean, known as the overturning circulation (Berx and Payne, 2017a).

Following the method of Häkkinen and Rhines (2004), the Subpolar Gyre index presented here (Berx and Payne, 2017b) was calculated from an analysis of sea surface height in the North Atlantic. The Subpolar Gyre index describes the current state of this complex circulation and has been found to be a useful indicator for understanding ecosystem variability in the Subpolar Gyre region and in the wider North Atlantic, including potential links with commercially important fish stocks (e.g. Hátún *et al.*, 2016). In 2012, ICES Working Group on Widely Distributed Stocks (WGWIDE) called for this product to be made more readily available; therefore, it is now included in the IROC.

The Subpolar Gyre index was high in the early 1990s, indicating a strong gyre circulation and a wide spread. This was shown to be linked to fresher and cooler conditions in the eastern North Atlantic. Between 1995 and 2005, the Subpolar Gyre index weakened and contracted (Figure 8). It is thought that a weaker Subpolar Gyre results in more water of subtropical origin; therefore, this phenomenon was linked to the trend in warming and salinification of the Atlantic water (AW) in the eastern North Atlantic (Holliday *et al.*, 2008). Since 2010, the Subpolar Gyre index can be described as weak and variable. The lowest annual value (−1.26) in the Subpolar Gyre index time-series was observed in 2013. The annual value of the index in 2015 was −0.63.

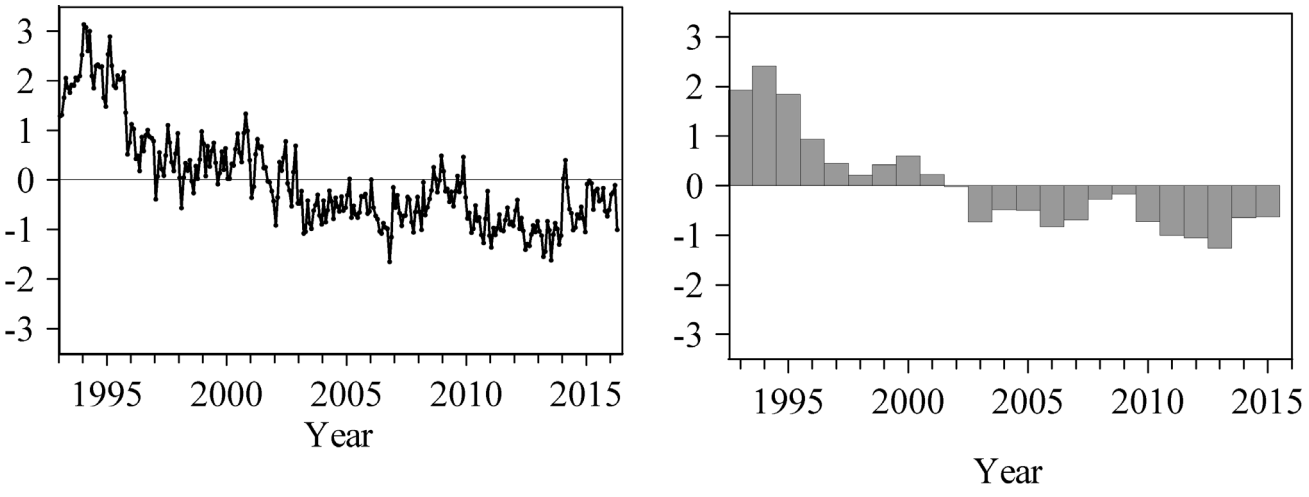

FIGURE 8.
The monthly (left) and annual (right) Subpolar Gyre index since 1992. Data source: Marine Scotland, UK (Berx and Payne, 2017b).

On board RV "Oceania". Photo: Agnieszka Beszczynska-Möller, Institute of Oceanology, Polish Academy of Sciences, Poland.

3. NORTH ATLANTIC ATMOSPHERE

The North Atlantic Oscillation (NAO) is a pattern of atmospheric variability that has a significant impact on oceanic conditions. It affects windspeed, precipitation, evaporation, and the exchange of heat between ocean and atmosphere, and its effects are most strongly felt in winter. The NAO index is a simple device used to describe the state of the NAO. It is a measure of the strength of the sea level air pressure gradient between Iceland and Lisbon, Portugal. When the NAO index is positive, there is a strengthening of the Icelandic low-pressure system and the Azores high-pressure system. This produces stronger mid-latitude westerly winds, with colder and drier conditions over the western North Atlantic and warmer and wetter conditions in the eastern North Atlantic. When the NAO index is negative the pressure gradient is reduced, and the effects tend to be reversed.

The NAO index calculated by various climate scientists comes in several slightly different versions. The Hurrell winter (December/January/February/March, or DJFM) NAO index (Hurrell *et al.*, 2003) is the one most commonly used and is particularly relevant to the eastern North Atlantic. Note that although we may think of winter as coming at the end of the year, here the "winter season" spans an annual boundary and precedes the year of interest, so the winter of December 2015 to March 2016 sets up conditions for summer 2016.

The NAO is the dominant pattern of atmospheric pressure variability in the North Atlantic. However, when the NAO itself is weak (i.e. the dominant atmospheric pattern is not an NAO type pattern), this may be caused by a different pattern occurring. Two other dominant atmospheric regimes have been identified as useful descriptors: (i) the Atlantic Ridge mode, when a strong anticyclonic ridge develops off western Europe (similar to the East Atlantic pattern); and (ii) the Blocking regime, when the anticyclonic ridge develops over Scandinavia. The four regimes (positive NAO, negative NAO, Atlantic Ridge, and Blocking) have all been occurring at around the same frequency (20–30% of all winter days) since 1950 (Hurrell and Deser, 2010). For this reason, we also include maps of SLP, windspeed, and air temperature as they offer a more detailed understanding of the North Atlantic atmospheric variability than the NAO index.

3.1 NORTH ATLANTIC OSCILLATION (NAO) INDEX

Following a long period of increase, from an extreme and persistent negative phase in the 1960s to a most extreme and persistent positive phase during the late 1980s and early 1990s, the Hurrell NAO index underwent a large and rapid decrease during winter 1995/1996. In many of the years between 1996 and 2009, the Hurrell winter NAO index was both weak and a less useful descriptor of atmospheric conditions, mainly because the SLP patterns were not typical of the NAO. In winter 2009/2010, the index was strongly negative (Figure 9), and its anomaly pattern exerted a dominant influence on atmospheric conditions. This was the strongest negative anomaly since 1969 and the second strongest negative value for the Hurrell winter

NAO index on record (starting in 1864). Winter 2014/2015 saw the strongest NAO index since 1995 and the fourth most positive NAO index in the last 110 years (Hurrell and National Center for Atmospheric Research Staff, 2017). The winter NAO index was positive (+0.98) for the third consecutive winter, but was weaker than the two preceding winters, both of which exceeded +3.0, and was the lowest magnitude (either positive or negative) index of this decade.

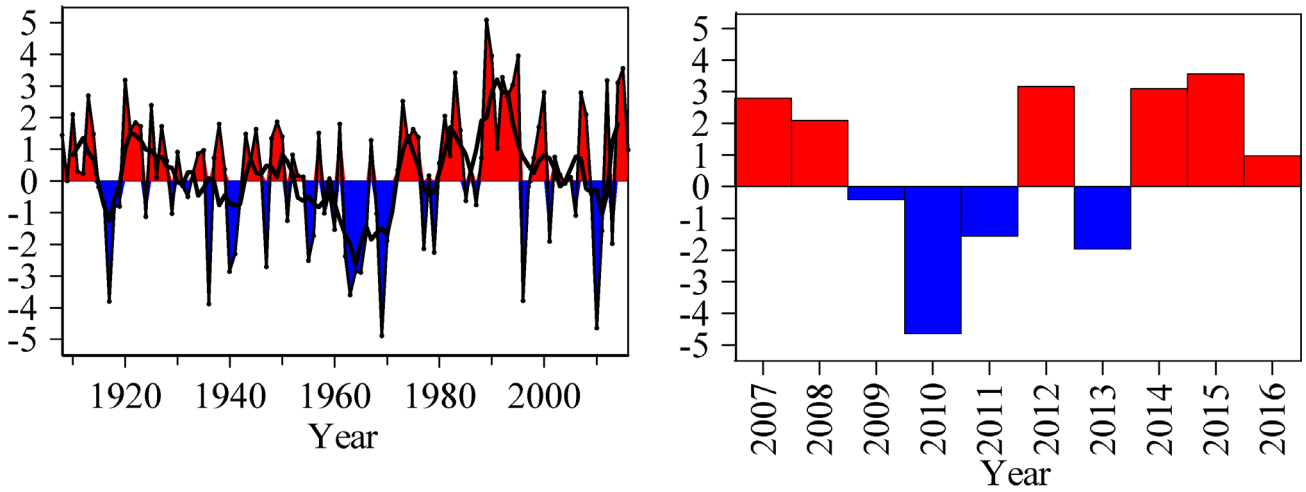

FIGURE 9.
The Hurrell winter (DJFM) NAO index for the past 100 years with a two-year running mean applied (left panel) and for the current decade (right panel). Data source: The Climate Analysis Section, NCAR, Boulder, USA (Hurrell and National Center for Atmospheric Research Staff, 2017).

3.2 SEA LEVEL PRESSURE AND WINDSPEED

Atmospheric conditions indicated by the NAO index are more understandable when the anomaly fields are mapped. Ocean properties are particularly dominated by winter conditions; hence, the inclusion of SLP and windspeed maps for the winter period (Figures 10 and 11).

The top panel of Figure 10 shows the winter SLP averaged over 30 years (1981–2010). The dominant features ("action centres") are the Iceland Low, situated southwest of Iceland, and the Azores High, west of Gibraltar. The middle panel of Figure 10 shows the mean SLP for winter 2015/2016 (DJFM), and the bottom panel shows the 2015/2016 winter SLP anomaly (i.e. the difference between the top and middle panels).

The pattern of SLP is closely related to patterns of wind. The geostrophic (or "gradient") wind blows parallel to the isobars, with lower pressure to the left; the closer the isobars, the stronger the wind. The strength of the winter mean surface wind averaged over the 30-year period (1981–2010) is shown in the upper panel of Figure 11, while the middle panel shows the mean surface wind for winter 2015/2016 and the lower panel the anomaly in winter 2015/2016.

In the SLP for winter 2015/2016 (Figure 10), the Azores High appeared relatively strong with a high pressure anomaly extending from Newfoundland across southern Europe, while the Iceland Low strengthened at its southern extent. The influence of this is seen in stronger-than-normal winds (Figure 11) along a track from the Flemish Cap to the Bay of Biscay and into the English Channel, as well as over the Labrador Sea. A band of weaker-than-average winds was evident from southwest of Iceland into the Norwegian Sea, extending to Svalbard and the western Barents Sea. Winds at the northeastern coast of North America were weaker than average, from the Carolinas to Newfoundland.

3.3 SURFACE AIR TEMPERATURE

North Atlantic winter mean surface air temperatures are shown in Figure 12 (Kalnay *et al*., 1996). The 1981–2010 mean conditions (Figure 12, top panel) show warm temperatures penetrating far to the north on the eastern side of the North Atlantic and the Nordic seas, caused by the northward movement of warm oceanic water. The middle panel of Figure 12 shows the conditions in winter 2015/2016 (DJFM), and the bottom panel shows the difference between the two.

Offshore wind park in the southern North Sea. Photo: Holger Klein, Bundesamt für Seeschifffahrt und Hydrographie, Germany.

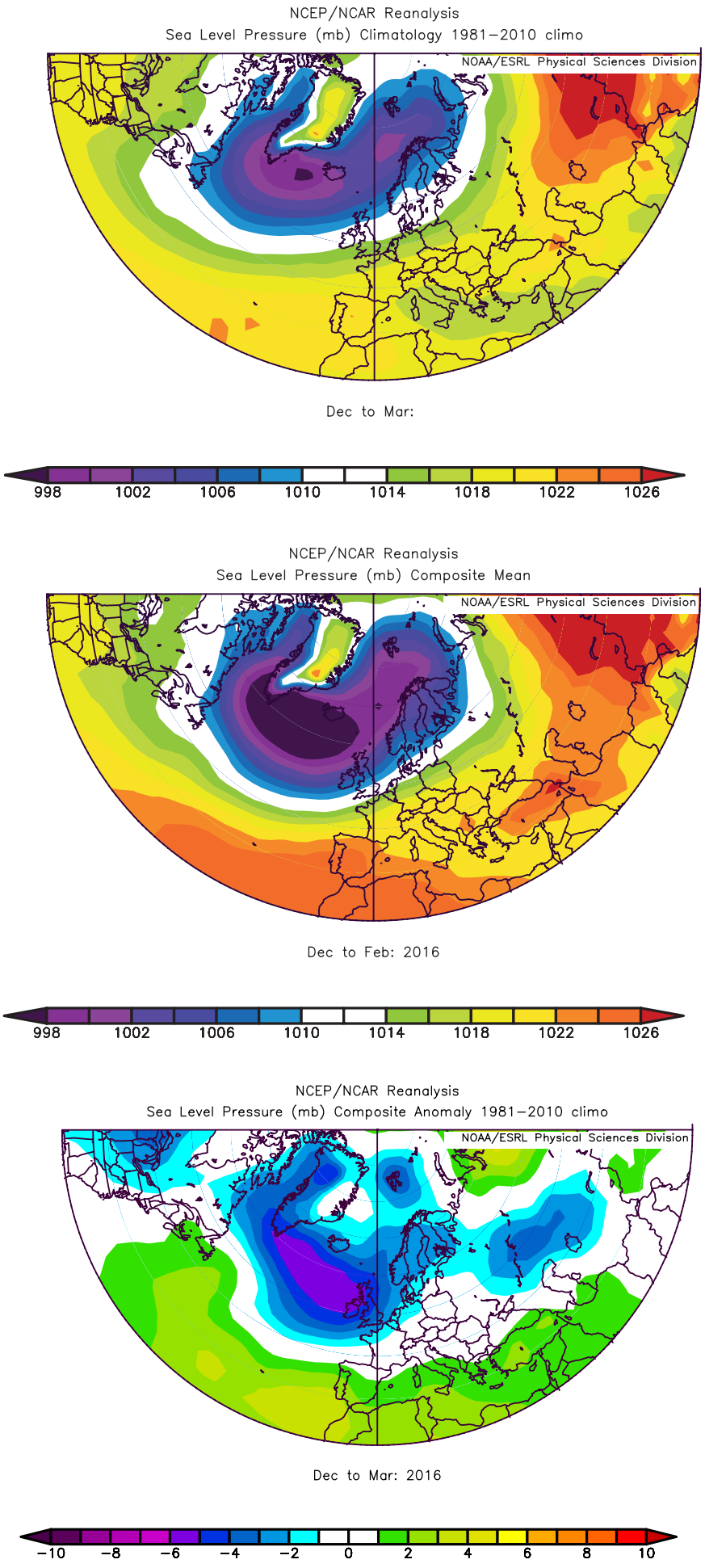

FIGURE 10.
Winter (DJFM) sea level pressure (SLP) fields. Top panel: SLP averaged over 30 years (1981–2010). Middle panel: SLP in winter 2015/2016. Bottom panel: winter 2015/2016 SLP anomaly, calculated as the difference between the top and middle panels. Images provided by the NOAA/ESRL Physical Sciences Division, Boulder, CO.

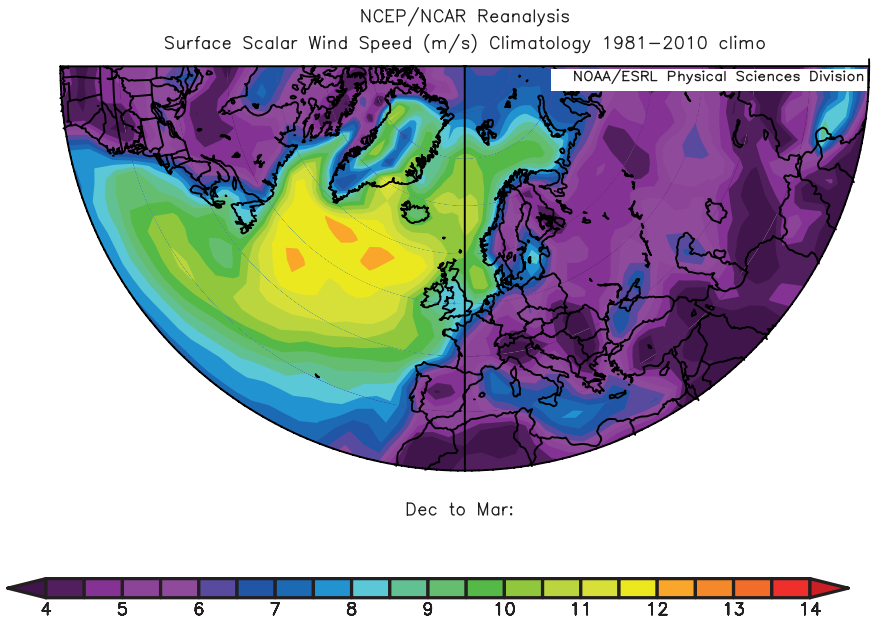

FIGURE 11.
Winter (DJFM) windspeed fields. Top panel: scalar wind-speed averaged over 30 years (1981–2010). Middle panel: scalar windspeed in winter 2015/2016. Bottom panel: winter 2015/2016 scalar windspeed anomaly, calculated as the difference between the top and middle panels. Images provided by the NOAA/ESRL Physical Sciences Division, Boulder, CO.

Winter 2015/2016 air temperatures were only below the long-term average (1981–2010) over the Subpolar Gyre. The influence of the cooler area appears to extend as far as the European shelf edge where air temperatures experienced from Portugal to Iceland, Faroe, and southern Norway were close to, rather than above the average of recent years. This lower-than-average pattern is consistent with the SST anomalies observed in the subpolar region. Temperatures elsewhere were generally higher than normal, particularly over the Mid-Atlantic Bight, Fram Strait, and the Barents Sea.

3.4 OUTLOOK BEYOND 2016

An initial assessment of the North Atlantic atmosphere at the end of the IROC year is included. Atmospheric conditions during winter are a determining factor of oceanic conditions for the following year; therefore, this outlook offers some predictive capability for spring–autumn 2017.

The SLP pattern for December 2016–March 2017 indicates that it will be the fourth consecutive positive NAO index winter, but again weaker than those preceding it. As expected for a weak NAO index, the SLP anomaly pattern is not a clear NAO pattern. An anticyclonic anomaly centred over the North Sea and a cyclonic anomaly over the Arctic extended southeast and southwest. Again, in concert with weakened NAO influence, there was no strong spatial pattern to the windspeed anomaly. Recent advances in understanding the predictability of the NAO are showing significant skill in seasonal predictions of the European winter through predictability of the winter NAO (Scaife *et al*., 2014), Arctic Oscillation (AO), and Sudden Stratospheric Warming (SSW) events (Scaife *et al*., 2015). Recent results published by the UK Met Office suggest that there is even significant skill in predicting the winter NAO index one year ahead (Dunstone *et al*., 2016) with a correlation coefficient (r) between the observed and the predicted NAO of about 0.4 for the second winter, comparing well with that of about 0.6 for the first winter (Scaife *et al*.,2014).

Air temperatures in winter 2016/2017 were cold over the Subpolar Gyre, including over the Irminger Sea and Iceland Basin. As in winter 2015/2016, there were warmer-than-average conditions around the margins of the Subpolar Gyre, but the colder-than-average conditions observed in 2016 over the gyre itself were not evident in winter 2016/2017, possibly indicating a weakening of the relatively cool conditions in that region for the last few years.

Experimental forecasts from the US (seasonal periods: NOAA Climate Prediction Center - The North American Multi-Model Ensemble) and the UK (1–5 years: Met Office Decadal forecast January 2017) also suggest an outlook for temperatures in the Subpolar Gyre region that is more typical of the long-term average (1981–2010) than has been seen in the last few cold anomaly years. As these are experimental forecasts at an early stage, they are noted here so that their performance may be tracked and their utility gauged as they develop.

RV "Delaware II" plunging through a large wave as it travels across the Bay of Fundy. Photo: Chris Melrose, NEFSC/NOAA, US.

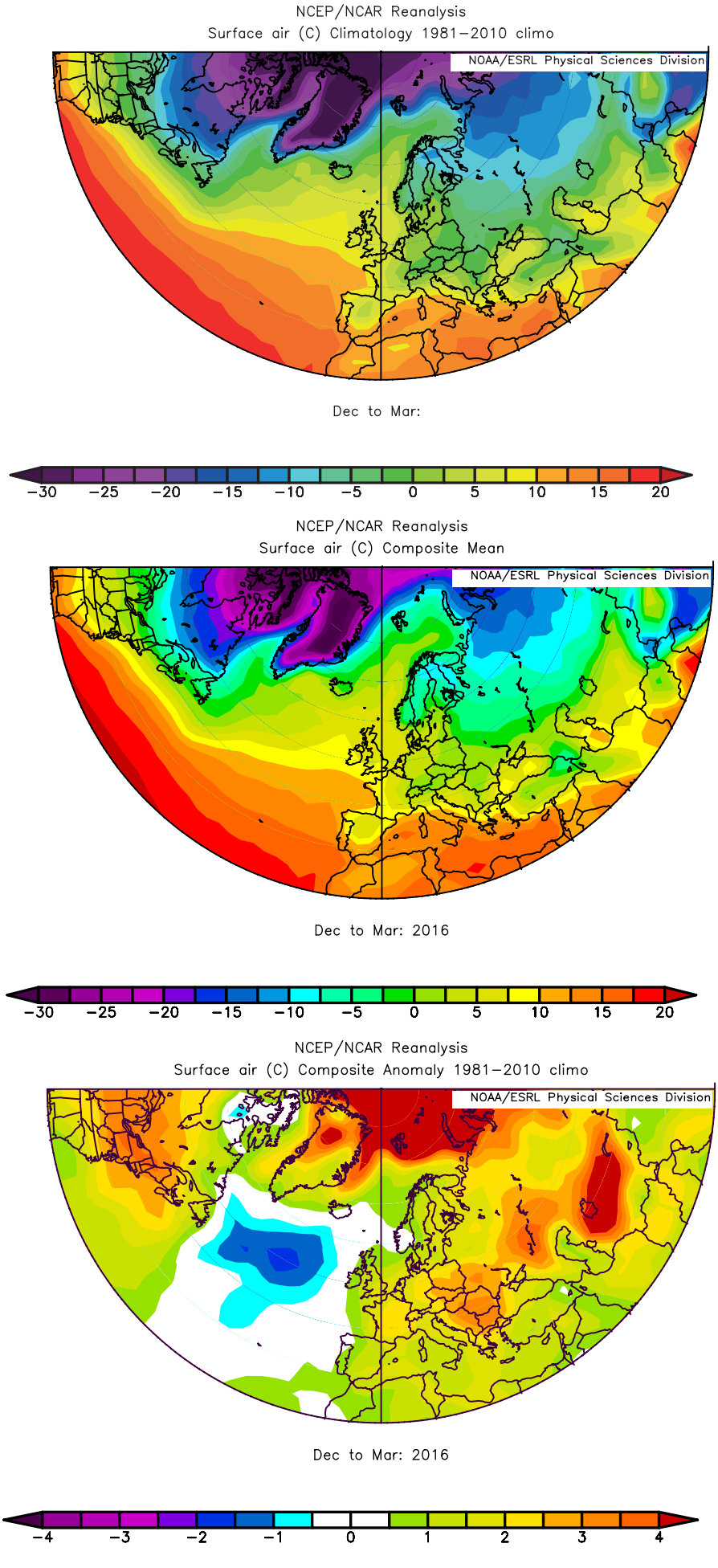

FIGURE 12.
Winter (DJFM) surface air temperature fields. Top panel: surface air temperature averaged over 30 years (1981–2010). Middle panel: surface air temperatures in winter 2015/2016. Bottom panel: winter 2015/2016 surface air temperature anomaly, calculated as the difference between the top and middle panels. Images provided by the NOAA/ESRL Physical Sciences Division, Boulder, CO (available online at http://www.cdc.noaa.gov/).

Steaming slowly back out to deep water through light sea ice. Photo: Penny Holliday, National Oceanography Centre Southampton, UK.

4. DETAILED AREA DESCRIPTIONS, PART I: THE UPPER OCEAN

4.1 INTRODUCTION

This section presents time-series from sustained observations in ICES areas (Figure 13). The general pattern of oceanic circulation in the upper layers of the North Atlantic, in relation to the areas described here, is shown in Figure 14. In addition to temperature and salinity, other indices are presented where available, such as air temperature and sea ice extent. The regional context of the sections and stations is summarized, noting any significant changes.

Most standard sections or stations are sampled annually or more frequently. Many of the time-series presented here have been extracted from larger datasets and have been chosen as indicators of the conditions in a particular area. Where appropriate, data are presented as anomalies to demonstrate how the values compare with the average or "normal" conditions (usually the long-term mean of each parameter during 1981–2010). For datasets that do not extend as far back as 1981, the average conditions have been calculated from the start of the dataset through 2010.

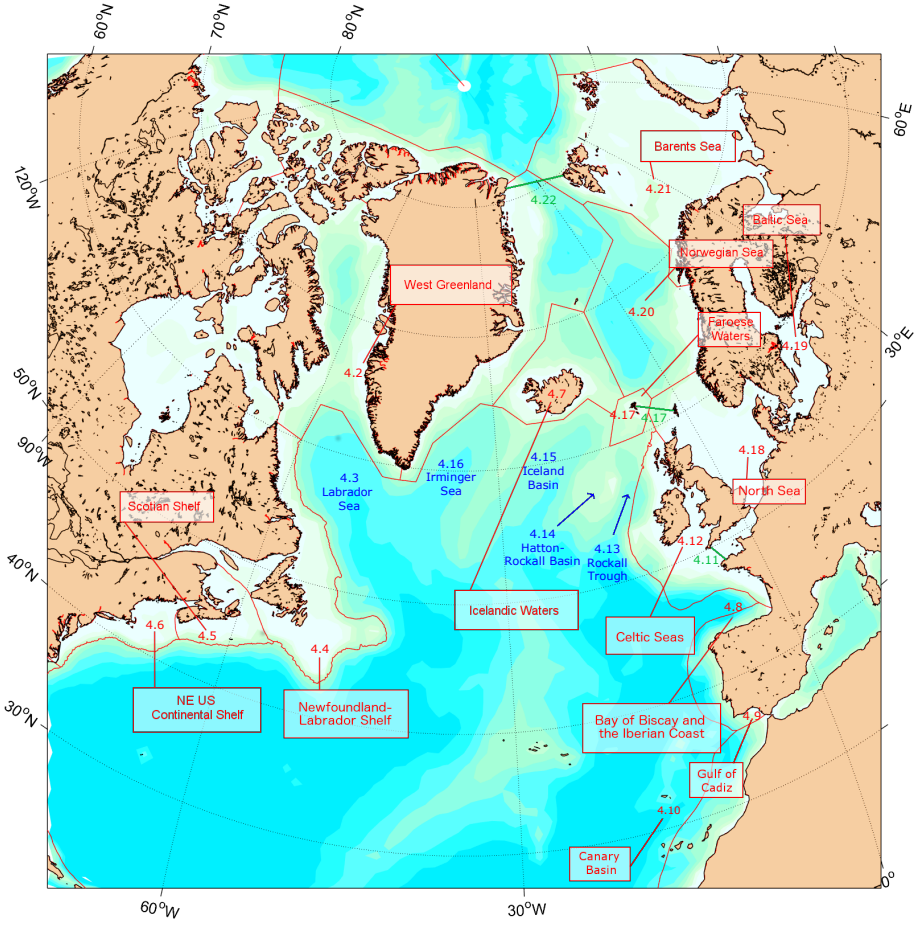

FIGURE 13.
Schematic of marine areas used to organize data presentation in this section. Numbers refer to the subsection number. Regions are labelled in red. Ocean basins are labelled in blue. Green numbers indicate straits. NOAA Large Marine Ecosystem (LME) boundaries (www.lme.noaa.gov) are shown as background reference, but hydrographic regions are loosely defined, so they do not perfectly overlap.

In places, the seasonal cycle has been removed from a dataset either by calculating the average seasonal cycle during 1981–2010 or by drawing on other sources, such as regional climatology datasets. Smoothed versions of most time-series are included using a "Loess smoother", a locally weighted regression with a two- or five-year window (chosen to be the most appropriate for each time-series).

In some areas, data are sampled regularly enough to allow a good description of the seasonal cycle. Where possible, monthly data from 2016 are presented and compared with the average seasonal conditions and statistics.

Although there are no real boundaries in the ocean, it is the intention that the data presented will represent conditions in a particular area. In this chapter, datasets are grouped into areas based on existing definitions such as ICES ecoregions[3] or NOAA LMEs[4], but the bathymetry of ocean basins[5] and the general pattern of ocean circulation is also taken into account (Figure 14).

Where there is overlap, ICES ecoregions and NOAA LMEs generally align, although there are some differences in the position of offshore boundaries. The offshore boundaries of ICES ecoregions are often aligned with management areas, typically the 200 nautical mile fishery limits, thereby representing economic limits rather than true ecosystem boundaries. Ocean currents tend to circulate around ocean basins, flowing at the margins of a sea/ocean area. As shelf areas are generally delineated by waters of coastal origin farther onshore and oceanic origin farther offshore, ocean currents could be used to define the boundary. However, the dynamic nature of ocean currents ensures that this will never be a fixed boundary; for this reason, the defined areas are nominal rather than definitive.

Although the data presented here offer the best available indicative time-series within a region, it should be noted that in large areas with complex circulation patterns, consideration should be given to how representative these data are of the whole ecoregion.

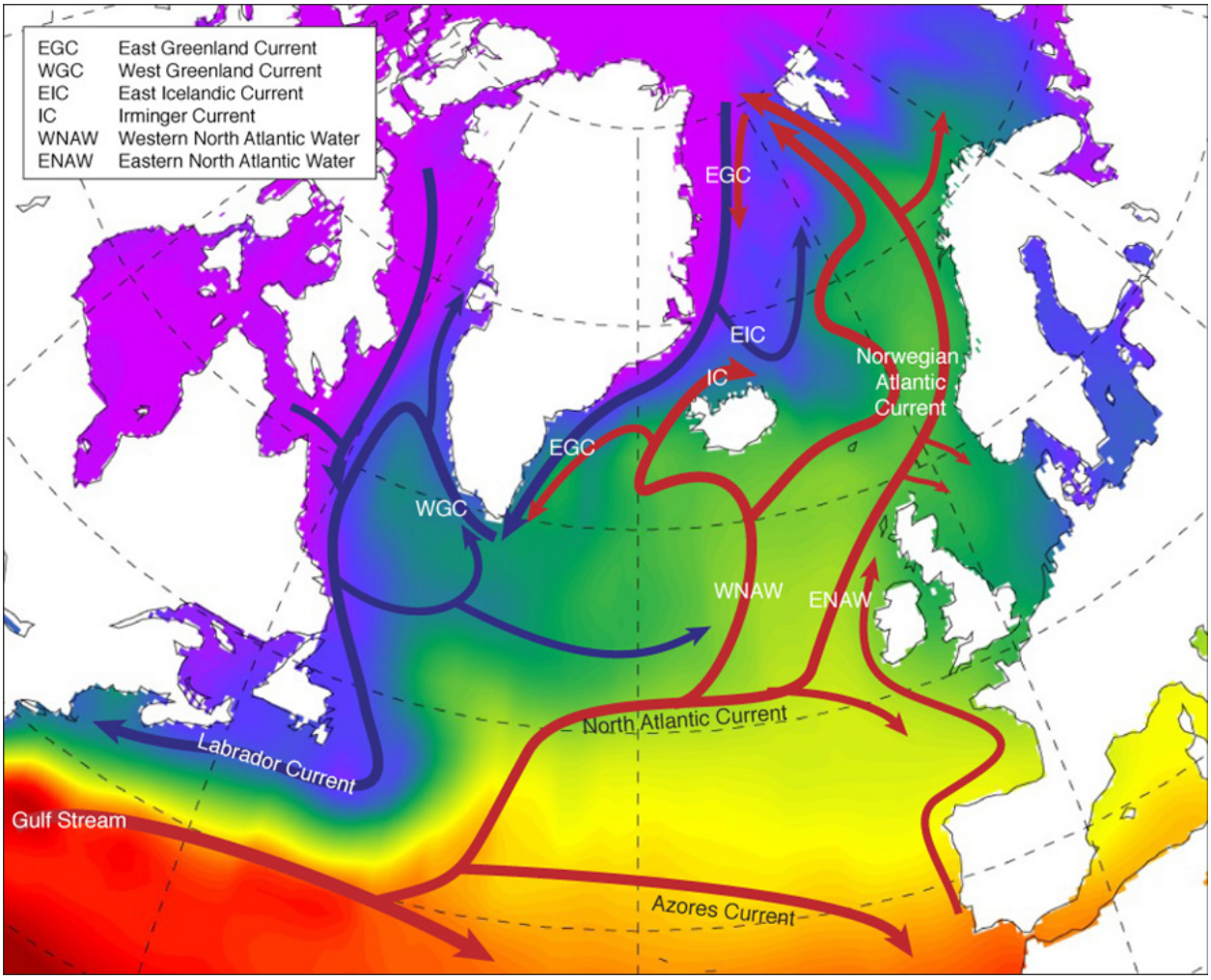

FIGURE 14.
Schematic of the general circulation of the upper ocean (0–1000 m) in the North Atlantic. Blue arrows = movement of cooler waters of the Subpolar Gyre; red arrows = movement of warmer waters of the Subtropical Gyre.

3) http://www.ices.dk/community/advisory-process/Pages/ICES-ecosystems-and-advisory-areas.aspx
4) http://www.lme.noaa.gov/
5) http://www.gebco.net/data_and_products/undersea_feature_names/

4.2 WEST GREENLAND

The US National Oceanic and Atmospheric Administration (NOAA) Large Marine Ecosystem (LME) project has identified the ecosystem of the Canadian Eastern Arctic–Western Greenland as an LME. Only conditions in the West Greenland portion of the region are examined here. The hydrographic conditions presented are monitored at two oceanographic sections across the continental slope of West Greenland in the southwestern part of the ecoregion, at a position that is influenced by the West Greenland Current (WGC; Figure 15). The WGC carries water northward along the west coast of Greenland and consists of two components: a cold and fresh inshore component, which is a mixture of polar water and melt water, and a warmer, saltier offshore component called Irminger Sea water. Being part of the cyclonic Subpolar Gyre, the WGC is subject to hydrographic variations on a range of time-scales associated with variability in the gyre.

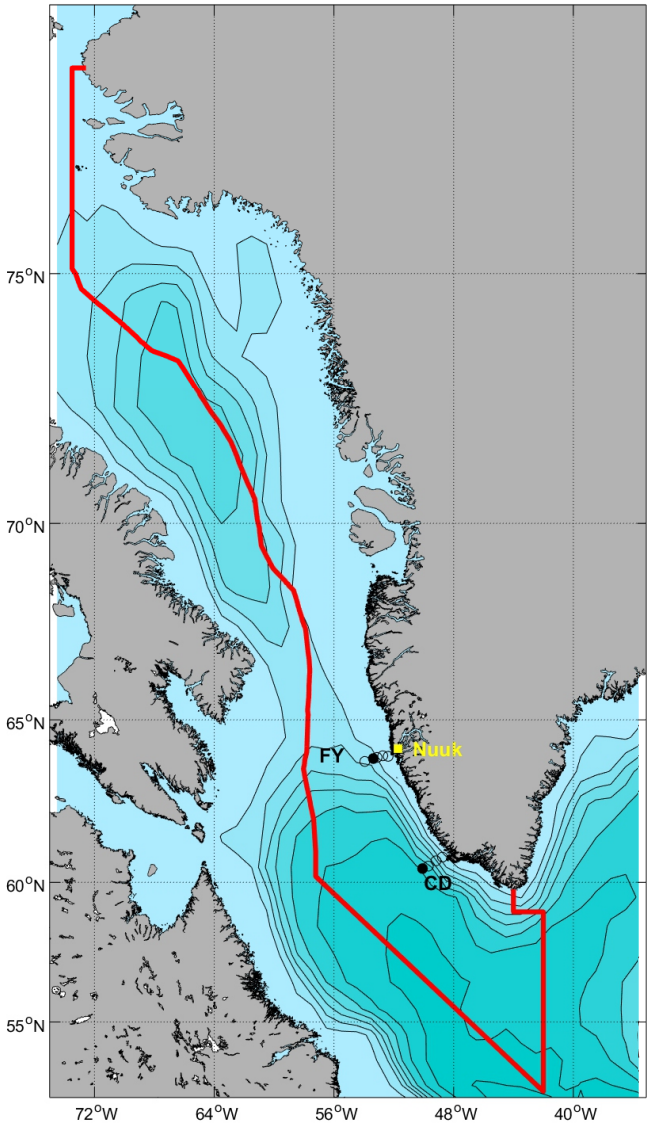

In winter 2015/2016, the NAO index was positive (0.98) for the third consecutive winter, but was weaker than the two preceding winters. The annual mean air temperature at Nuuk Weather Station in West Greenland was 0.6°C in 2016, which was 2.0°C above the long-term mean (1981–2010). The daily air temperature at Nuuk (Figure 16) reached 24°C on 9 June 2016, marking the warmest temperature ever recorded in the Arctic country during June.

The water properties between 0 and 50 m depth at Fyllas Bank Station 4 (Figure 17) are used to monitor the variability of the fresh polar water component of the WGC. However, the Fyllas Bank section had to be abandoned due to severe weather conditions.

The temperature and salinity of the Irminger Sea water component of the WGC began increasing in the late 1990s, coinciding with the slowing down of the Subpolar Gyre. The warming trend lasted until 2014. In 2016, the water temperature in the 75–200 m layer at Cape Desolation Station 3 (Figure 18) was 5.44°C with a salinity of 34.84, which was 0.27°C and 0.08 below the long-term mean, respectively.

FIGURE 15.
Circulation schematic for the Labrador Sea and Davis Strait. The location of Nuuk is marked in yellow. The red lines show the extent of NAFO Division 1a, Western Greenland. The circles labeled "FY" are Fyllas Bank hydrographic section stations, Station 4 is marked as a black circle. The circles labeled "CD" are stations of the Cape Desolation hydrographic section; Station 3 is marked as a black circle.

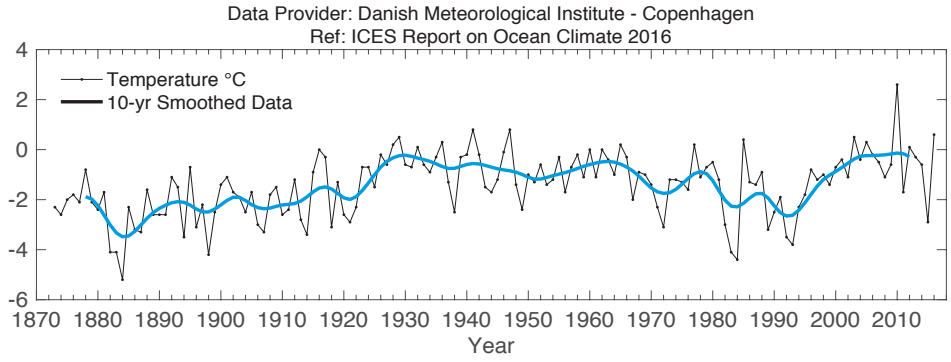

FIGURE 16.
West Greenland. Annual mean air temperature at Nuuk station (64.16°N 51.75°W). Data source: Cappelen (2017).

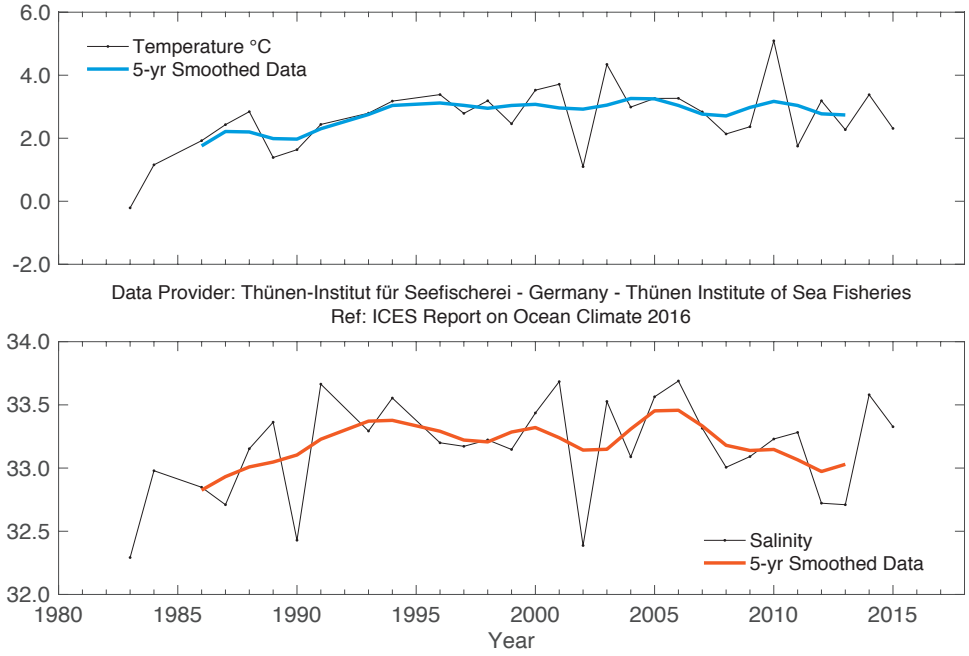

FIGURE 17.
West Greenland. Mean temperature (upper panel) and salinity (lower panel) in the 0–50 m water layer at Fyllas Bank Station 4 (63.88°N 53.37°W).

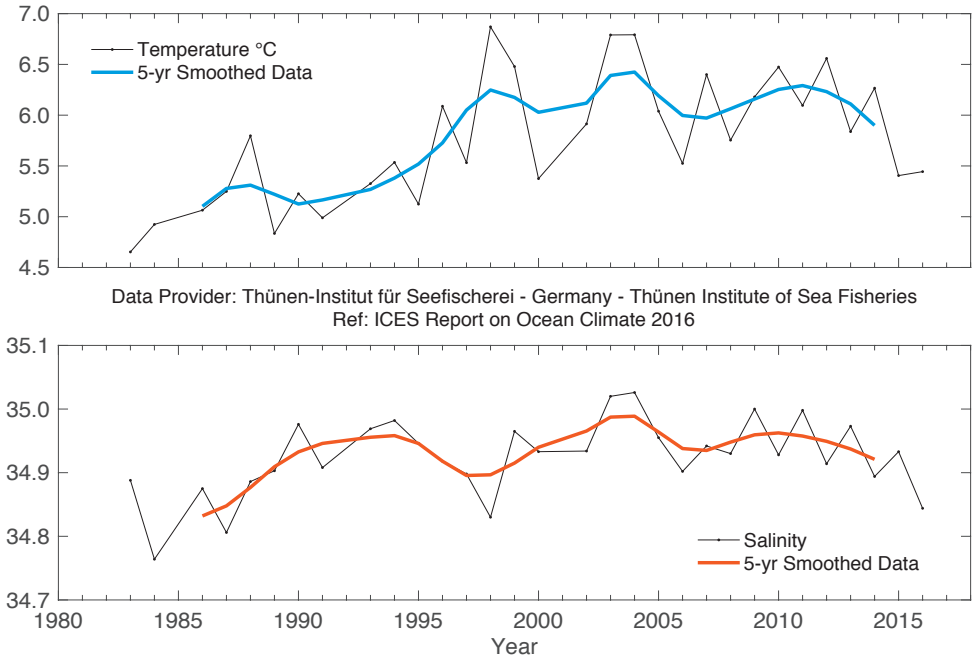

FIGURE 18.
West Greenland. Temperature (upper panel) and salinity (lower panel) in 75–200 m water layer at Cape Desolation Station 3 (60.47°N 50°W).

4.3 LABRADOR SEA

The Labrador Sea is located between Greenland and the Labrador coast of eastern Canada. It is an ocean basin that lies offshore from the West Greenland and Newfoundland–Labrador Shelf ecoregions. Cold, low-salinity waters of polar origin circle the Labrador Sea in an anticlockwise current system that includes both the north-flowing WGC on the eastern side and the south-flowing Labrador Current on the western side. Warm and saline Atlantic waters originating in the subtropics flow north into the Labrador Sea on the Greenland side and become colder and fresher as they circulate.

Changes in Labrador Sea hydrographic conditions on interannual time-scales depend on the variable influences of heat loss to the atmosphere, heat and salt gain from Atlantic waters, and freshwater gain from Arctic outflow, melting sea ice, precipitation, and run-off. In the Labrador Sea, surface heat losses in winter result in the formation of dense waters. This process makes the Labrador Sea the primary region in the Northern Hemisphere for the atmospheric ventilation of the Atlantic Ocean's intermediate depth waters. Through winter cooling of surface water and subsequent sinking to depths of 500–2500 m (depending on the severity of the winter), a denser water mass known as Labrador Sea water (LSW) is formed. This water spreads over the Atlantic Ocean, ventilating its deep layers and driving and feeding the global ocean's overturning circulation or ocean conveyor belt.

The Atlantic Zone Off-Shelf Monitoring Program (AZOMP) of Fisheries and Oceans Canada provides observations of variability in the ocean climate and plankton affecting regional climate and ecosystems of the North Atlantic and global climate system. The 27th annual survey of the AR7W Line in the Labrador Sea (presently the core part of AZOMP) took place on CCGS "Hudson" during the period of 30 April–24 May 2016.

A sequence of severe winters in the early 1990s led to deep convection that peaked in 1993–1994, filling the upper two kilometres of the water column with cold freshwater. Conditions have generally become milder since the mid-1990s. Between 1995 and 2011, the upper levels of the Labrador Sea became warmer and more saline as heat losses to the atmosphere decreased and Atlantic waters became increasingly dominant. However, over the past six years, the upper and intermediate layers have exhibited a cooling and freshening trend.

The surface heat loss experienced by the mid-high latitude North Atlantic in winter 2015/2016 was reduced in comparison to the previous (2014/2015) winter (Yashayaev and Loder, 2017). However, the strength and depth of winter convection and thereby production of newly-ventilated LSW were the largest since 1994. The key factor responsible for the further deepening of convection in winter 2015/2016, ultimately exceeding 2000 m, was preconditioning of vertical stratification by convective mixing of the previous winters. The recent period of intensified ventilation period and the resulting LSW year class (LSW 2012–2016) were probably the largest since 1938, outside the 1987–1994 period of progressive development of record-strong convection. A reservoir filled with this newly ventilated, cold and fairly fresh LSW is also rich in carbon dioxide and other dissolved gases, suggesting that the strong winter convection in 2015–2016 led to increased gas (dissolved oxygen, anthropogenic gases, and carbon dioxide) uptakes in the Labrador Sea that spread to, and even below 2000 m.

Further intensification of cooling, convective mixing, and intermediate water mass production in the Labrador Sea during winter 2015/2016.

Above-average regional cooling during winter in 2012–2016 has driven a progressive increase in the depth to which cooled waters sink, reaching 2100 m in 2016. As a result of this intermittent recurrence of intensified LSW formation, the annual average temperature and density in the region's upper 2000 m have predominantly varied on a bi-decadal time scale, rather than having a long-term trend, as might be expected from anthropogenic climate change.

SST anomalies in the Labrador Sea (Figure 19) were near normal in winter, while positive anomalies were dominant in summer. The surface freshening that had reached its peak in the central Labrador Sea in 2012 was

reduced and reversed in the following years, resulting in the upper layer salinity being highest in 2016.

The intermediate waters at depths between 400 and 2000 m experienced significant cooling after 2011, continuing in 2012 and 2014–2016, while salinity has largely decreased since 2011 due to intensified deep mixing and increased export of freshwater from the upper layer. The progressively deepening convective mixing that reoccurred in the Labrador Sea during four of five recent winters (2011–2012, 2013–2014, 2014–2015, and 2015–2016) has reversed the general warming trend that was observed in the intermediate waters of the Labrador Sea during 1994–2011.

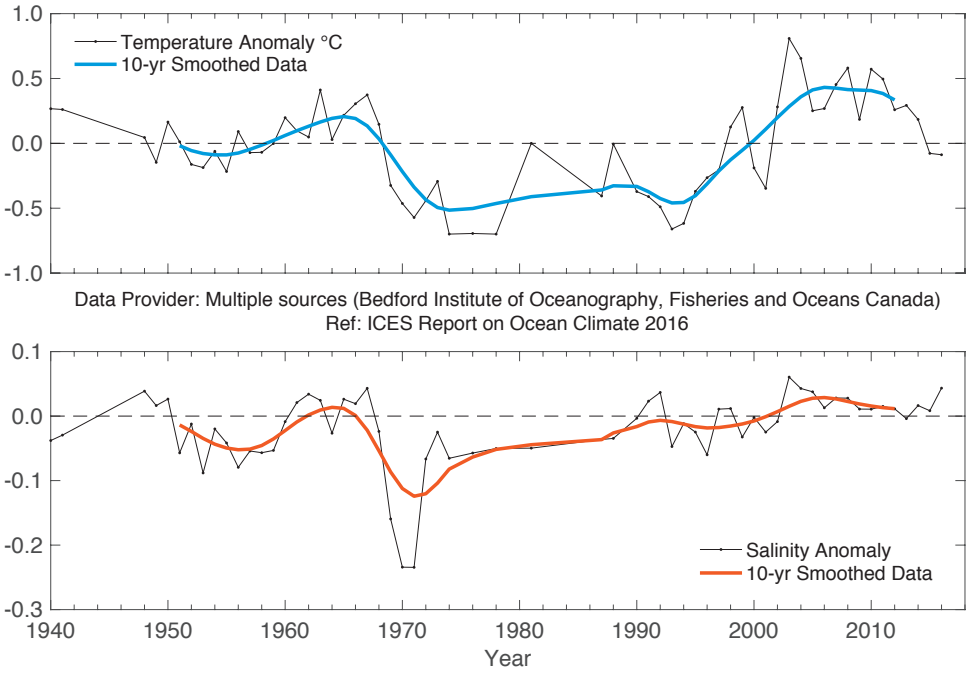

FIGURE 19.
Labrador Sea. Potential temperature (upper panel) and salinity (lower panel) anomalies at 50–200 m from CTD and Argo data in the west-central Labrador Sea (centred at 56.7°N 52.5°W). Estimates of seasonal cycle (derived from all data in the time-series) have been removed from the observations.

4.4 NEWFOUNDLAND-LABRADOR SHELF

The Newfoundland–Labrador shelf is identified as a LME. This ecoregion is situated on the western side of the Labrador Sea, stretching from the Hudson Strait in the north to the southern Grand Banks of Newfoundland. The Newfoundland–Labrador shelf is dominated by shallow banks, cross-shelf channels or saddles, and deep marginal troughs near the coast. Circulation is dominated by the south-flowing Labrador Current, which brings relatively cold freshwater from the north as well as sea ice and icebergs to southern areas of the Grand Banks.

Hydrographic conditions are determined in part by the strength of the winter atmospheric circulation over the Northwest Atlantic (NAO), advection by the Labrador Current, cross-shelf exchange with warmer continental slope water, and bottom topography. Superimposed are large seasonal and interannual variations in solar heat input, sea ice cover, and storm-forced mixing. The resulting water mass on the shelf exhibits large annual cycles, with strong horizontal and vertical temperature and salinity gradients.

The annual NAO index (December–February, Iceland–Azores), a key indicator of climate conditions in the Northwest Atlantic, decreased after the record-high in 2015, but remained in a positive phase at 0.5 s.d. above normal. As a result, Arctic air outflow to the Northwest Atlantic decreased in most areas compared to the previous year.

Annual air temperatures over Labrador at Cartwright increased from 1.5°C (1.2 s.d.) below normal in 2015 to 0.4°C (0.3 s.d.) below normal in 2016. Farther south at St. John's, air temperature anomalies were above normal by 0.6°C (0.7 s.d.). Sea ice extent on the Newfoundland–Labrador shelf was lighter than normal (0.3 s.d.) in 2016. As a result of these and other fac-

Ocean temperatures off Newfoundland and Labrador have returned to near normal or slightly above normal after the cold conditions experienced in 2015.

tors, local water temperatures on the shelf in 2016 increased over the previous year.

At the standard monitoring site off eastern Newfoundland (Station 27), the depth-averaged annual water temperature has experienced a decreasing trend during the past several years from the record-high in 2011, when it was +1.1°C (2.8 s.d.) above normal. In 2016, the water-column-averaged temperature at Station 27 was above normal by 0.3°C (0.7 s.d.), whereas salinity was below normal by 0.5 s.d.

A robust index of ocean climate conditions in eastern Canadian waters is the extent of the cold intermediate layer (CIL) comprised of < 0°C water overlying the continental shelf. This winter-cooled water remains isolated between the seasonally heated upper layer and the underlying warmer shelf-slope water throughout the summer and early autumn months. During the 1960s when the NAO was well below normal and had the lowest value ever in the 20th century, the volume of CIL water was at a minimum (warmer-than-normal conditions), and during the high NAO years of the early 1990s, the CIL volume reached near-record-high values (colder-than-normal conditions). Since the late 1990s, as ocean temperatures increased, the area of CIL water experienced a downward trend that lasted until 2011. Since then, however, the CIL area has trended upward and in 2015 reached its highest level since 1970 on the Grand Banks (2.2 s.d. above normal) during spring. In 2016, the CIL area was below normal off southern Labrador (0.8 s.d.) and near normal off eastern Newfoundland during the summer months.

RV "Sanna". Photo: John Mortensen, Greenland Institute of Natural Resources.

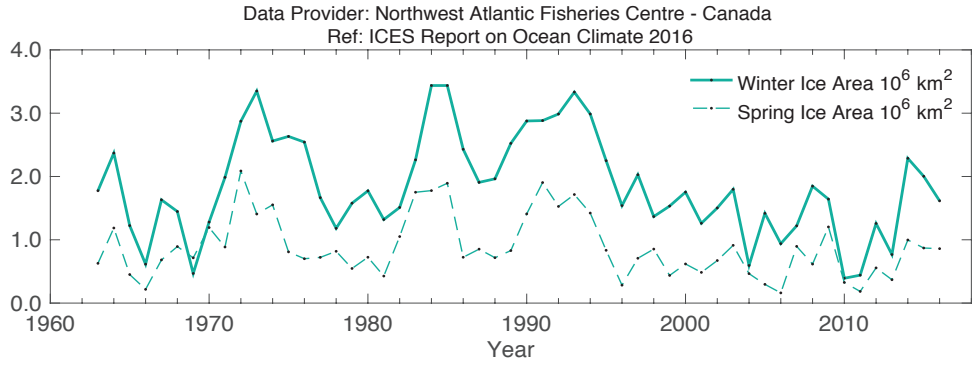

FIGURE 20.
Northwest Atlantic: Newfoundland–Labrador shelf. Winter and spring sea ice areas off Newfoundland–Labrador between 45°N and 55°N.

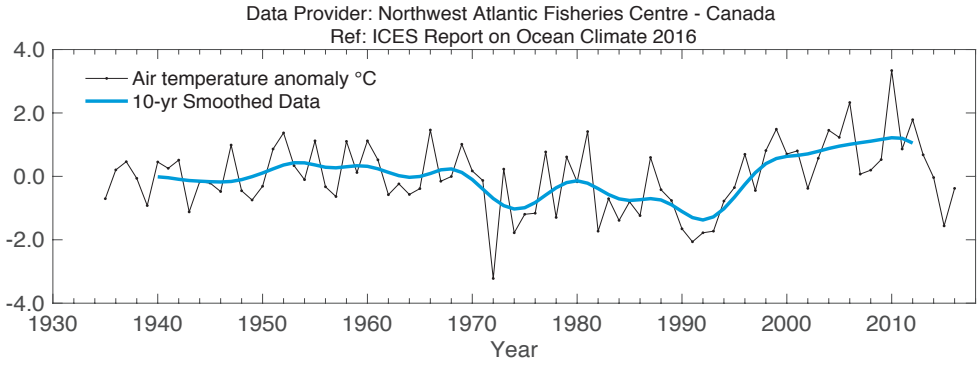

FIGURE 21.
Northwest Atlantic: Newfoundland–Labrador shelf. Annual air temperature anomalies at Cartwright on the Labrador coast.

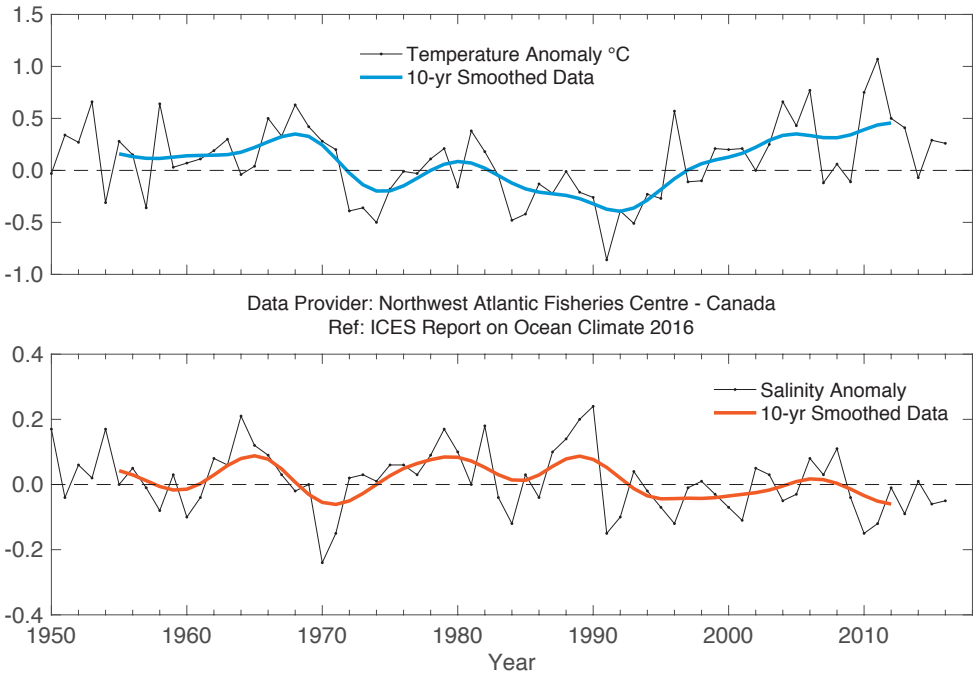

FIGURE 22.
Northwest Atlantic: Newfoundland–Labrador shelf. Annual depth-averaged Newfoundland shelf temperature (upper panel) and salinity (lower panel) anomalies at Station 27 (47.55°N 52.59°W).

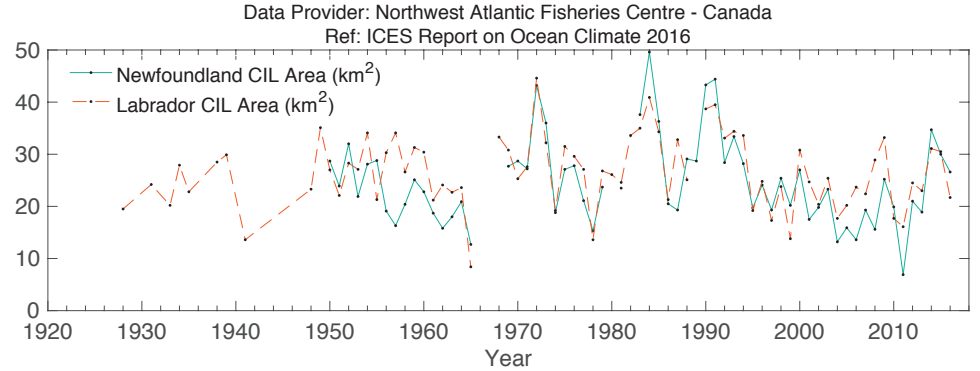

FIGURE 23.
Spatial extent of cold intermediate layer (CIL).

4.5 SCOTIAN SHELF

The Scotian shelf is the continental shelf off the coast of Nova Scotia and is identified as a LME. It is characterized by complex topography consisting of many offshore shallow banks and deep mid-shelf basins. It is separated from the Newfoundland shelf in the northeast by the Laurentian Channel and borders the Gulf of Maine to the southwest. Surface circulation is dominated by a general flow towards the southwest, interrupted by a clockwise movement around the banks and an anticlockwise movement around the basins, with the strengths varying seasonally.

Hydrographic conditions on the Scotian shelf are determined by heat transfer between the ocean and atmosphere, inflow from the Gulf of St Lawrence and the Newfoundland shelf, and exchange with offshore slope waters. Water properties have large seasonal cycles and are modified by freshwater run-off, precipitation, and melting of sea ice. Temperature and salinity exhibit strong horizontal and vertical gradients that are modified by diffusion, mixing, currents, and shelf topography.

In 2016, annual mean air temperature over the Scotian shelf, represented by Sable Island observations, was +1.2°C (+1.8 s.d.) above the long-term mean (1981–2010). The amount of sea ice on the Scotian shelf in 2016, as measured by the total area of ice seaward of Cabot Strait between Nova Scotia and Newfoundland from January to April, was 100 km^2, well below the long-term mean coverage of 32 000 km^2. This was similar to the 2010–2013 period, which had extremely low coverage after an above-average year in 2015.

Topography separates the northeastern Scotian shelf from the rest of the shelf. In the northeast, the bottom tends to be covered by relatively cold waters (1–4°C), whereas the basins in the central and southwestern regions typically have bottom temperatures of 8–10°C. The origin of the latter is the offshore slope waters, whereas in the northeast, the water comes principally from the Gulf of St Lawrence. The interannual variability of the two water masses differs.

Measurements of temperatures at 100 m at the Misaine Bank station capture the changes in the northeast. They revealed well above-average conditions in 2016, with temperature and salinity above normal, +1.2°C (+1.9 s.d.) and +0.16 (+1.2 s.d.), respectively. The deep Emerald Basin anomalies represent the slope water intrusions onto the shelf that are subsequently trapped in the inner basins. In 2016, the 250 m temperature and salinity anomalies were well above normal, +1.6°C (+1.9 s.d.) and +0.31 (+2.0 s.d.), respectively, but not as large as in 2014. Model simulations of the region showed a large flux of warm salty water from the slope region.

Warm water continued on the Scotian Shelf and sea ice levels were above normal.

Deployment of current meter in Arnarfjordur in Iceland.
Photo: Hedinn Valdimarsson, Marine Research Institute, Iceland.

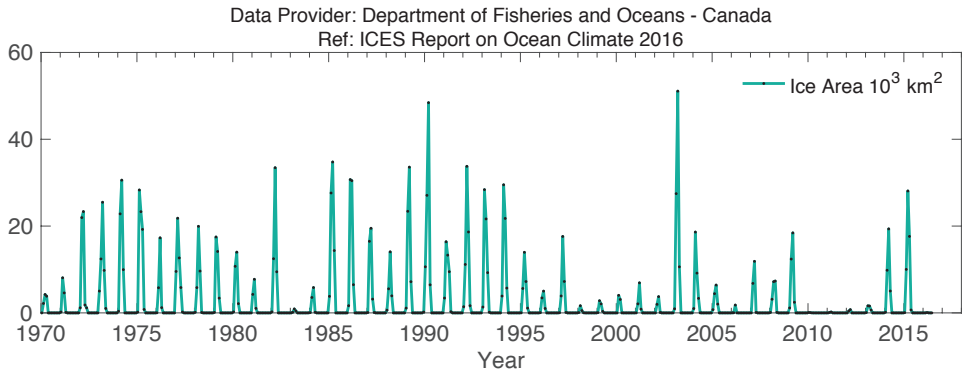

FIGURE 24.
Northwest Atlantic: Scotian shelf. Monthly means of ice area seaward of Cabot Strait.

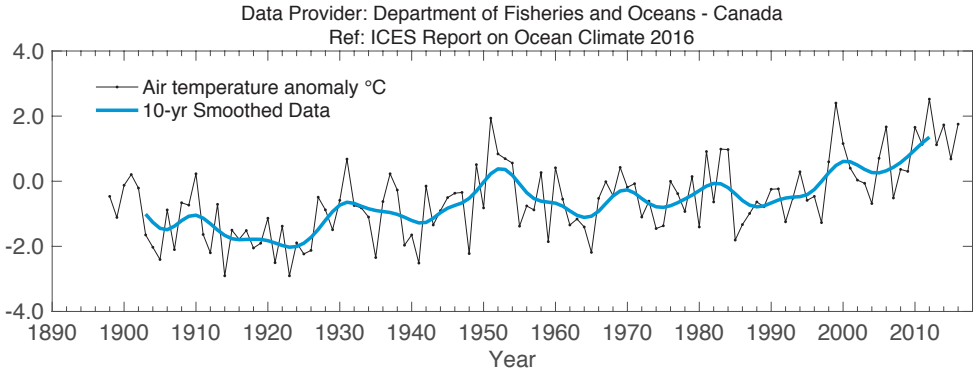

FIGURE 25.
Air temperature anomalies at Sable Island on the Scotian shelf.

Glass sampler for organic contaminants. Photo: Holger Klein, Bundesamt für Seeschifffahrt und Hydrographie, Germany.

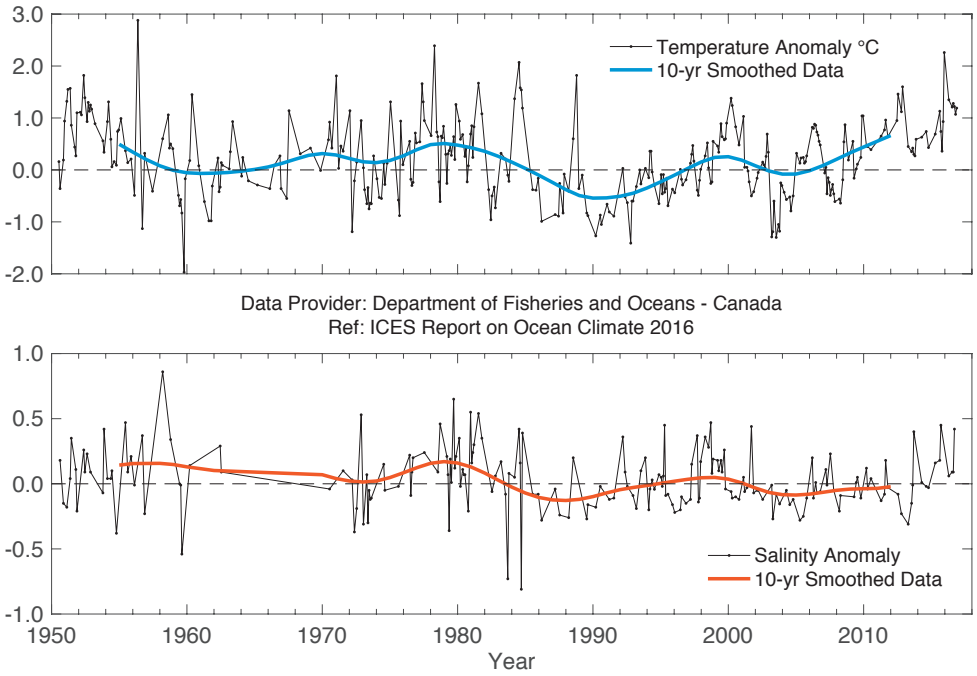

FIGURE 26.
Near-bottom temperature (upper panel) and salinity (lower panel) anomalies at Misaine Bank (100 m).

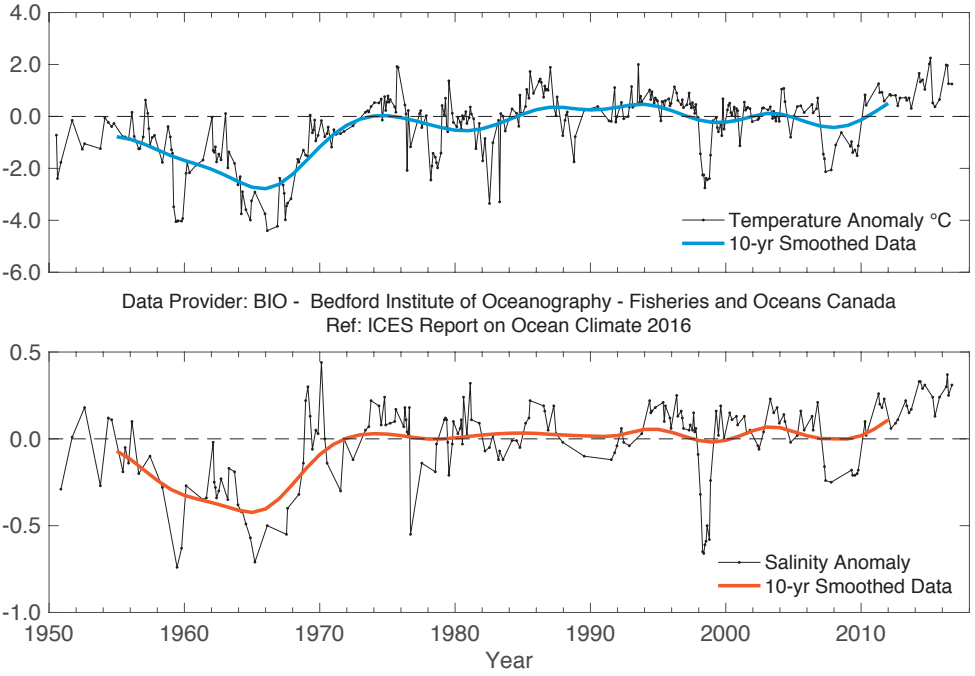

FIGURE 27.
Near-bottom temperature (upper panel) and salinity (lower panel) anomalies in the central Scotian shelf (Emerald Basin, 250 m).

4.6 NORTHEAST US CONTINENTAL SHELF

The Northeast US continental shelf extends from the southern tip of Nova Scotia, Canada, southwestward through the Gulf of Maine and the Mid-Atlantic Bight to Cape Hatteras, North Carolina (Figure 28). Contrasting water masses from the Subtropical and Subpolar gyres influence the hydrography in this region. Located at the downstream end of an extensive interconnected coastal boundary current system, the Northeast US continental shelf is the direct recipient of cold/fresh Arctic-origin water, accumulated coastal discharge, and ice melt that has been advected thousands of kilometres around the boundary of the subpolar North Atlantic. Likewise, subtropical water masses, advected by the Gulf Stream, slope currents, and associated eddies, also influence the composition of water masses within this shelf region. The western boundary currents of the Subpolar and Subtropical gyres respond to variations in basin-scale forcing through changes in position, volume transport, and/or water mass composition, and it is partly through these changes that basin-scale climate variability is communicated to the local Northeast US continental shelf. Shelf-wide hydrographic conditions have been monitored annually in this region since 1977 as part of quarterly ecosystem monitoring and twice-yearly bottom-trawl surveys conducted by the NOAA National Marine Fisheries Service, Northeast Fisheries Science Center.

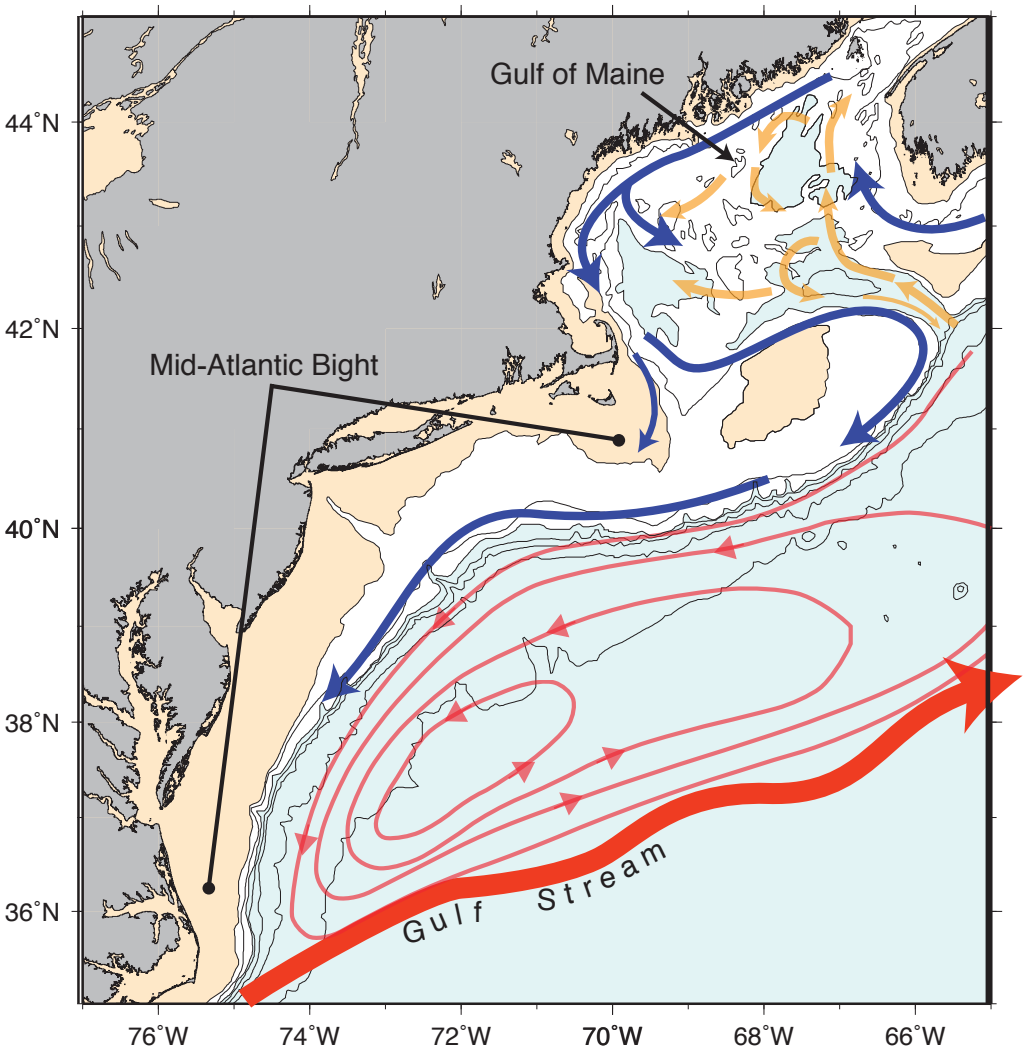

FIGURE 28.
Circulation schematic for the Northeast US shelf region, where blue arrows represent shelf water circulation and orange arrows represent deeper slope water circulation pathways. Water depths deeper than 200 m are shaded blue. Water depths shallower than 50 m are shaded tan.

Observations indicate that the entire Northeast US shelf was significantly warmer in 2016 than the mean for the period 1981–2010. Annually, 0–30 m temperatures were 1–1.5°C warmer than normal everywhere (Figures 30–34), with the largest anomalies observed in the southern Mid-Atlantic Bight (Figure 30) and eastern Gulf of Maine (Figure 33). Seasonal warming exceeded 1 s.d. from spring through early autumn in the Gulf of Maine and on Georges Bank (Figure 33), but was significantly enhanced during autumn in the Mid-Atlantic Bight. Warming extended to the bottom across the entire shelf, with near-bottom annual temperature anomalies exceeding upper-layer anomalies by up to 0.4°C in the Mid-Atlantic Bight (not shown). Upper-level (0–30 m) waters were more saline across the entire Northeast US continental shelf in 2016, averaging 0.2–0.5 units more saline than normal. The largest annual anomalies were observed in the Mid-Atlantic Bight (Figures 30 and 31). Seasonally, the largest positive anomalies were observed during autumn, where salinities were close to 2 s.d. higher than normal on Georges Bank and in the northern Mid-Atlantic Bight (e.g. Figure 35). Saline conditions during autumn coincide with extremes in temperature as well, particularly along the shelf edge in the northern Mid-Atlantic Bight. The extreme conditions reflect the presence of a large Gulf Stream warm core ring and resulting intrusion of Gulf Stream water onto the shelf.

Temperature and salinity anomalies derived from hydrographic observations collected within the deep layer (150–200 m) in the Northeast Channel indicate that deep inflow to the Gulf of Maine remained warmer and saltier in 2016 compared with the long-term mean (Figure 36). These deep waters are not influenced by seasonal atmospheric forcing and represent deep inflow conditions for one of the dominant water mass sources to the Gulf of Maine, the slope waters (Mountain, 2012).

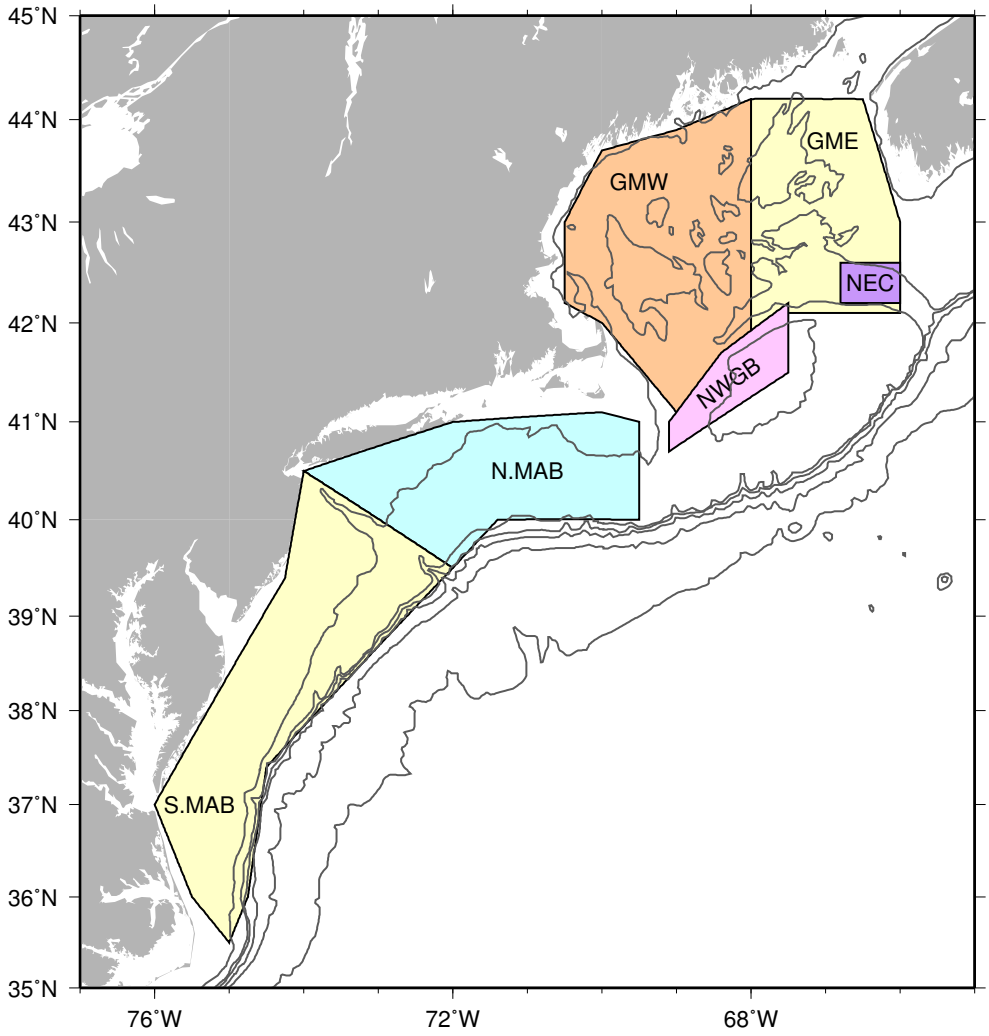

FIGURE 29.
Northeast US continental shelf. The six regions within which CTD observations are used to compute regional average time-series: eastern and western Gulf of Maine (GME and GMW); northern and southern Mid-Atlantic Bight (N.MAB and S.MAB); Northeast Channel (NEC); and Northwest Georges Bank (NWGB). The 50, 200, 500, 1000, 2000, and 3000 m isobaths are also shown.

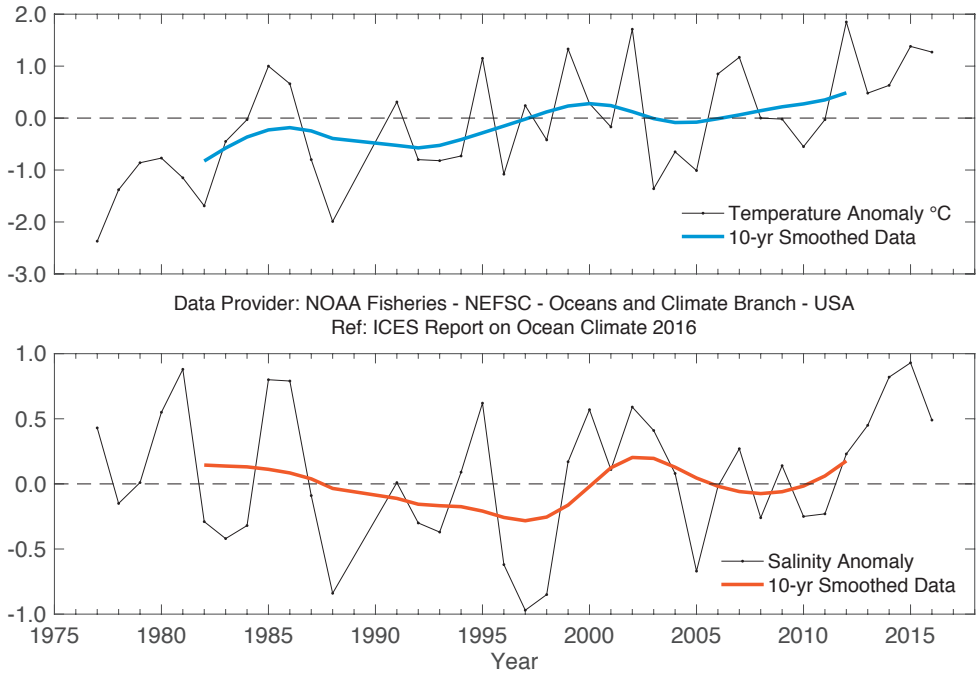

FIGURE 30.
Time-series plots of 0–30 m averaged temperature anomaly (upper panel) and salinity anomaly (lower panel) in the region between Cape Hatteras, North Carolina, and Hudson Canyon. Anomalies are calculated relative to the period 1981–2010 using hydrographic data from shelf-wide surveys.

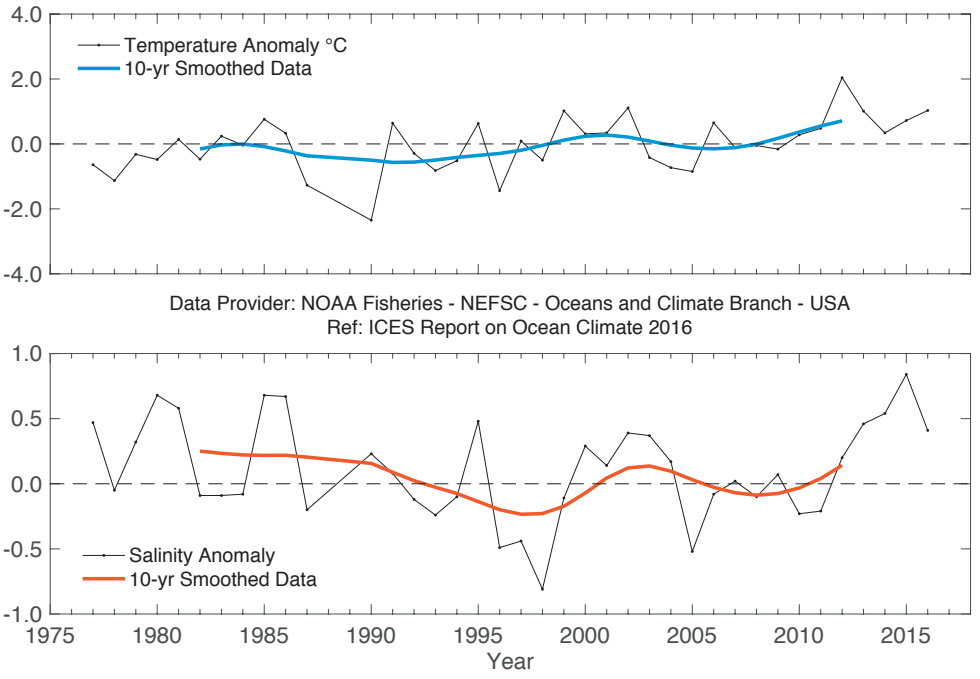

FIGURE 31.
Time-series plots of 0–30 m averaged temperature anomaly (upper panel) and salinity anomaly (lower panel) in the region between Hudson Canyon and Cape Cod, Massachusetts. Anomalies are calculated relative to the period 1981–2010, using hydrographic data from shelf-wide surveys.

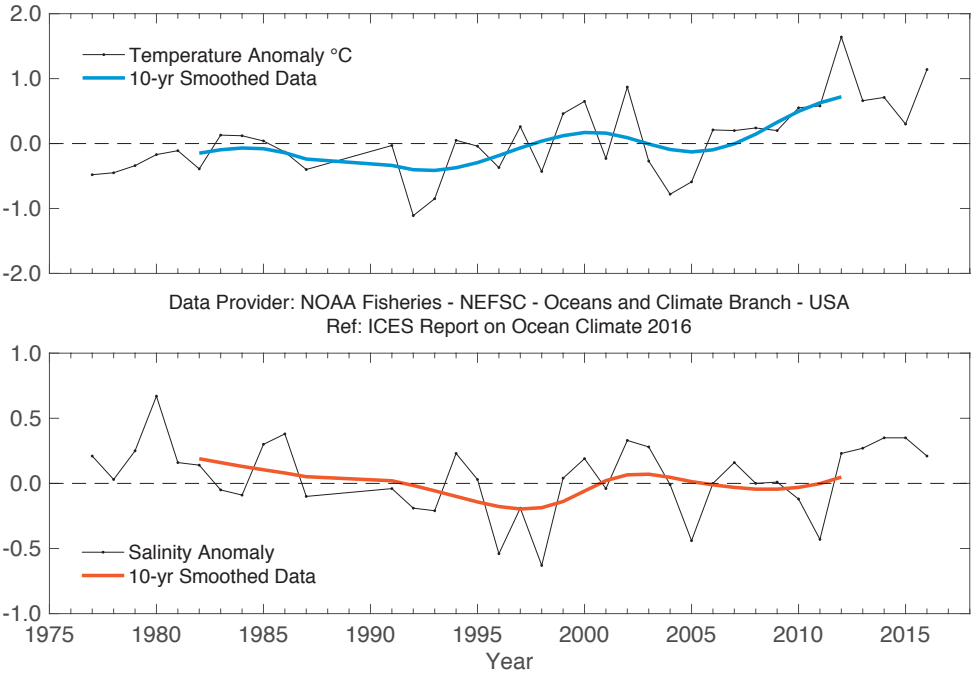

FIGURE 32.
Time-series plots of 0–30 m averaged temperature anomaly (upper panel) and salinity anomaly (lower panel) in the western Gulf of Maine. Anomalies are calculated relative to the period 1981–2010, using hydrographic data from shelf-wide surveys.

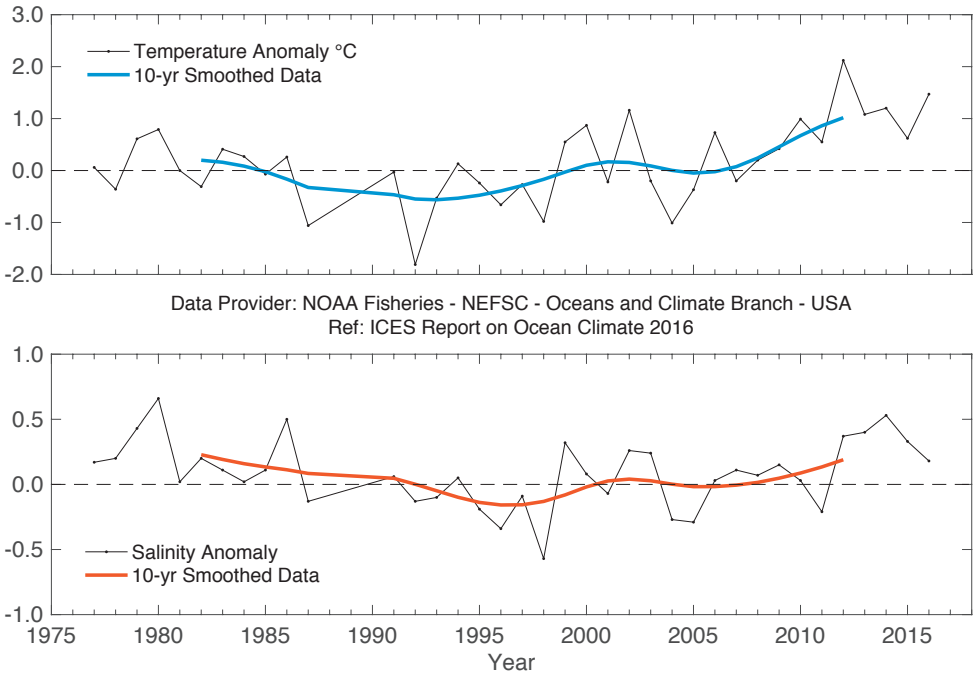

FIGURE 33.
Time-series plots of 0–30 m averaged temperature anomaly (upper panel) and salinity anomaly (lower panel) in the eastern Gulf of Maine. Anomalies are calculated relative to the period 1981–2010, using hydrographic data from shelf-wide surveys.

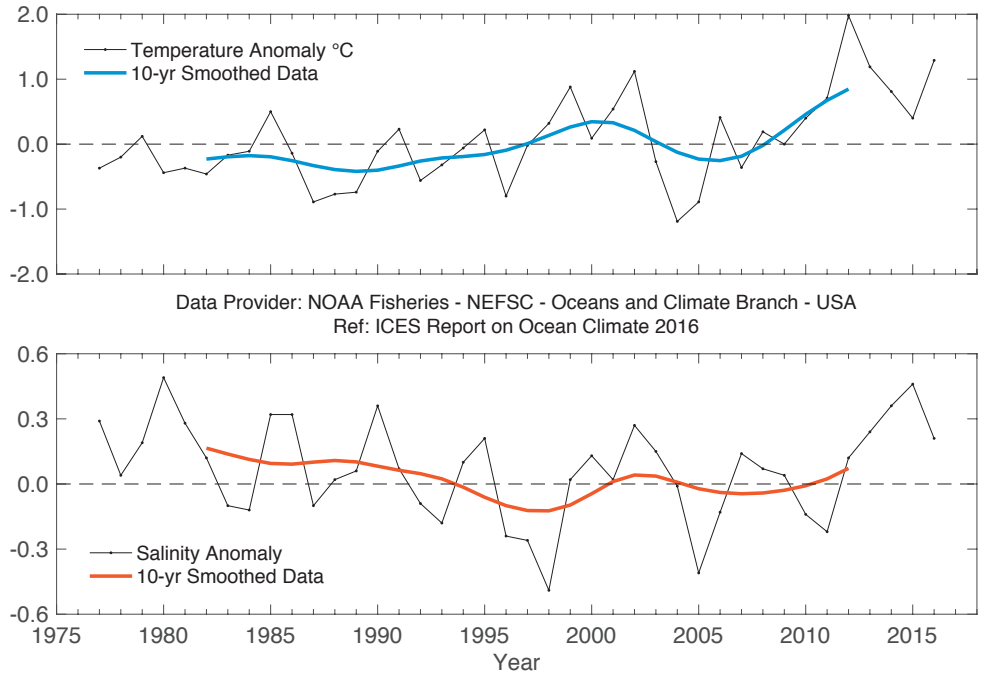

FIGURE 34.
Time-series plots of 0–30 m averaged temperature anomaly (upper panel) and salinity anomaly (lower panel) on Georges Bank. Anomalies are calculated relative to the period 1981–2010, using hydrographic data from shelf-wide surveys.

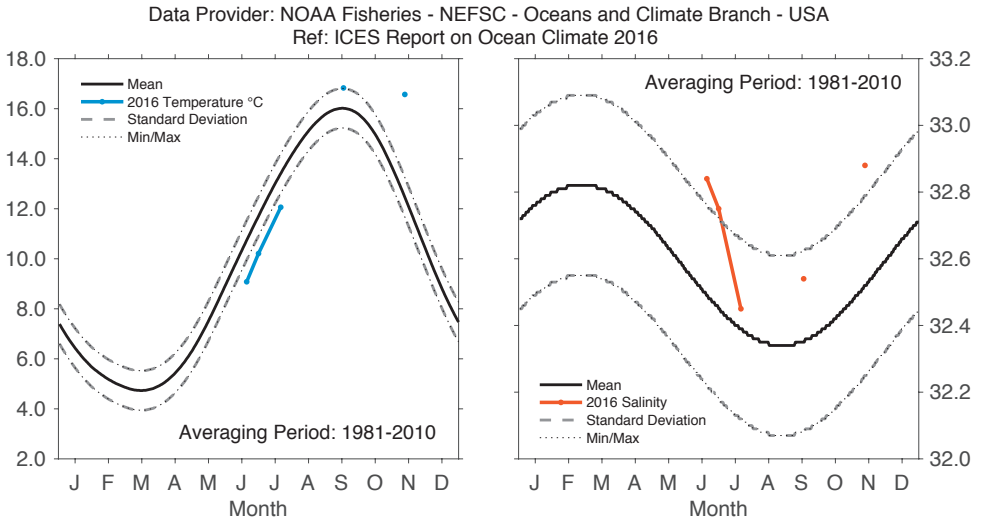

FIGURE 35.
2016 temperature (left) and salinity (right) averaged over 0–30 m at northwest Georges Bank, relative to the annual cycle calculated relative to the period 1981–2010. The envelope corresponding to the monthly range and 1 s.d. are shown.

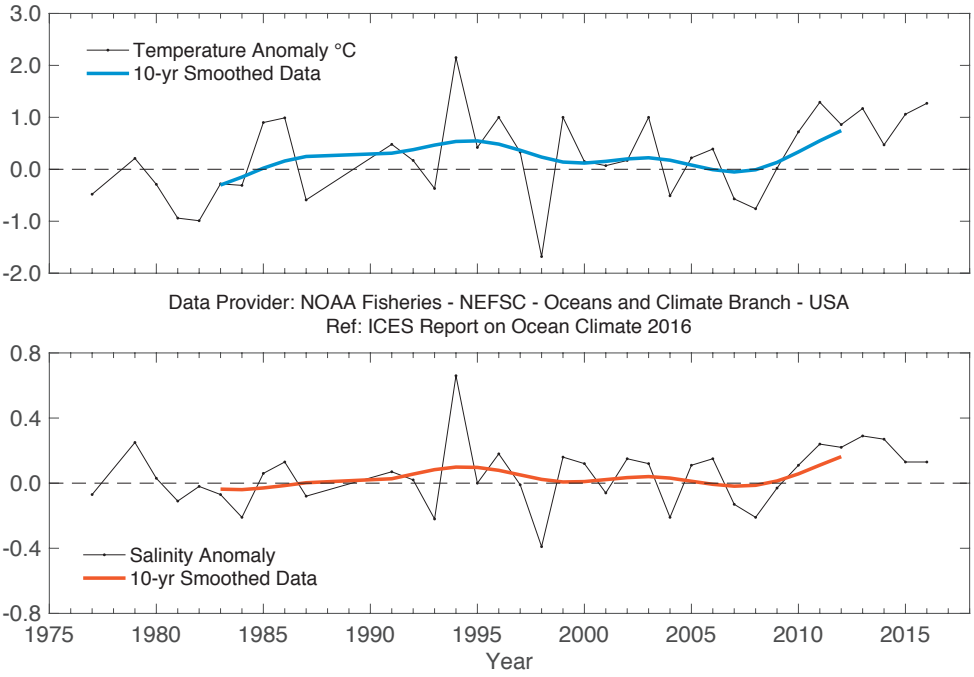

FIGURE 36.
Time-series plots of 150–200 m averaged temperature anomaly (upper panel) and salinity anomaly (lower panel) in the Northeast Channel. Anomalies are calculated relative to the period 1981–2010, using hydrographic data from shelf-wide surveys.

4.7 ICELANDIC WATERS

The Iceland Shelf and Sea are identified as an LME and an ICES ecoregion. Iceland is at the meeting place of warm and cold currents, which converge in an area of submarine ridges (Greenland–Scotland Ridge, Reykjanes Ridge, Kolbeinsey Ridge) that form natural barriers to the main ocean currents (Figure 37). The warm Irminger Current (6–8°C), a branch of the North Atlantic Current (NAC), flows from the south, and the cold East Greenland and East Icelandic currents (–1°C to 2°C) flow from the north. Deep and bottom currents in the seas around Iceland are principally the overflow of cold water from the Nordic seas and the Arctic Ocean over the submarine ridges into the North Atlantic.

Hydrographic conditions in Icelandic waters are generally closely related to atmospheric or climatic conditions in and over the country and the surrounding seas, mainly through the Icelandic low-pressure and Greenland high-pressure systems. These conditions in the atmosphere and the surrounding seas affect biological conditions, expressed through the food chain in the waters, including recruitment and abundance of commercially important fish stocks.

Annual mean air temperatures for south (Reykjavik) and north (Akureyri) were among the highest observed. Temperature and especially salinity in the AW from the south was lower in 2016 than it has been since before 2000. Salinity and temperature north and east of Iceland were both above average; well above average in the latter half of the year and well above the long-term average.

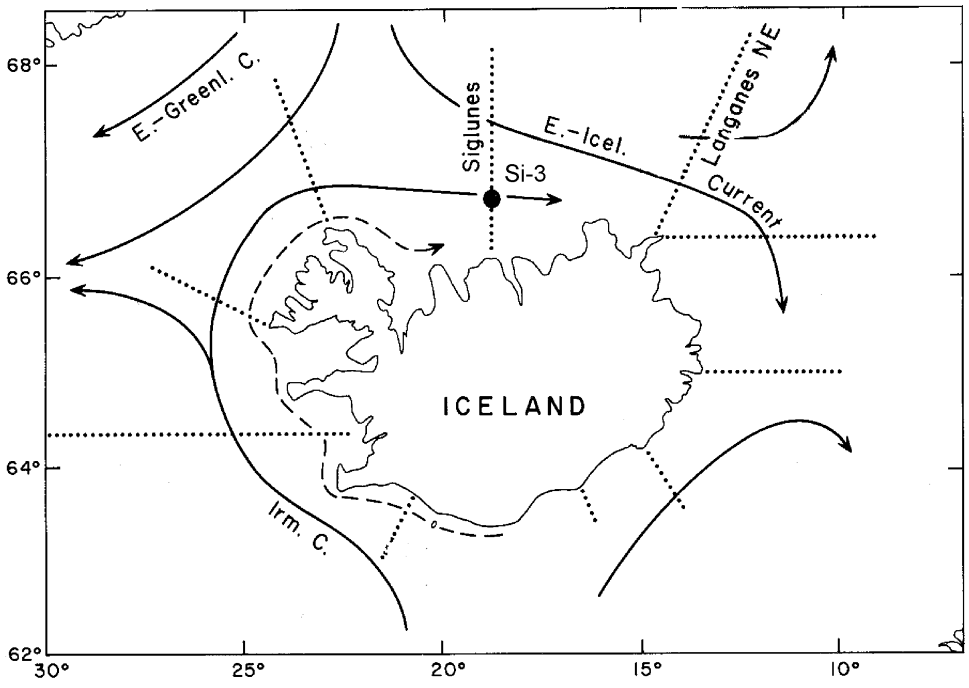

FIGURE 37.
Main currents and location of standard sections in Icelandic waters.

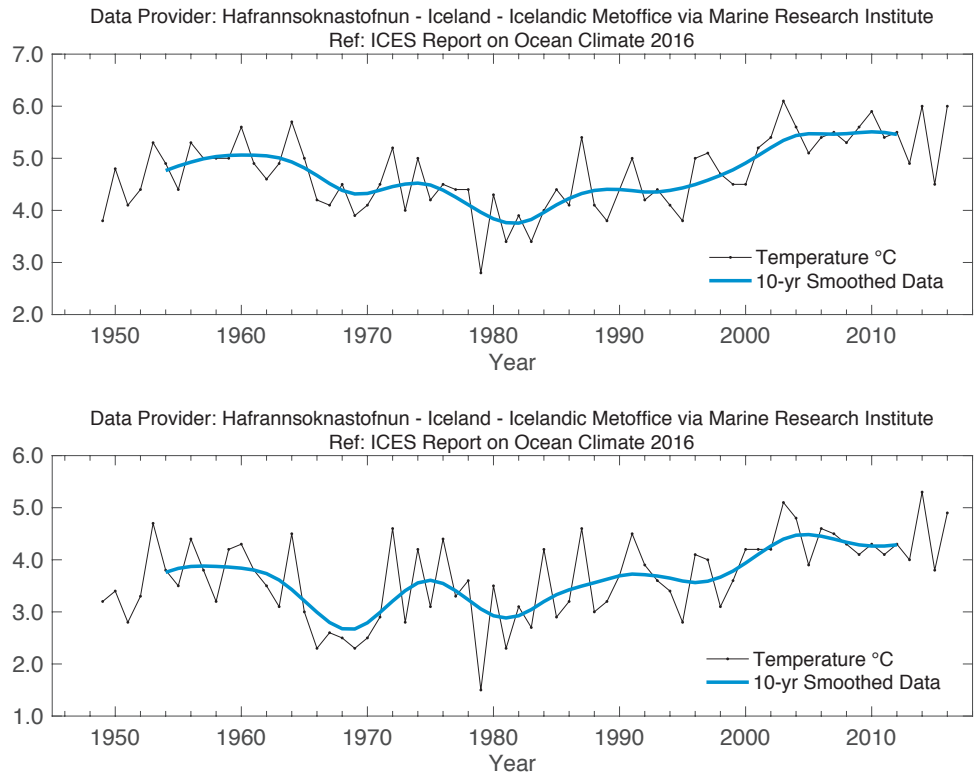

FIGURE 38.
Icelandic waters. Mean annual air temperature at Reykjavik (upper panel) and Akureyri (lower panel).

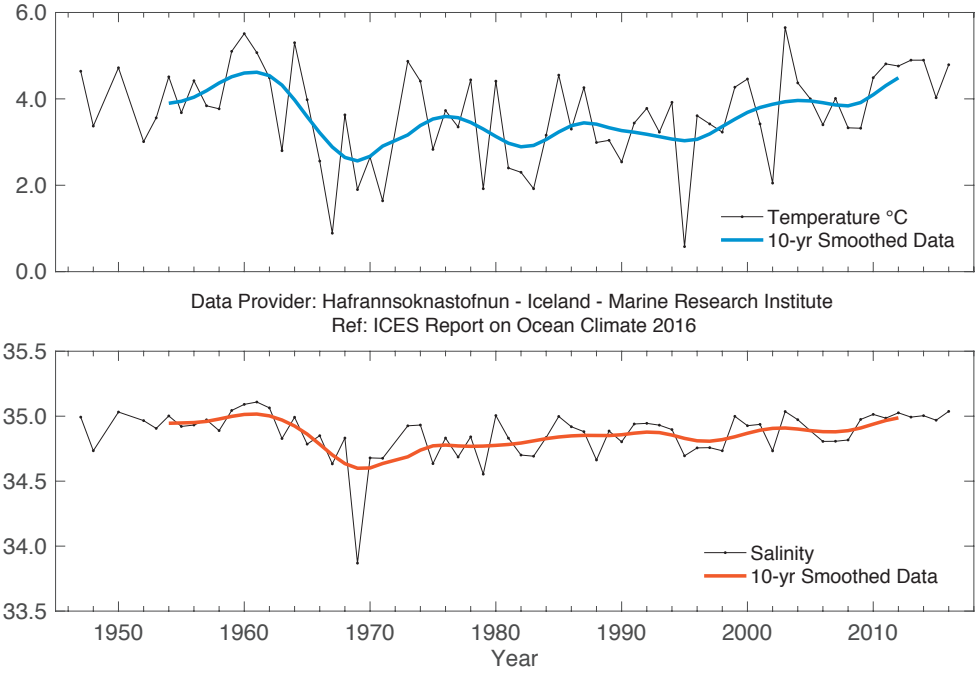

FIGURE 39.
Icelandic waters. Temperature (upper panel) and salinity (lower panel) at 50–150 m at Siglunes Stations 2–4 in North Icelandic waters.

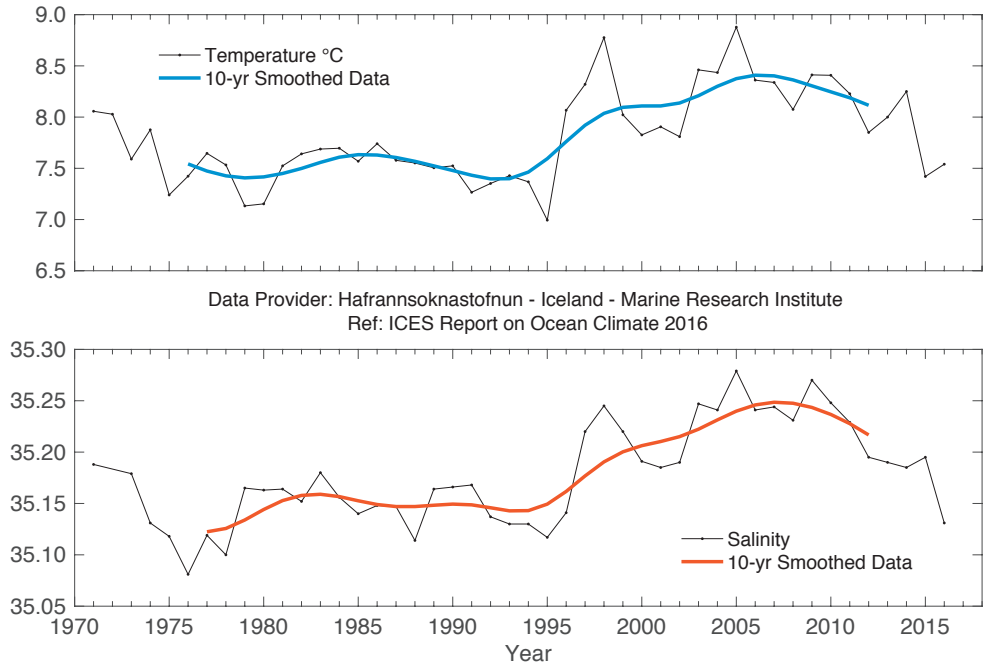

FIGURE 40.
Icelandic waters. Temperature (upper panel) and salinity (lower panel) at 0–200 m at Selvogsbanki Station 5 in southern Icelandic waters.

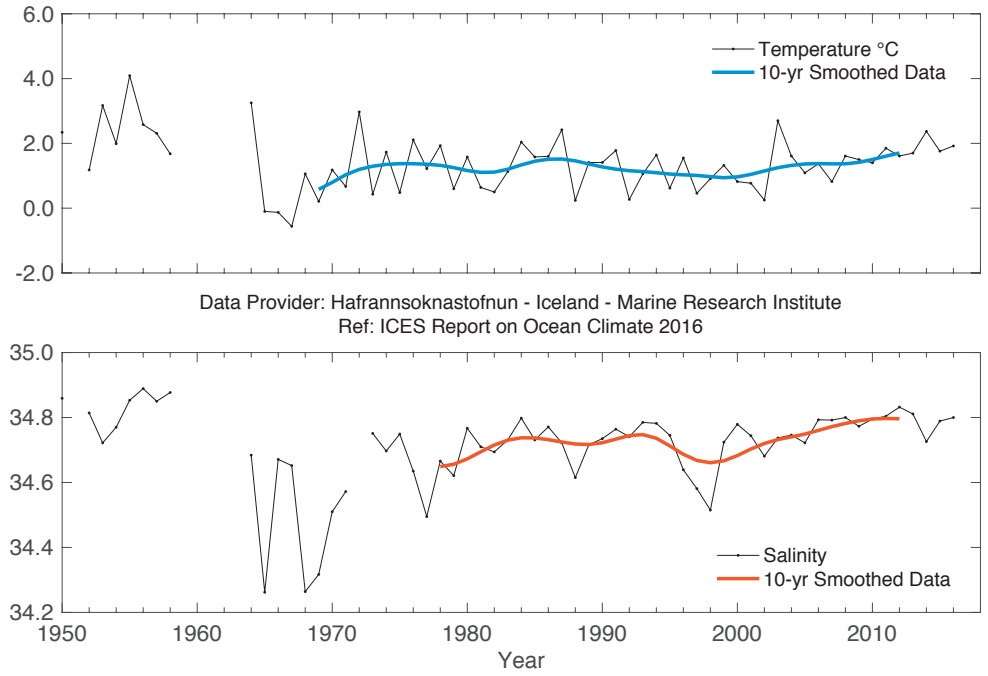

FIGURE 41.
Icelandic waters. Temperature (upper panel) and salinity (lower panel) at 0–50 m in the East Icelandic Current (Langanes Stations 2–6).

4.8 BAY OF BISCAY AND IBERIAN COAST

The Bay of Biscay and the Iberian coast are defined as one ICES ecoregion, while under NOAAs LME programme, the Bay of Biscay is grouped with the Celtic seas and the Iberian coast is identified as a separate region. The ICES ecoregion used here is located in the eastern North Atlantic at the northeastern edge of the subtropical anticyclonic gyre or within the intergyre area. It could be considered an adjacent sea with weak anticyclonic circulation. Shelf and slope currents are important in the system, characterized by coastal upwelling events in spring and summer and the dominance of a geostrophic balanced poleward flow (known as the Iberian Poleward Current) in autumn and winter.

From the atmospheric point of view, 2016 can be considered warm with respect to the long-term mean in the Iberian Peninsula and southern Bay of Biscay. Overall, average temperature exceeded 0.5°C with respect to the reference period (1981–2010), but was slightly colder than in 2015. The seasonal cycle of the air temperature was characterized by the prevalence of normal-to-warm conditions all year except for March and November, which were cold. In terms of precipitation, 2016 can be considered wet, particularly in northwest Spain during the first half of the year. Precipitation was average in southeastern Biscay.

SST remained warm in comparison to the long-term record, with a positive anomaly slightly above 0.4°C at the coastal long-term series of San Sebastian (Figure 43). Towards the west, upwelling pulses lowered SST to below average in August–September. Low salinity conditions that started in 2013 continued, contrasting with the high salinity period peaking in 2011–2012. The entry of the Iberian Poleward Current was evident around January after two years of very weak signature. The subsurface waters were fresh in 2016, though slightly saltier than in 2015. This is the third consecutive year that fresh conditions were observed. Temperature recovered from 2015, measuring slighter warmer than average in 2016. This is consistent with local atmospheric conditions (warm and locally dry, but wet towards the northwest) enhanced by upwelling and likely by advective influences from northern regions. For the upper ocean influenced by the mixed-layer development (0–300 dbar), the result is a rather average year, warmer and slightly saltier than 2015.

The upper ocean remained relatively warm. The freshening initiated around 2013 ceased, with 2016 being slightly saltier than 2015.

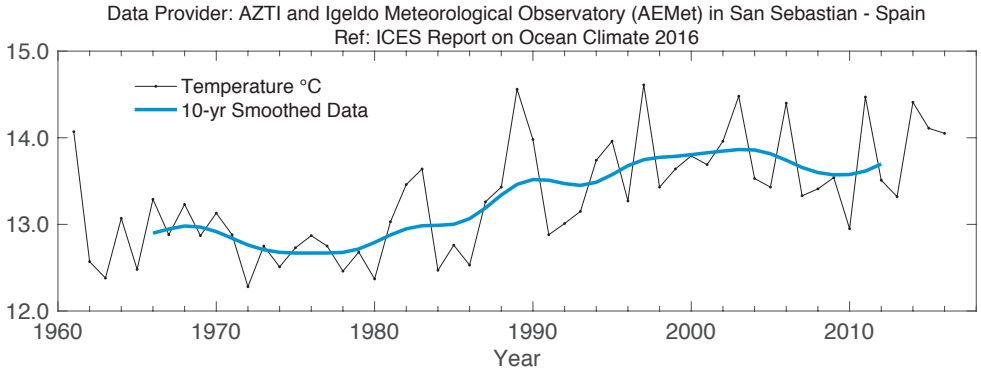

FIGURE 42.
Bay of Biscay and eastern North Atlantic. Air temperature at San Sebastian (43°18.50'N 2°2.37'W).

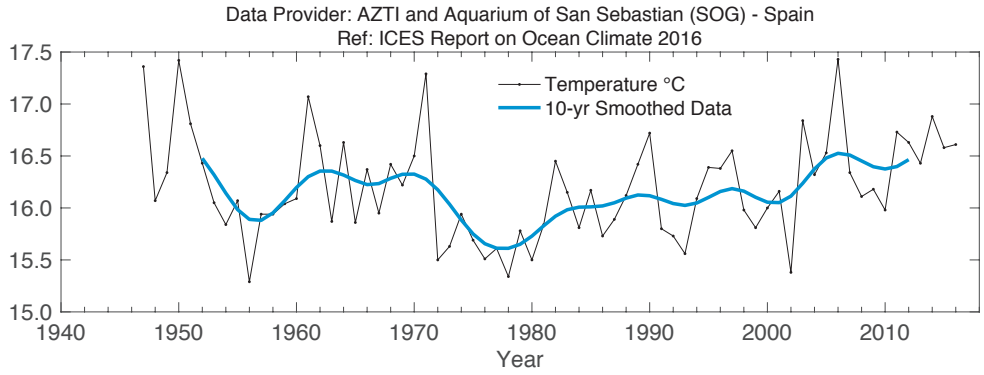

FIGURE 43.
Bay of Biscay and eastern North Atlantic. Sea surface temperature (SST) at San Sebastian (43°18.50'N 2°2.37'W).

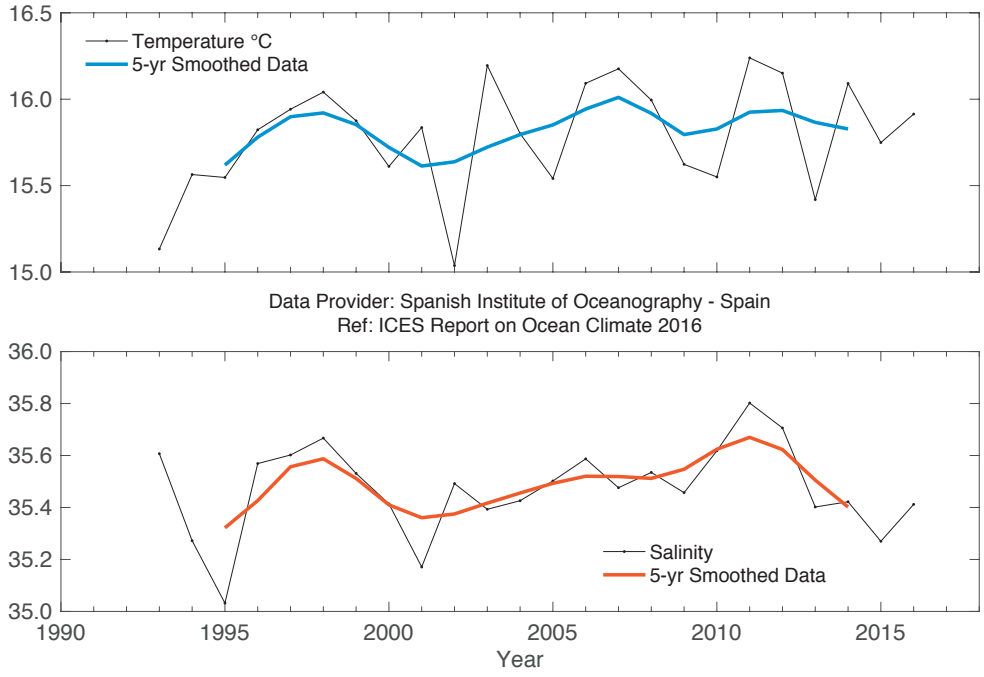

FIGURE 44.
Bay of Biscay and eastern North Atlantic. Potential temperature (upper panel) and salinity (lower panel) at Santander Station 6, 5–300 m (43°42.50'N 3°47.00'W).

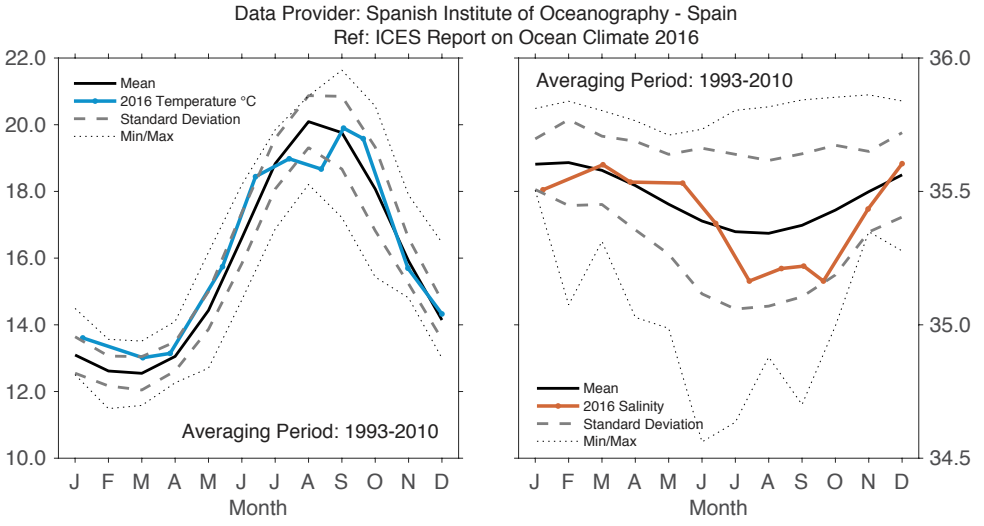

FIGURE 45.
Bay of Biscay and eastern North Atlantic. 2016 monthly temperature (left panel) and salinity (right panel) at Santander Station 6, 10 m (43°42.50'N 3°47.00'W).

4.9 GULF OF CADIZ

The Gulf of Cadiz is located southwest of the Iberian Peninsula, where the Atlantic Ocean and the Mediterranean Sea connect through the Strait of Gibraltar. Here, the water exchange is governed by a two-layered inverse estuarine circulation: Mediterranean water (MW) flows into the Gulf of Cadiz beneath the Atlantic water (AW) that flows into the Mediterranean Sea.

The traditional view of the surface circulation in the Gulf of Cadiz presents a clockwise flow on the slope as part of a larger-scale anticyclonic gyre and a countercurrent on the inner shelf. The clockwise flow conveys both eastern North Atlantic central waters (ENACW) from the Portuguese coastal transition zone (CTZ) and the Azores Current towards the Mediterranean Sea. The inshore countercurrent transports waters westward most of the year. A number of mechanisms have been proposed as responsible for this pattern.

Seasonal displacements of the Azores High have been related to its convergence with the Azores Current and the local upwelling-favourable winds. Besides local wind forcing, alongshore pressure gradients generated by the spatially heterogeneous wind field and the buoyancy flux associated with continental run-off seem to be the trigger for the onset of the inshore coastal countercurrent.

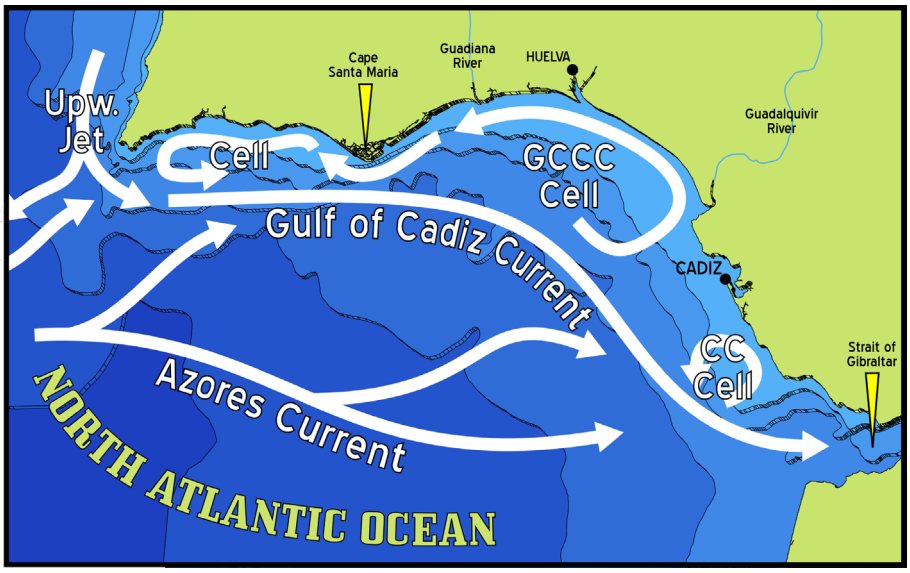

FIGURE 46.
Upper ocean circulation schematic for the Gulf of Cadiz. GCCC stands for the Gulf of Cadiz Countercurrent which, together with the Gulf of Cadiz Current, shapes a number of cyclonic cells on the inner shelf. CC Cell stands for the tidally-steered cyclonic patch off Trafalgar.

In the Gulf of Cadiz, air temperatures and SSTs continue to display the increasing trend observed since the beginning of 2000 (0.20 ± 0.03°C per decade for air and 0.16 ± 0.02°C per decade for SSTs). Accordingly, 2016 was warm with respect to the 1997–2017 mean. Overall, average air temperature exceeded 0.5°C with respect to the reference period, being slightly colder than the former warm period observed during 2010–2011. SST was also warm compared to the recorded series. Positive temperature anomalies occurred steadily from 2013, reaching up to 0.4°C by the end of 2016. In spite of the strong surface warming, water column-averaged (0–600 m) temperatures at the central Gulf of Cadiz, retrieved from the STOCA monitoring programme (Series Temporales de datos Oceanográficos en el golfo de CAdiz), show a slightly decreasing trend from 2008, likely pushed by the contribution of the ENACW between 50 and 300 m. This is consistent with a slight freshening of the water column over the same depth span. Strong seasonality in hydrographic series became increasingly noticeable from 2013, coincident with a larger observational effort.

In spite of warming surface waters, the upper ocean exhibited steady cooling and freshening from 2008.

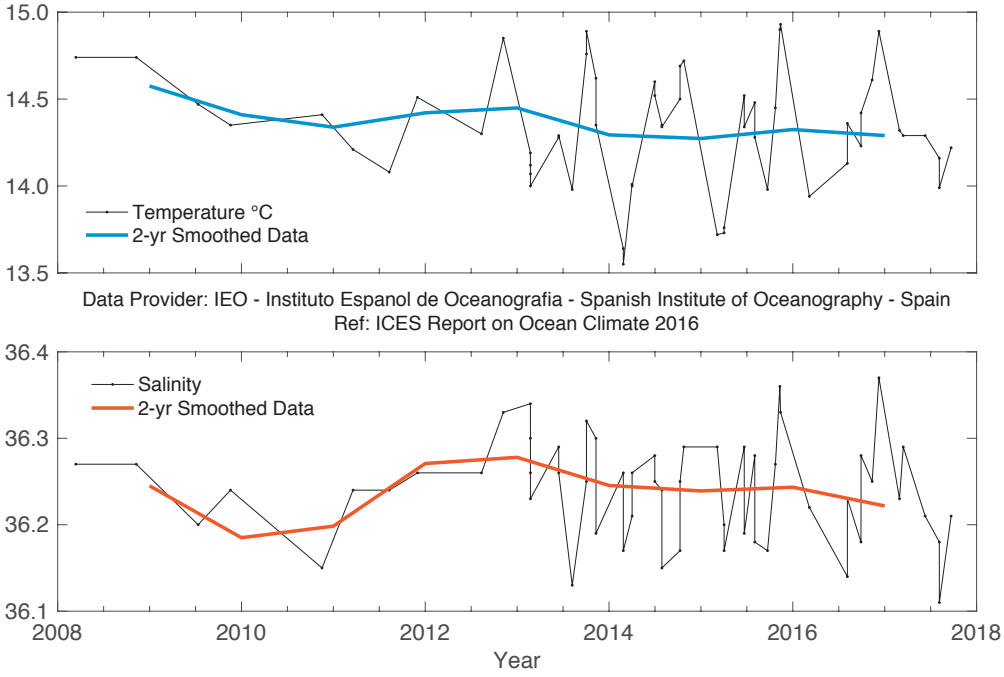

FIGURE 47.
Gulf of Cadiz. Potential temperature (upper panel) and salinity (lower panel) for the whole 600 m water column at Station SP6 (36.14°N 6.71°W) of the STOCA programme.

4.10 CANARY BASIN

The Canary Basin sits at the boundary between the oceanic waters of the Subtropical Atlantic Gyre and the upwelling waters from the Canary Current LME (CCLME) off the coast of Northwest Africa. Since the early 2000s, the Canary Islands archipelago region has been monitored by the Spanish Institute of Oceanography: the oceanic waters west of Lanzarote (Stations 11–23, Figure 48) and the CTZ of the upwelling region of the CCLME (Stations 1–10, Figure 48). At the upper levels, the area is under the influence of the southward flowing Canary Current and the Canary Upwelling Current associated with the upwelling front. At intermediate levels, it is influenced by the tongue of slowly propagating Mediterranean waters and the slope current known as the Canary Intermediate Poleward Current.

Waters above the seasonal thermocline, γ_n < 26.850 kg m^{-3}, are characterized by widely varying temperature and salinity due to seasonal heating and evaporation. These waters occupy the upper 300 m in the oceanic region and the upper 100 m in the stations under the influence of the coastal upwelling, which are considered the surface waters. Below the seasonal thermocline and through the permanent thermocline is the North Atlantic central water (NACW), roughly delimited by 26.850 < γ_n < 27.380 kg m^{-3}, between 300 and 700 m depth.

These waters are characterized on the θ/S diagram by an approximately straight-line relationship between potential temperature (11.4°C < θ < 14.9°C) and salinity (35.6 < S < 36.1). At intermediate levels between 27.380 < γ_n < 27.820 kg m^{-3}, two distinct water masses are observed in the Canary Islands region, the fresher (S < 35.3) and slightly lighter Antarctic intermediate waters (AAIW), and the saltier (S > 35.4) and heavier Mediterranean waters.

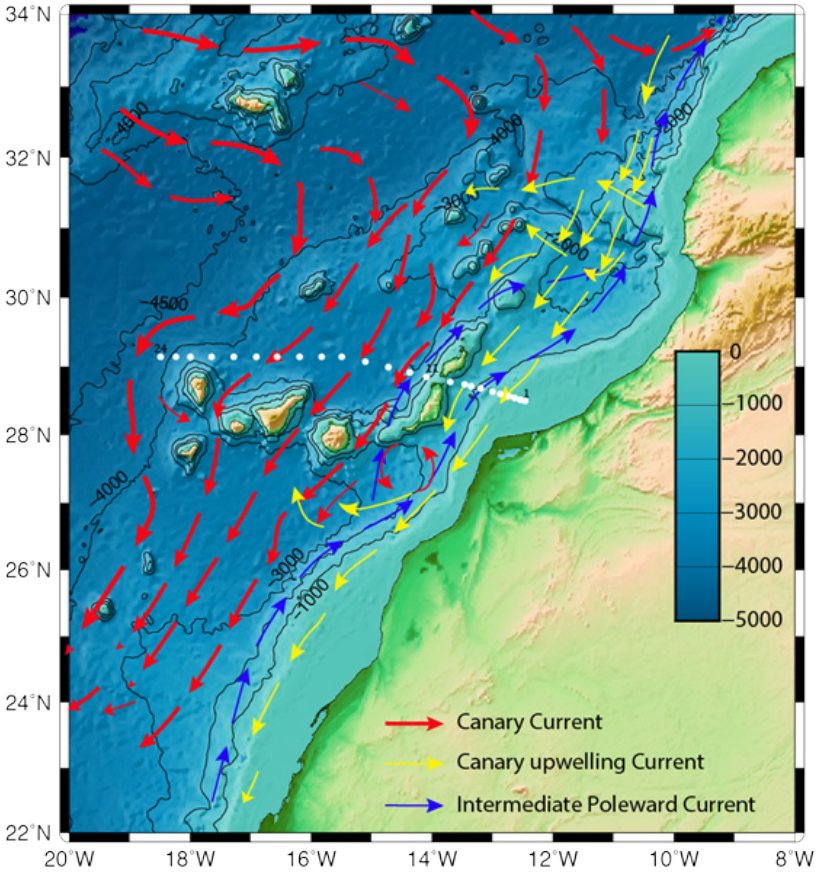

FIGURE 48.
Circulation schematic for the Canary Basin. Red arrows show the southward Canary Current carrying mainly NACW and intermediate waters. Yellow arrows show the Canary Upwelling Current that flows in thermocline layers. The white dots represent the distribution of the hydrographic stations sampled in the Canary Islands archipelago region since 1997.

During 2016, there was a slight decrease in warming and an increase in salinity compared to the previous year; 2014 was the saltiest and warmest year on record for NACW. The upwelling of the CCLME continues to strengthen.

In the oceanic region, between the 1990s and the early 2000s, there was a decrease in the temperature and salinity in all upper-layer waters. However, since the mid-2000s, there has been a marked increase in both temperature and salinity. In the depth stratum associated with the NACW (200–800 dbar), statistically significant warming was observed, measuring 0.14 ± 0.07°C decade^{-1} along with an increase in salinity of 0.020 ± 0.012 decade^{-1}. During 2016, there was a slight decrease in the warming and increase in salinity compared with the previous year, although 2014 was the saltiest and warmest year on record for the NACW (Figure 49). The increases in temperature and salinity almost compensate in density, corroborating that the observed trends are due to deepening of the isoneutral surfaces rather than changes along the isoneutral surfaces. This overall increase in salinity and temperature for the NACW was also observed in the CTZ, although with slightly smaller values for the trend due to the influence of upwelling. The hydrographic variability in the CTZ is higher due to the proximity of the upwelling region and the frequent intrusions of upwelling filaments. For the same reason, the uncertainty is higher in the trend estimations.

Surface waters in the CTZ shows a non-statistically significant cooling of −0.27 ± 0.51°C decade^{-1} and a non-statistically significant decrease in salinity of −0.051 ± 0.064 decade^{-1}, both coherent with an increase in the upwelling in the CCLME. Compared to 2015, there was a decrease in the cooling and a decrease in salinity. The upwelling of the CCLME continues to strengthen, and 2015 was the coldest and freshest year on record for the surface waters influenced by upwelling.

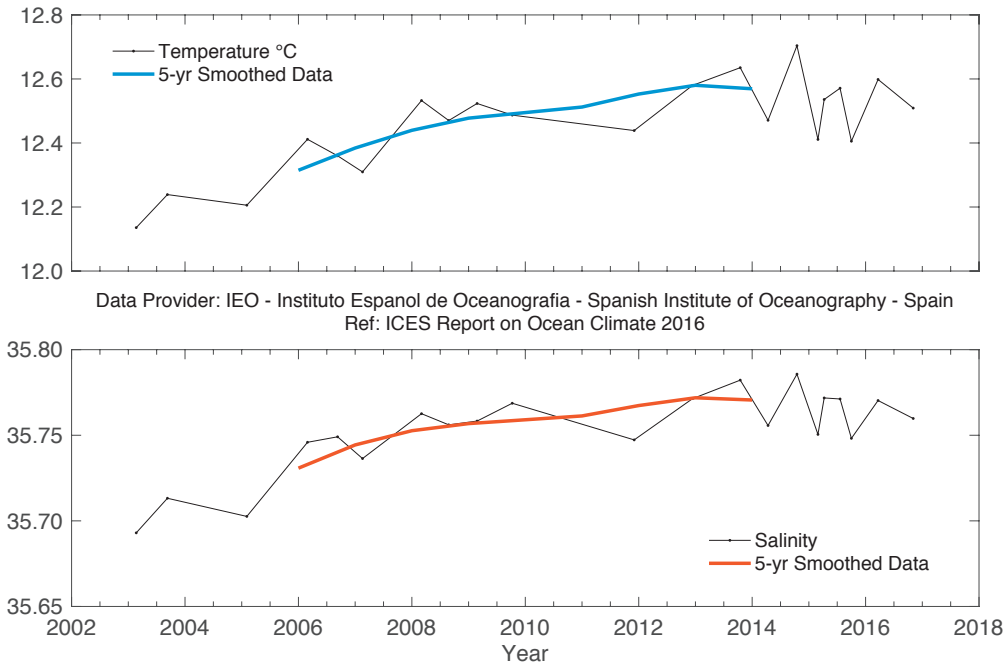

FIGURE 49.
Potential temperature (upper panel) and salinity (lower panel) for the 200-800 m layer in the oceanic waters of the Canary Basin.

4.11 SOUTHWEST APPROACHES

The datasets presented here lie at the western end of the English Channel and the boundary of the Celtic Seas and the Bay of Biscay ecoregions. The area is commonly referred to as the Southwest Approaches, which relates to the passage of shipping through the English Channel. As these data lie on a boundary between different ecoregions, this terminology has been adopted here and relates to the region forming a pathway for AW to enter the southern North Sea.

The Astan Site (48.77°N 3.94°W) is located 3.5 km offshore of the north coast of Brittany, France, in the western English Channel. Measurements began in the late 1990s and are collected twice a month at this coastal station. Properties at this site are typical of western Channel waters. Bottom depth is ca. 60 m, and the water column is well mixed for most of the surveys.

At the Astan station, temperatures in 2016 were higher than the climatology values, especially in winter, returning to about average in spring and summer and being again above average in late autumn. Overall anomaly is ca. 0.50°C above the 1998–2010 climatology.

The salinity cycle was atypical in comparison with the average pattern; minimum salinity values were not observed simply because a dry winter with low precipitation reduced the river inputs in the western Channel. A similar cycle with no spring salinity low values occurred in 2005, 2007, 2012, and 2015. Average 2016 salinity was slightly higher (ca. 0.04) than climatology.

Station E1 (50.03°N 4.37°W) is situated on the southern coast of England in the western English Channel. The water depth is 75 m, and the station is tidally influenced by a 1.1-knot maximum surface stream at mean spring tide. The seabed is mainly sand, resulting in a low bottom stress (12 ergs cm^{-2} s^{-1}). The station may be described as oceanic with the development of a seasonal thermocline; stratification typically starts in early April, persists throughout summer, and is eroded by the end of October. The typical depth of the summer thermocline is ca. 20 m. The station is greatly affected by ambient weather.

Measurements have been taken at this station since the end of the 19th century, with data currently available since 1903. The series is unbroken, apart from the gaps for the two world wars and a hiatus in funding between 1985 and 2002. The data takes the form of vertical profiles of temperature and salinity. Early measurements were taken with reversing mercury-in-glass thermometers and discrete salinity bottles. More recently, electronic equipment (Seabird CTD) has been utilized.

The time-series demonstrates considerable interannual variability in temperature. As was the case in 2015, the monthly average temperatures were slightly below (ca. 0.1−0.2°C) the long-term mean for the spring and summer seasons during 2016. In contrast, the winter months (January, February) and autumn (September, October, and November) were markedly warm (ca. 1.0–2.0°C).

The salinity recorded in early 2016 (between January and April) was close to the long-term mean for this period of the year (ca. 35.2–35.3), whereas for the late spring until the close of the year, it was consistently 0.1–0.2 above (May-December average about 35.1–35.3).

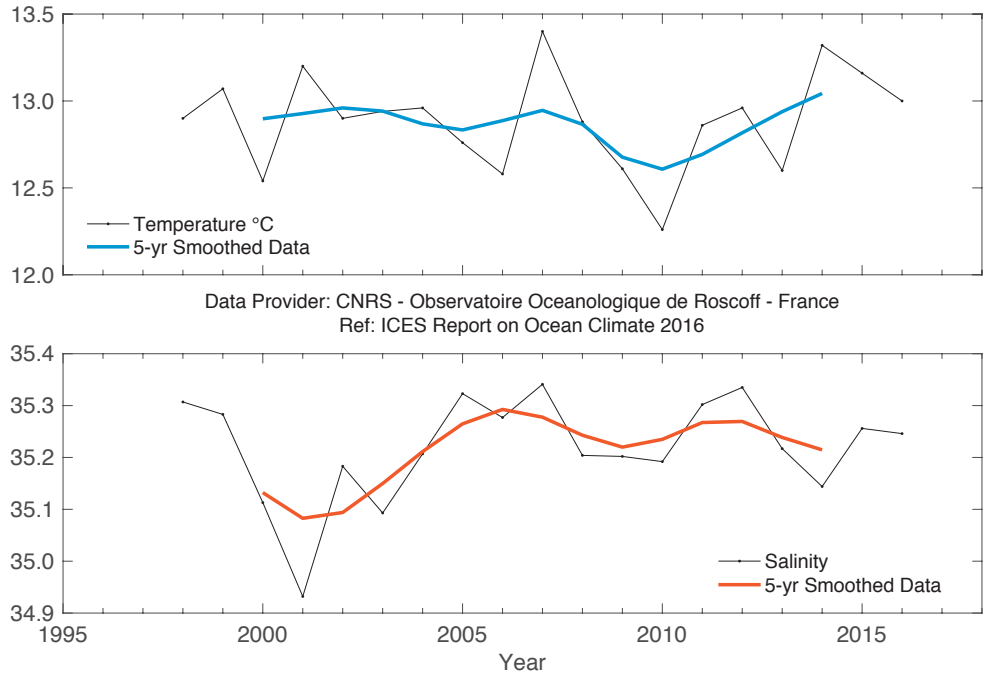

FIGURE 50.
Temperature (upper panel) and salinity (lower panel) anomalies of surface water at the Astan station (48.77°N 3.94°W) base period (1998–2010).

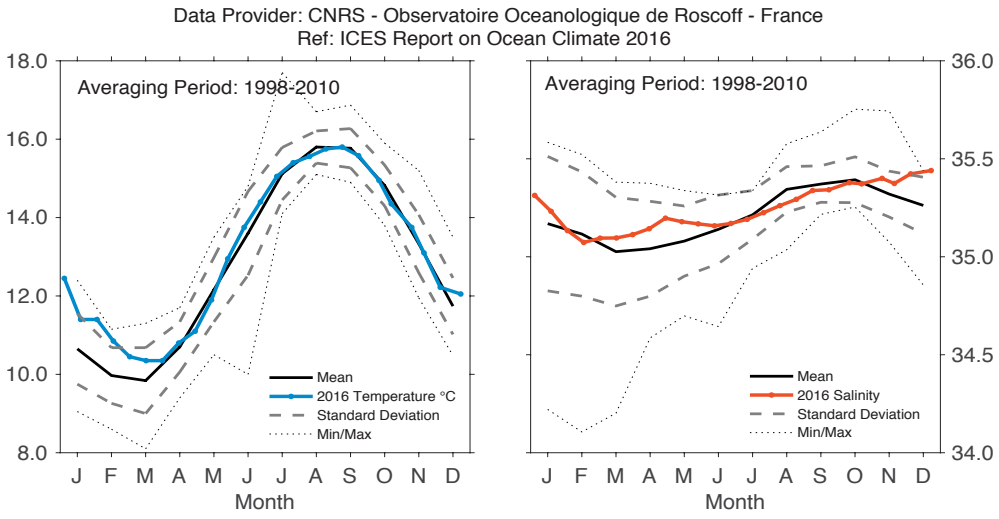

FIGURE 51.
Monthly average seasonal cycle with 2016 temperature (left panel) and salinity (right panel) observations of surface water at the Astan station (48.77°N 3.94°W). Note: Month markers are placed mid-month.

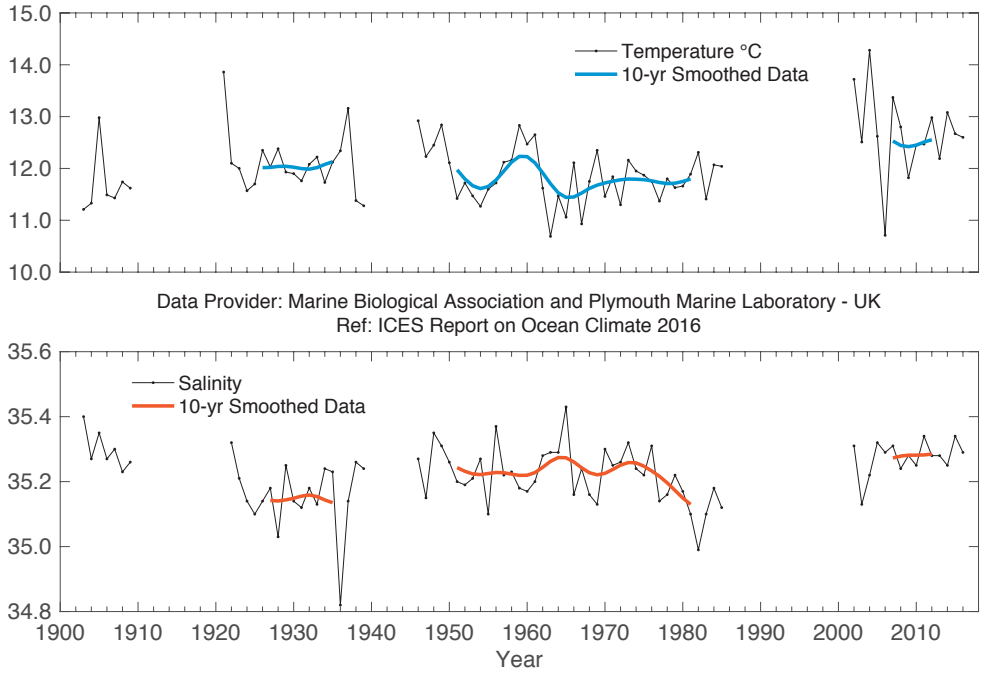

FIGURE 52.
Temperature (upper panel) and salinity (lower panel) anomalies of surface (0–40 m) water at Station E1 in the western English Channel (50.03°N 4.37°W).

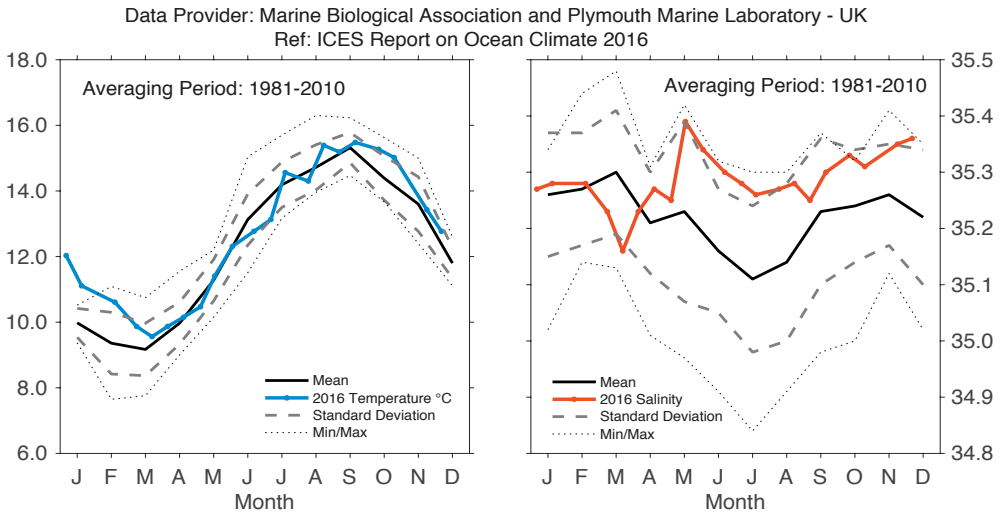

FIGURE 53.
Monthly average seasonal cycle with 2016 temperature (left panel) and salinity (right panel) observations of surface (0–40 m) water at Station E1 in the western English Channel (50.03°N 4.37°W).

4.12 CELTIC SEAS

The Celtic Seas ecoregion relates to the area west of the UK and Ireland, as well as the Irish Sea. It is bounded by France in the south and the Faroes in the north. In addition to the influence of coastal waters on the shelf, the area is strongly influenced by the poleward transport of AW as well as the continental slope current that brings waters northward from the Biscay region. The time-series of surface observations at the Malin Head coastal station (the most northerly point of Ireland) is inshore of coastal currents and is influenced by run-off. The measurement methodology has changed over the years, beginning with a hand-held thermometer and currently utilizing a high-precision SBE 39 temperature sensor (since 2008). M3, an offshore weather buoy, has been maintained at 51.22°N 10.55°W off the southwestern coast of Ireland since mid-2002, where SST data are collected hourly.

At Malin Head, SST has shown a dramatic rise since the end of the 1980s. The mean temperature for 2016 is 0.72°C above the 1981–2010 mean. Monthly mean temperatures for 2016 are mostly above average, especially in the winter months. The long-term winter mean shows significant warming since the late 1990s, with the 2015/2016 winter being the warmest of all at 1.63°C above the long-term winter mean.

At the M3 buoy, there is considerable interannual variability, but the trend here is for mean annual temperatures to be lower than average over recent years. However, this trend should be treated with caution as the "long-term mean" used to calculate the anomalies is only over the last eight years of the 1981–2010 period. The mean temperature for 2016 was −0.08°C below average. Monthly temperatures are about average for the whole year.

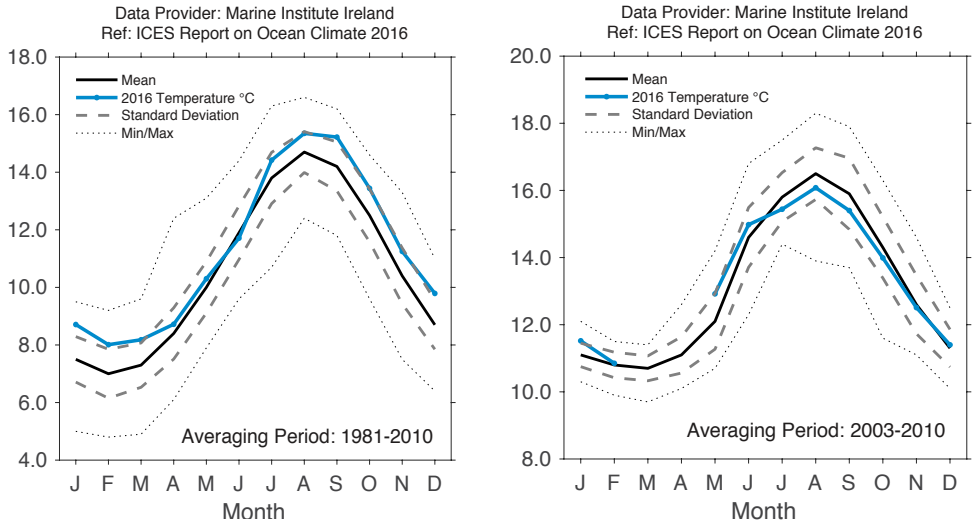

FIGURE 54.
Celtic Seas. Monthly average seasonal cycle with 2016 monthly temperature at Malin Head (left panel) and the M3 Weather Buoy (right panel, 51.22°N 10.55°W).

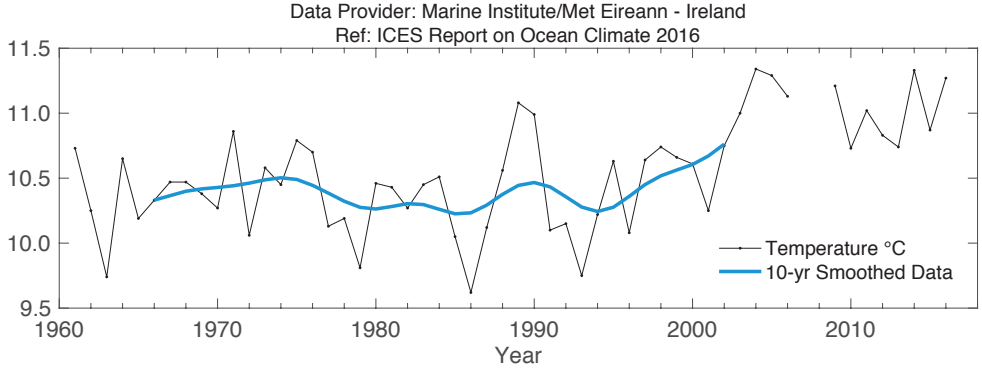

FIGURE 55.
Celtic Seas: Temperature at Malin Head coastal station (55.39°N 7.38°W).

4.13 ROCKALL TROUGH

Rockall Trough is a deep ocean basin situated west of Britain and Ireland and sits within the Celtic Seas and Oceanic Northeast Atlantic ecoregions. With significantly different oceanographic characteristics than the shallower shelf sea areas, Rockall Trough is separated from the Iceland Basin by Hatton and Rockall banks and from the Norwegian Sea by the shallow (500 m) Wyville Thomson Ridge. It is a route for warm North Atlantic upper water to reach the Norwegian Sea, where it is converted into cold, dense overflow water as part of the thermohaline overturning in the North Atlantic. The upper water column is characterized by poleward-moving eastern North Atlantic water (ENAW), which is warmer and more saline than the waters of the Iceland Basin that also contribute to the Norwegian Sea inflow.

The potential temperature of the upper 800 m was close to the 1981–2010 mean in 2016. The upper ocean has been cooling relative to a peak of 9.8°C in 2007 (Figure 56). The salinity of the upper 800 m has also been decreasing since the end of the 2000s and decreased sharply in 2016 to 0.07 psu below the long-term mean.

Rapid freshening in Rockall Trough since 2015.

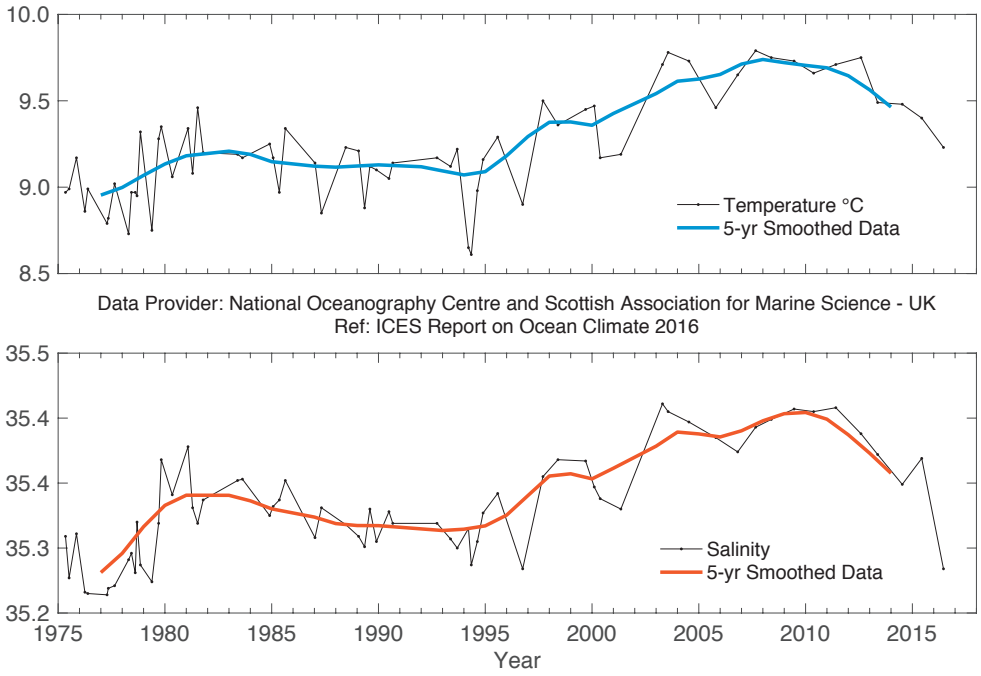

FIGURE 56.
Rockall Trough. Temperature (upper panel) and salinity (lower panel) for the upper ocean (potential density 27.2–27.50, representing the top 800 m, but excluding the seasonally warmed surface layer).

4.14 HATTON-ROCKALL BASIN

The shallow Hatton–Rockall Basin (1000 m) lies between the Iceland Basin to the west and Rockall Trough to the east and is bounded by the Hatton and Rockall banks. The basin is filled with well-mixed subpolar-mode water (SPMW) moving northward as part of the NAC complex. Winter mixing reaches 800–1000 m here. Temperature and salinity vary considerably, depending on the type of NAC water that enters the basin. The region is in the transition zone between cold, fresh, central subpolar water and warm, saline, eastern subpolar water. When the NAC fronts shift westward, the basin becomes warmer and more saline.

The range of basin mean temperature and salinity in the upper 1000 m is more than 1°C and 0.1 psu, higher than in the Iceland Basin to the west and Rockall Trough to the east. The lowest values were seen at the beginning of the time-series in 1996, followed by a steady rise to maximum values in the late 2000s. Since 2010, there has been a decrease in temperature and salinity; in 2016, both were lower than the 1996–2010 average, and the magnitude of these anomalies is second only to the 1996 values (Figure 57).

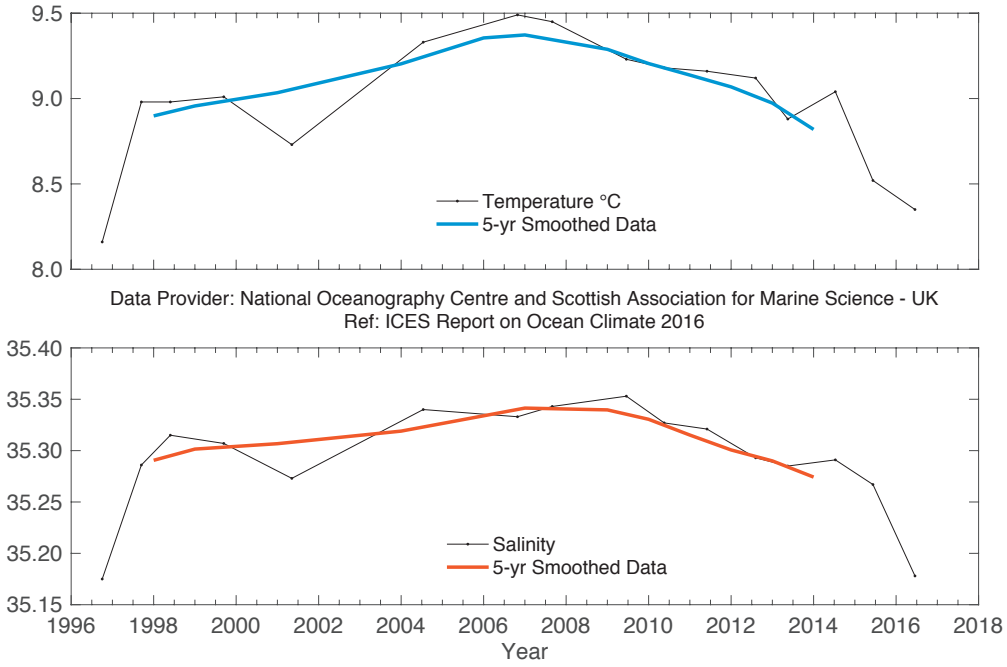

FIGURE 57.
Hatton–Rockall Basin. Temperature (upper panel) and salinity (lower panel) for the upper ocean (potential density 27.20–27.50, representing the top 600 m and excluding the seasonally warmed surface layer).

4.15 ICELAND BASIN

A major part of the NAC flows into the Iceland Basin adjacent to the shallow Hatton Bank on the southeast side of the basin. The NAC typically consists of one or two fronts between warmer, more saline water in the east and colder, fresher water to the north and west. The region is rich in eddy activity and the water properties are quite variable in time and space. Most of the water entering the Iceland Basin from the south flows through into the Norwegian Sea over the Iceland–Scotland Ridge. A smaller fraction of the NAC water recirculates south of Iceland in the boundary currents of the main anticlockwise circulation of the Subpolar Gyre.

The temperature and salinity of the upper ocean (ca. the top 500–600 m) vary from year to year, but also exhibit multiyear changes. From 1996 to the late 2000s, both temperature and salinity increased but have since been decreasing (Holliday *et al.*, 2015). In 2016, the temperature and salinity values were the lowest recorded since 1996 (Figure 58). The change since 2010 implies that the basin is receiving more water originating in the west and central subpolar region and less warm, saline water from the eastern intergyre regions. Superimposed on that multiyear trend is rapid cooling between 2014 and 2015, caused by a high flux of heat from the ocean to the atmosphere (Duchez *et al.*, 2016) and rapid freshening between 2015 and 2016, which has as yet unidentified origins.

Record-low salinity observed in the Iceland Basin upper ocean.

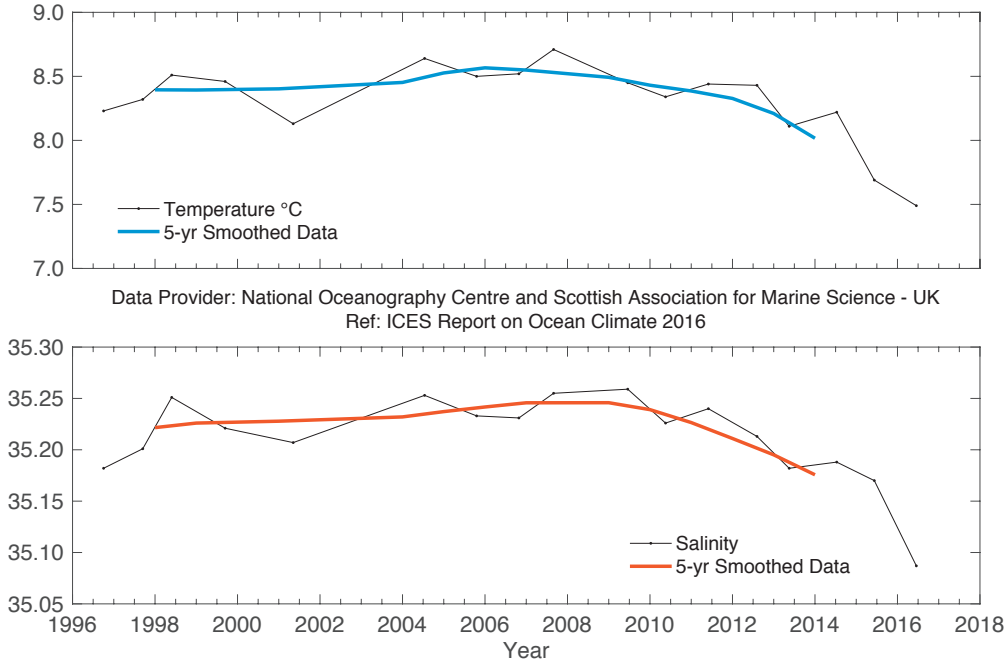

FIGURE 58.
Iceland Basin. Temperature (upper panel) and salinity (lower panel) for the upper ocean (potential density 27.20–27.50, representing the top 500 m and excluding the seasonally warmed surface layer).

4.16 IRMINGER SEA

The Irminger Sea is the ocean basin between southern Greenland, the Reykjanes Ridge, and Iceland. This area forms part of the North Atlantic subarctic cyclonic gyre. Due to this gyre, the exchange of water between the Irminger and Labrador seas proceeds relatively fast. In the bottom layers of the Irminger Sea, cold water originating from the (sub)arctic seas flows from Denmark Strait southwards over the continental slope of Greenland.

In 2004, SPMW in the central Irminger Sea (200–400 dbar) reached the highest recorded temperature and salinity since 1991. Since then, temperature has exhibited well-correlated interannual variations, suggesting that variations in wind-driven circulation were the main cause of this hydrographic variability.

Since 2014, a negative trend has been observed in temperature, but not in salinity until 2016. The temperature of SPMW in the central Irminger Sea was nearly 0.4°C below the long-term mean, while salinity was 0.015 above the mean.

Deep convection occurred over the winter of 2014/2015 until the end of April, leading to mixed layers as deep as 1400 m. Deep mixed layers were again seen in winter 2015/2016. Both winters led up to the cold anomaly observed in the Irminger Sea.

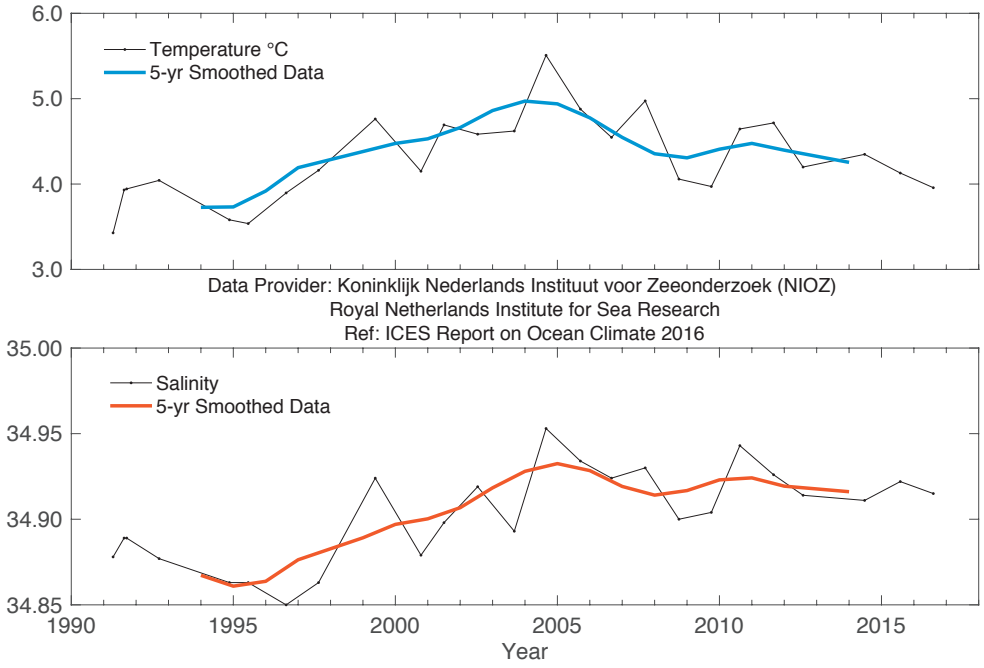

FIGURE 59.
Irminger Sea. Temperature (upper panel) and salinity (lower panel) of subpolar-mode water in the central Irminger Sea (averaged over 200–400 m).

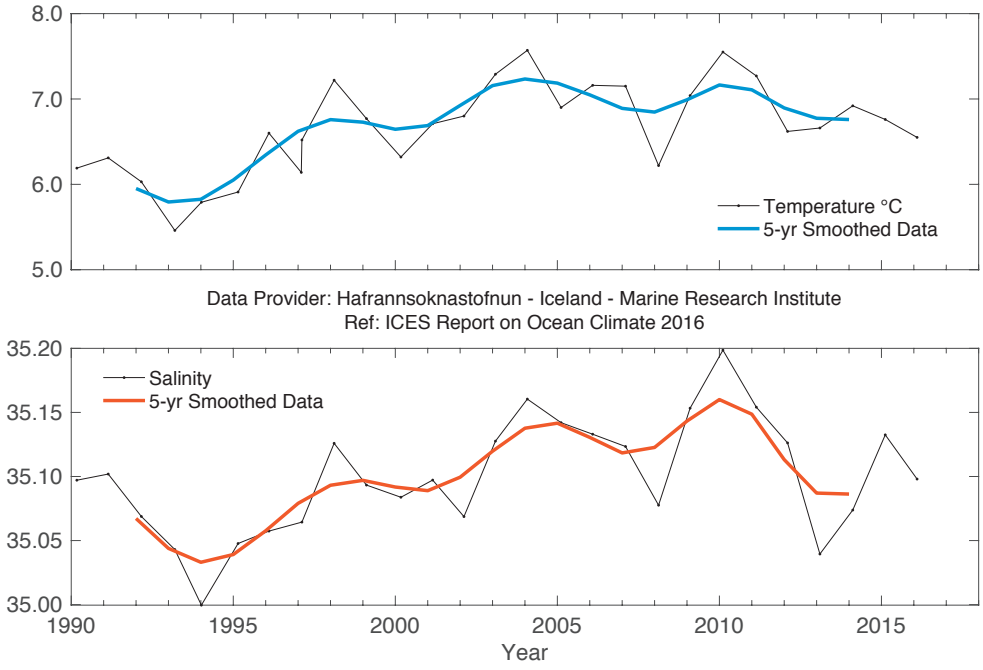

FIGURE 60.
Irminger Sea. Temperature (upper panel) and salinity (lower panel) of subpolar-mode water in the northern Irminger Sea (Station FX9, 64.33°N 28°W) from winter observations averaged over 200–500 m).

4.17 FAROESE WATERS AND THE FAROE-SHETLAND CHANNEL

Data from the Faroes ecoregion are grouped together with data from the Faroe-Shetland Channel. This small region sits at the boundary between the Celtic Seas, North Sea, and Norwegian Sea ecoregions and at the boundary between the North Atlantic and Nordic seas.

One branch of the NAC crosses the Greenland-Scotland Ridge (Figure 61), flowing on either side of the Faroes. Its properties are sampled by the Faroe Bank Channel before it crosses the ridge, and by the Faroe Current after it crosses the ridge. Some of this water recirculates and is sampled within the Faroe-Shetland Channel as modified North Atlantic water (MNAW).

Farther to the east, the continental slope current flows along the edge of the northwest European continental shelf; it carries warm, saline AW, originating in the southern Rockall Trough, into the Faroe-Shetland Channel. A proportion of this AW crosses onto the shelf itself and enters the North Sea, where it is diluted with coastal water and eventually leaves in the Norwegian Coastal Current. The remainder enters the Norwegian Sea and joins the water coming from north of the Faroes to become the Norwegian Atlantic Current (NAC).

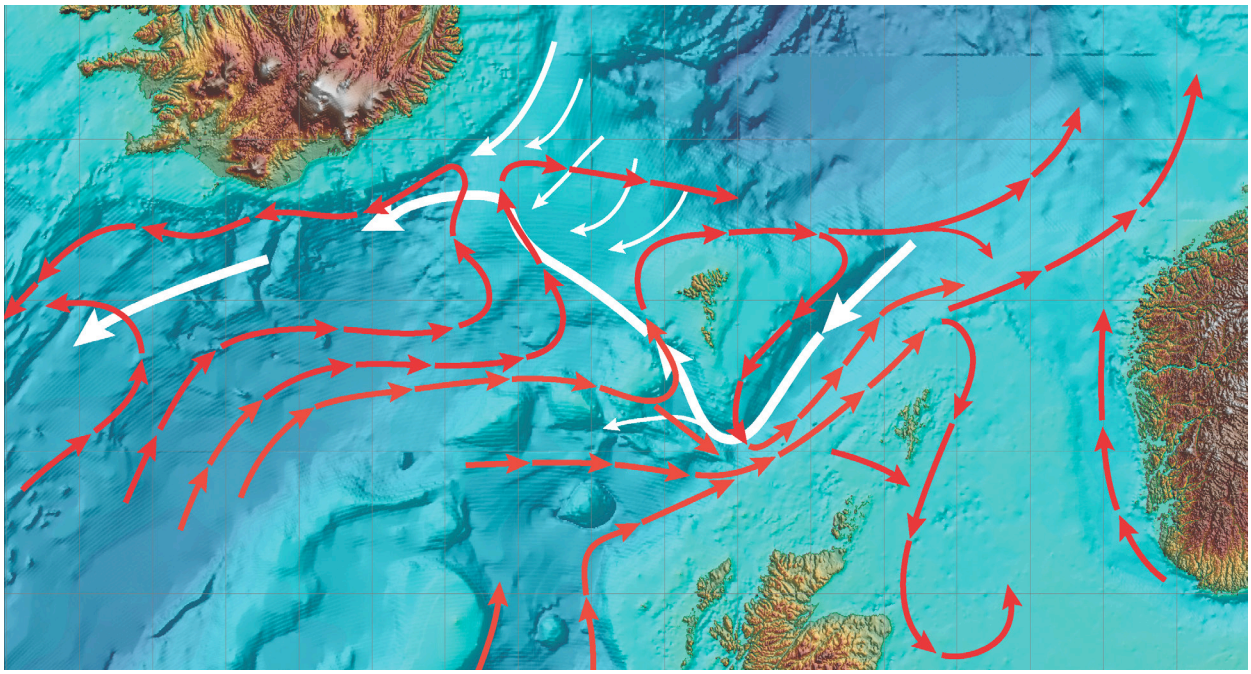

FIGURE 61.
Circulation schematic for the Faroes ecoregion and the Faroe-Shetland Channel. Red lines show the poleward movement of Atlantic water (AW). Thick white lines show the return circulation (at depth) of waters from the Nordic seas.

Generally, both temperature and salinity in all upper-layer waters around the Faroes and the Faroe–Shetland Channel increased markedly during the 1990s and 2000s. Both temperature and salinity decreased during the first half of the 2010s. Salinities were at a maximum around 2010 and have decreased since then, with an exceptionally large decrease observed in the Faroe Bank Channel in autumn 2016 (Figure 62). Temperatures have remained close to or below the long-term mean.

After the record-high salinities observed in the Faroe Bank Channel (Figure 62) and the Faroe Current (Figure 63) in November 2009, salinities decreased at both locations. In the Faroe Bank Channel, the salinities decreased from average values in 2015 to record-low values in autumn 2016. In the Faroe Current, there was a smaller decrease in salinity in 2016 compared to 2015.

Temperatures in the Faroe Bank Channel have been relatively high and stable since the mid-2000s and into the early 2010s. In 2012, they decreased and have been

close to the long-term mean in recent years; temperature decreased slightly from 2015 to 2016 and is now equal to the long-term mean. Normally, the characteristics of water in the Faroe Current change in the same way as the characteristics of the Faroe Bank Channel, but with a delay; thus, in the Faroe Current, similar temperature variability was observed, but here the temperature now is somewhat below the long-term mean.

On the Faroe Shelf, the annual average temperature has been relatively high since the early 2000s, but in 2015, the annual average temperature was the lowest observed since 2000 (Figure 64). In 2016, the temperature increased slightly compared to 2015. The long-term trend in salinity on the Faroe Shelf follows the trend observed in off-shelf waters. Thus, salinities increased from the start of the observations in 1995 to record-high values in 2010. Since 2010, salinities have been decreasing, and the record-low values observed in the Faroe Bank Channel in autumn 2016 were evident in the Faroe Shelf salinities, also being record-low in the last four months of 2016.

The temperature and salinity of the surface waters of the Faroe–Shetland Channel have generally increased over the past two decades. MNAW on the western slopes of the Channel experienced record-high temperature and salinity in 2010 (Figure 65). Temperature and salinity of AW masses on both sides of the Faroe–Shetland Channel have decreased significantly since then (Figure 66), and values are now lower than the long-term mean.

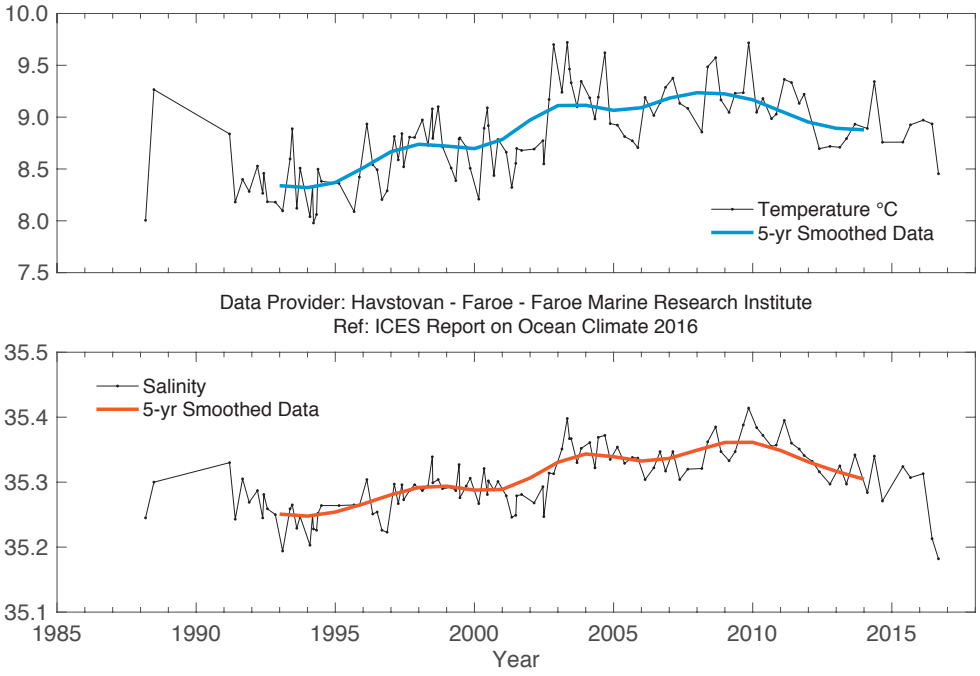

FIGURE 62.
Faroese waters. Temperature (upper panel) and salinity (lower panel) in the high salinity core of Atlantic water (AW) over the Faroe Bank Channel (maximum salinity averaged over a 50 m deep layer).

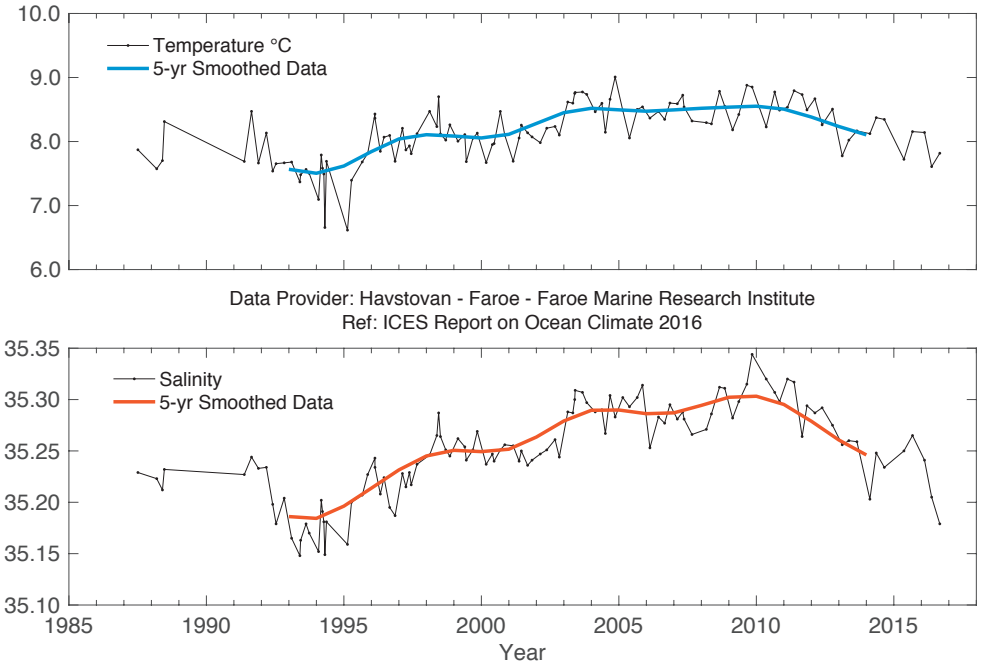

FIGURE 63.
Faroese waters. Temperature (upper panel) and salinity (lower panel) in the high salinity core of the Faroe Current north of the Faroes (maximum salinity averaged over a 50 m deep layer).

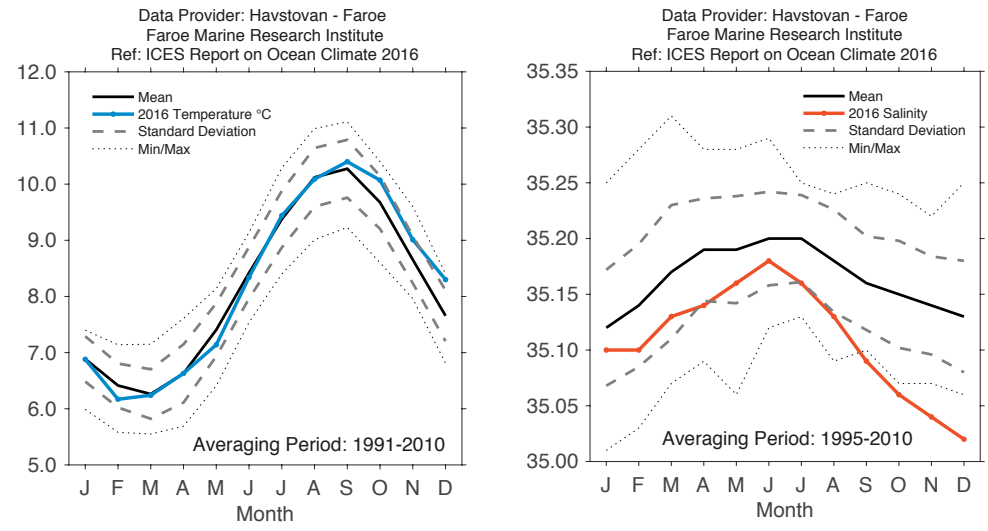

FIGURE 64.
2016 monthly temperature (left) from the Faroe coastal station at Oyrargjogv (62.12°N 7.17°W) and monthly salinity (right) from the Faroe coastal station at Skopun (61.91°N 6.88°W). Note that the temperature averaging period has been changed and is now based on data from Oyrargjogv in the period 1991–2010. The salinity averaging period is 1995–2016.

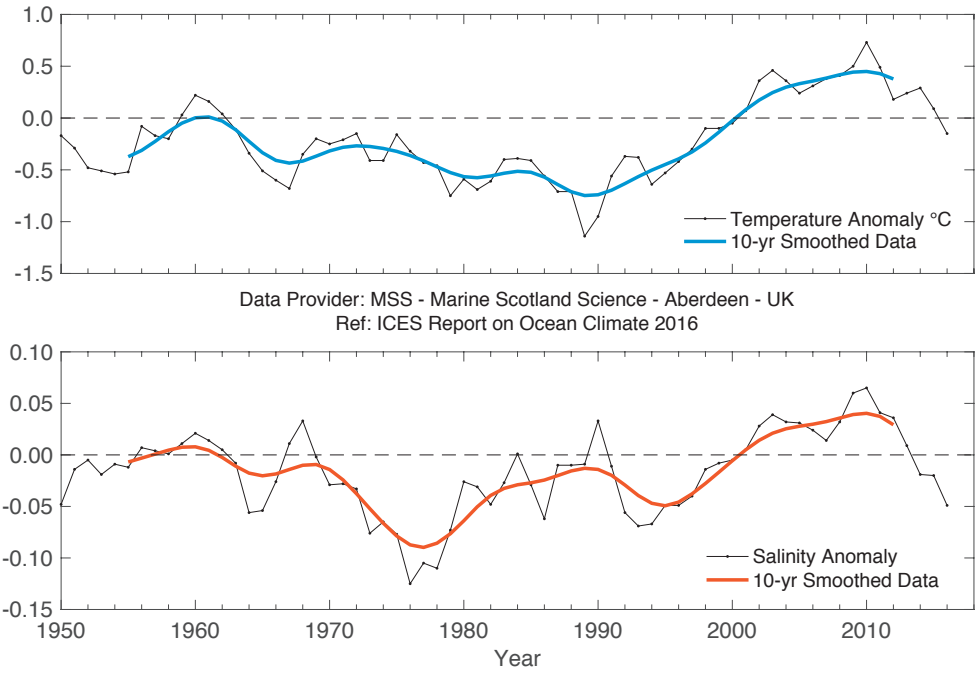

FIGURE 65.
Temperature anomaly (upper panel) and salinity anomaly (lower panel) in the modified Atlantic water (MNAW) entering the Faroe–Shetland Channel from the north after circulating around the Faroes.

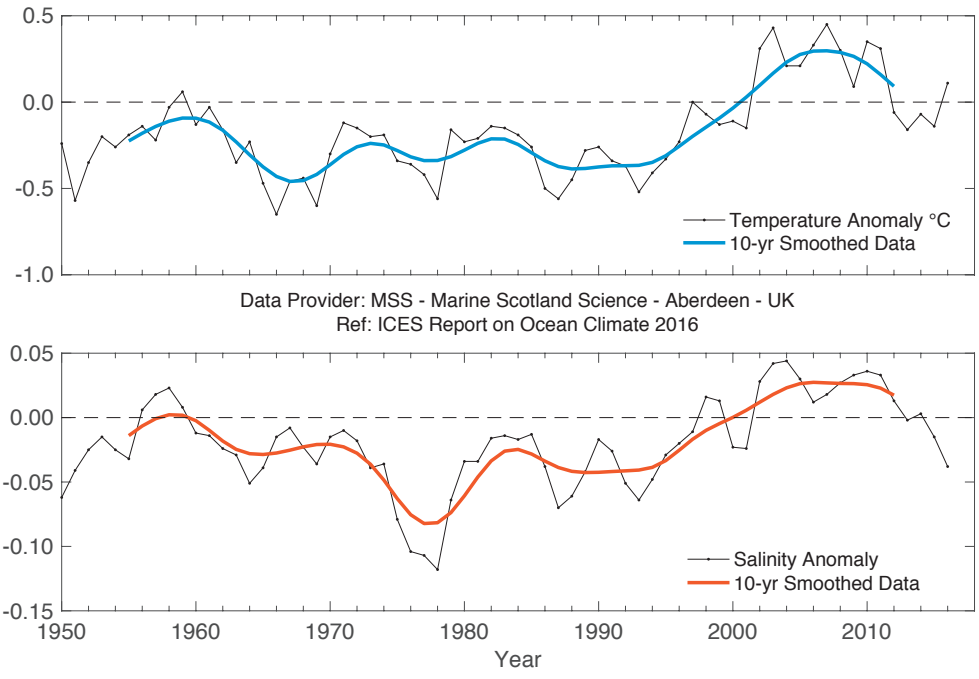

FIGURE 66.
Faroe–Shetland Channel. Temperature anomaly (upper panel) and salinity anomaly (lower panel) in the Atlantic water (AW) in the slope current.

4.18 NORTH SEA

North Sea oceanographic conditions are determined by the inflow of saline AW (Figure 67) and the ocean–atmosphere heat exchange. The inflow through the northern entrances (and, to a lesser degree, through the English Channel) can be strongly influenced by the NAO. Numerical model simulations also demonstrate strong differences in the North Sea circulation, depending on the state of the NAO. The AW mixes with river run-off and lower-salinity Baltic outflow along the Norwegian coast. A balance of tidal mixing and local heating forces the development of a seasonal stratification from April/May to September in most parts of the North Sea.

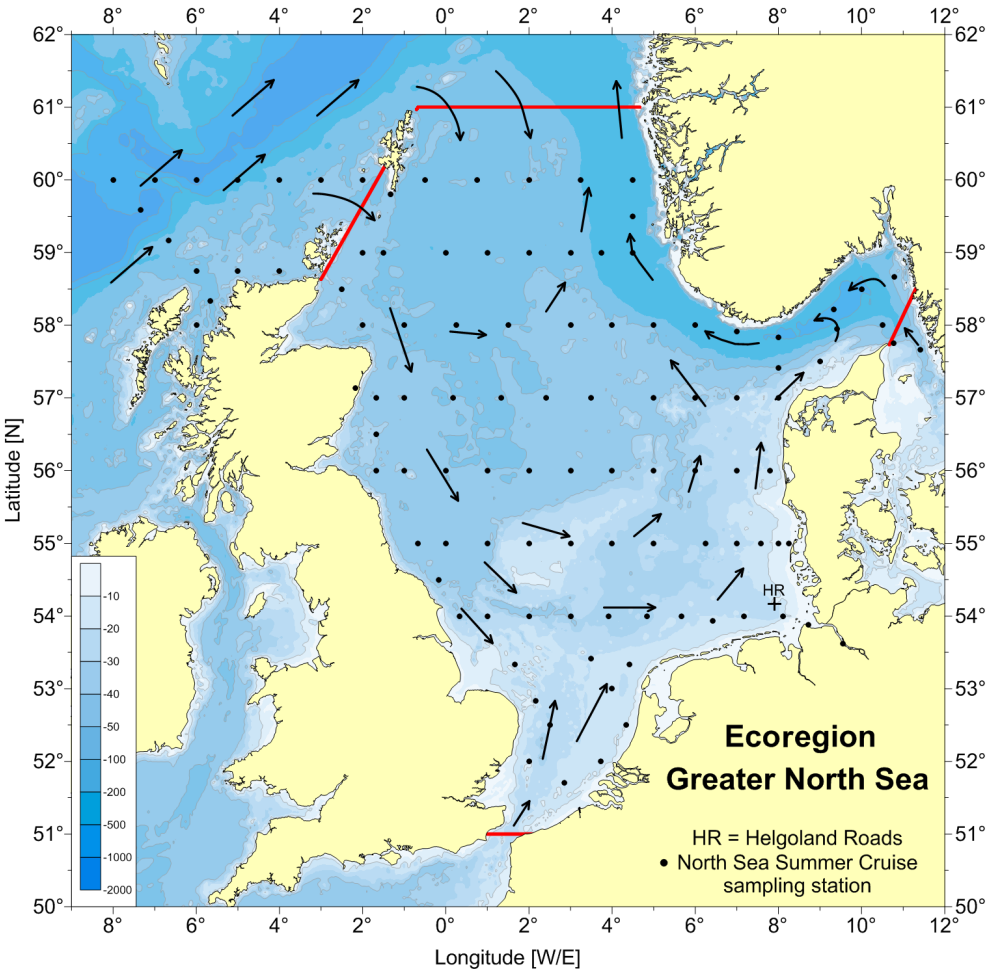

FIGURE 67. Circulation schematic for the North Sea. Red lines show the extent of the North Sea region. The sampling station at Helgoland Roads is marked with a HR+. Black arrows indicate mean residual circulation patterns. Black dots show the summer sampling undertaken in the North Sea by the Bundesamt für Seeschifffahrt und Hydrographie (BSH), Germany.

In 2016, the monthly area-averaged North Sea SST fell between 0.2 and 1.8°C above the mean of the reference period 1981–2010. 2016 is the first year since 1969 in which the seasonal SST maximum occurred in September instead of August (or July, in the case of 1973 and 1987). The September mean of 16.2°C was, together with 2002, the warmest since 1971. The 2016 annual mean of area-averaged North Sea SST was, together with 2003, the second highest value since 1971, measuring 11.0°C with an anomaly of +0.8°C. Besides the inflow of warmer AW at the northern boundary and through the English Channel, much of the North Sea SST variability is caused by local ocean–atmosphere heat flux.

During summer, surface temperatures in the southern North Sea exceeded the long-term mean (2000–2010) by 0.5–1.0°C, with coastal areas locally exceeding 1.5°C. North of 54°N, the temperatures measured up to 1.5°C below the long-term mean over large areas. Southwest of Norway, the negative anomalies over the Eigersund and Fischer Bank exceeded −2°C. The bottom temperatures exceeded the long-term mean over large areas with anomalies greater than 3°C over

Dogger Bank, Jyske Rev, and west of Jutland. Negative anomalies up to −1°C occurred west of Dogger Bank and in the northern North Sea.

The maximum vertical temperature gradient in the thermocline was 3°C m^{-1} at 56°N, and the 54°N section was mostly vertically mixed with vertical gradients < 0.5°C m^{-1}. Generally, the thermocline depth in the North Sea varied between 22 and 48 m. There was a strong thermocline in the central North Sea and a weakening of thermocline strength from south to north. The differences between surface and bottom temperatures were generally smaller compared to previous years, exceeding 8°C only in a small patch over the Norwegian Trench. Compared to 2015, the total heat content decreased slightly to 1.652 × 1021 J and exceeded the reference mean of 1.631 × 1021 J by 0.2 standard deviations only.

The southern boundary of AW > 35 psu intruding from the north was located at about 56°N in the surface and bottom layer. At the surface, AW intruded in a small tongue which disintegrated into several patches, while in the bottom layer, AW intruded in a broad front. In both layers, the general special pattern showed only minor deviations from the reference period, with negative anomalies occurring mainly in the eastern part of the North Sea and at the entrance of the English Channel. Compared to 2015, the total salt content decreased slightly to 1.092 × 1012 t, which is the lowest value since 2001.

In 2016, all monthly run-off volumes were below the reference period 1981–2000. Though the annual run-off volume of 15.3 km^3 $year^{-1}$ was, as in 2014 and 2015, relatively low, the values still fell within the 95% band, and no significant impacts on salinity in the German Bight have been observed.

In 2016, the annual area-averaged North Sea SST exceeded the climatological means. The September SST mean is, together with 2002, the warmest September since recording began in 1971, with an anomaly of +1.8°C.

Temperature and salinity at two positions in the northern North Sea illustrate conditions in the Atlantic inflow (Figure 68). The first (Location A) is near bottom in the northwestern part of the North Sea, and the second (Location B) is in the core of the AW at the western shelf edge of the Norwegian Trench. Measurements were taken during summer and represent the previous winter's conditions. The average temperature at Location A was 1–2°C lower than at Location B, and salinity was also slightly lower. In both locations, there were above-average temperatures and salinities in 2009, and there has been an increase in both salinities and temperatures since 2008.

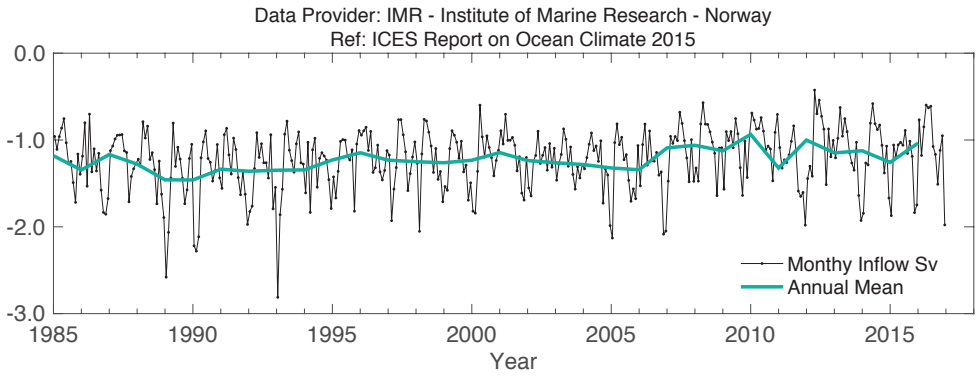

FIGURE 68.
Northern North Sea. Modelled annual mean (bold) and monthly mean volume transport of Atlantic water (AW) into the northern and central North Sea southwards between the Orkney Islands and Utsire, Norway.

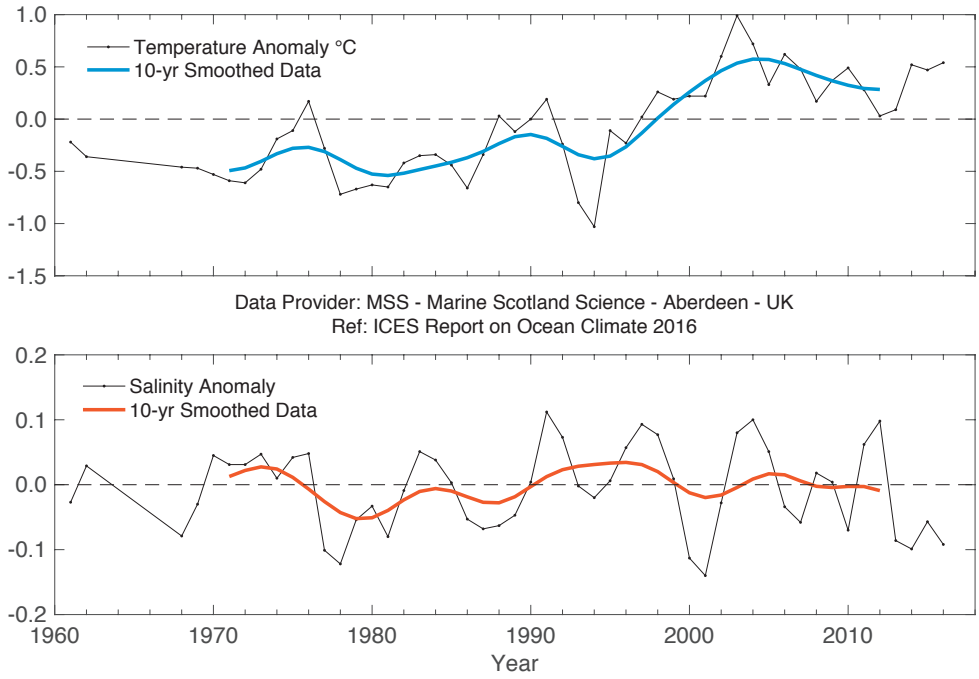

FIGURE 69.
Northern North Sea. Temperature anomaly (upper panel) and salinity anomaly (lower panel) in the Fair Isle Current entering the North Sea from the North Atlantic.

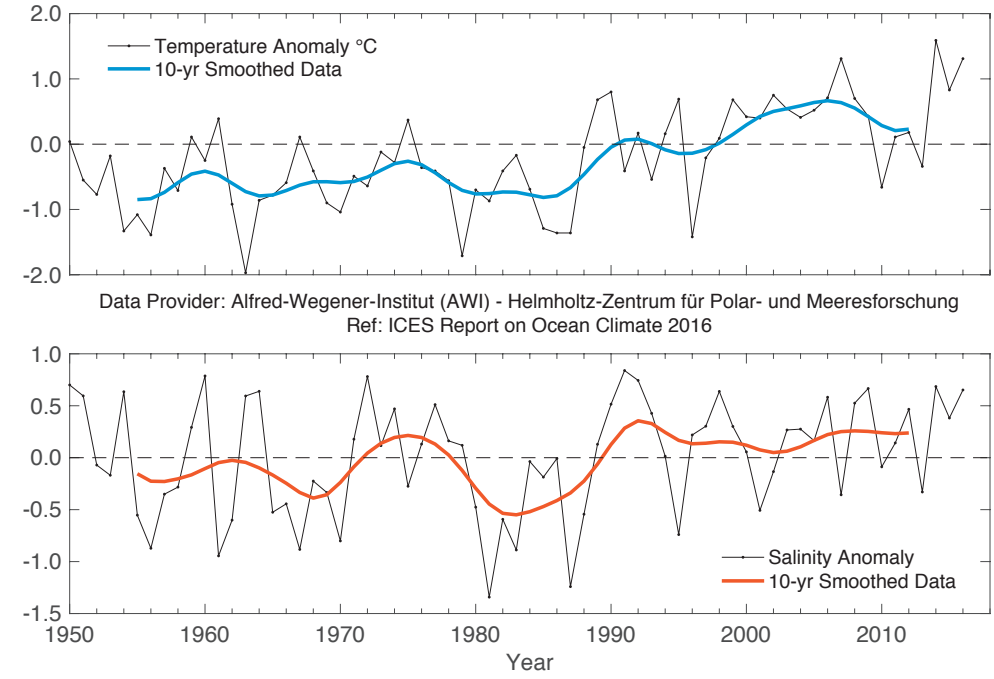

FIGURE 70.
Southern North Sea. Annual mean surface temperature anomaly (upper panel) and salinity anomaly (lower panel) at Station Helgoland Roads. Data until 2015.

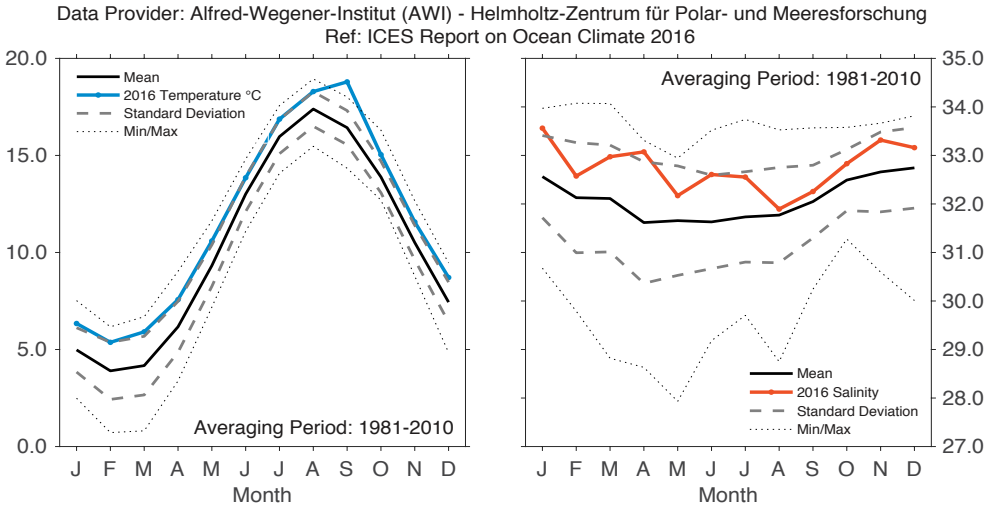

FIGURE 71.
Southern North Sea. Monthly surface temperature (left panel) and salinity (right panel) at Station Helgoland Roads.

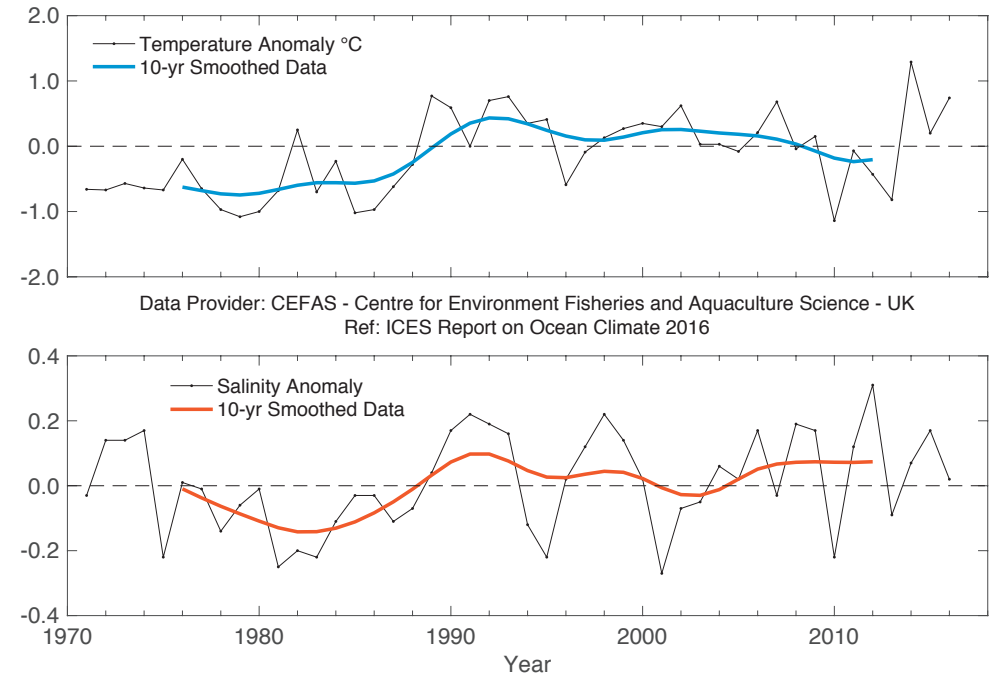

FIGURE 72.
Annual sea surface temperature (SST) anomaly (upper panel) and salinity anomaly (lower panel) relative to 1981–2010 from the merged Harwich Ferry Route and West Gabbard Smartbuoy time-series located at 52°N 003°E. Between 1971 and 2002, this was measured as part of a regular ferry route along 52°N between Harwich and Rotterdam. Data from 2002 are from the Cefas West Gabbard 2 site.

4.19 SKAGERRAK, KATTEGAT, AND THE BALTIC

The shallow seas of the Skagerrak, Kattegat, and the Baltic are characterized by large salinity variations. In the Skagerrak, water masses from different parts of the North Sea are present. The Kattegat is a transition area between the Baltic and the Skagerrak. The water is strongly stratified, with a permanent halocline (sharp change in salinity at depth). The deep water in the Baltic Proper, which enters through the Belts and the Sound, can be stagnant for long periods in the inner basins. In the relatively shallow area in the southern Baltic, smaller inflows pass relatively quickly, and conditions in the deep water are extremely variable. Surface salinity is very low in the Baltic Proper and its gulfs. The Gulf of Bothnia and the Gulf of Finland are ice-covered during winter.

Globally, 2016 was the warmest year, but the mean air temperature in Sweden did not reach record levels. The mean air temperature was higher than normal, especially in early spring and late summer, but due to a cold January, it is not in line with the warm Swedish years of 2014 and 2015. Owing to its central location relative to the Skagerrak, Kattegat, and Baltic, the weather in Sweden can be taken as representative for the area. Mean precipitation was lower than normal in most parts of Sweden; September and October were especially dry months. The number of sun hours was close to normal in the north, but above normal elsewhere.

The SST was above normal at the beginning of the year in the Baltic. In the Skagerrak, the year started with temperatures close to normal. In summer, water temperatures were slightly above normal for most stations, with September as outstanding in high SST after a period of warm weather. Surface salinities were mostly normal in the Skagerrak and the Kattegat except for Station P2, where half of the monthly values were more than ±1 s.d. away from the mean value. In the southern Baltic, surface salinities higher than normal were observed through the entire year until November. The rest of the Baltic Proper showed close to normal values, except during August and September, when they were lower than normal.

There was an inflow of more saline water into the Baltic between the end of January and early February, which means that the period of higher frequency of inflows, starting in 2014, continues. Despite the inflows, ca. 17% of the bottom waters in the Baltic Proper are anoxic and 28% are hypoxic, but the inflows have lowered the concentration of hydrogen sulphide in the eastern and western Gotland Basin.

A warm year with continuing low oxygen conditions in the deep waters of the Baltic Proper.

The ice season 2015/2016 had a late start and was shorter than normal. Nevertheless, the cold period in January covered most of the Bay of Bothnia (except the central parts), the Quark, and the Gulf of Finland with ice. The maximum ice extent of 110 000 km^2 was reached already on 23 January, more than 2.5-fold larger than the record-low in 2014. The ice season ended on 12 May, about two weeks earlier than normal.

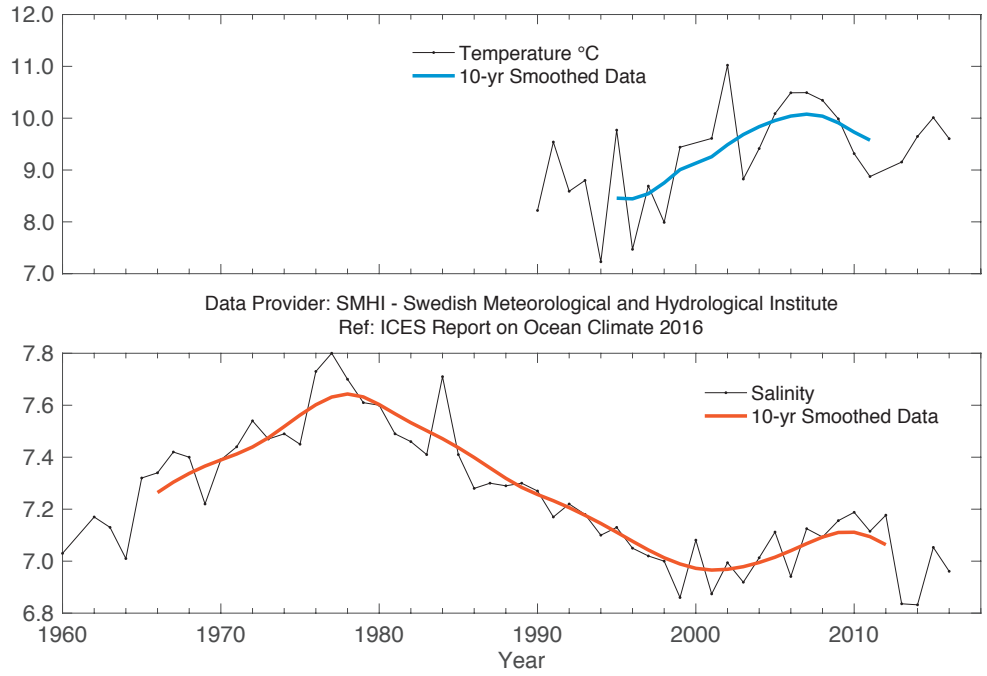

FIGURE 73.
Skagerrak, Kattegat, and the Baltic. Surface temperature, yearly mean (upper panel) and surface salinity, yearly mean (lower panel) at Station BY15 (east of Gotland) in the Baltic Proper.

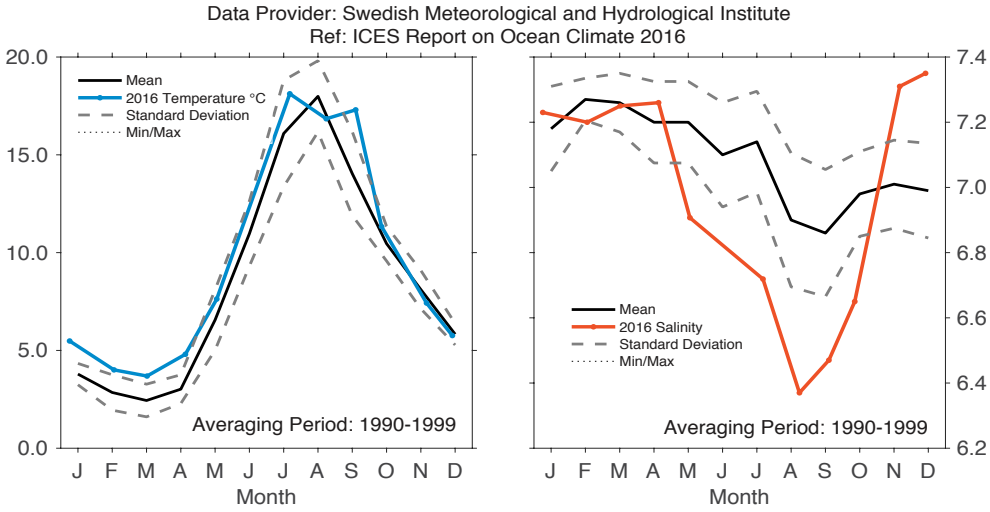

FIGURE 74.
Skagerrak, Kattegat, and the Baltic. Monthly surface temperature (left panel) and salinity (right panel) at Station BY15 (east of Gotland) in the Baltic Proper.

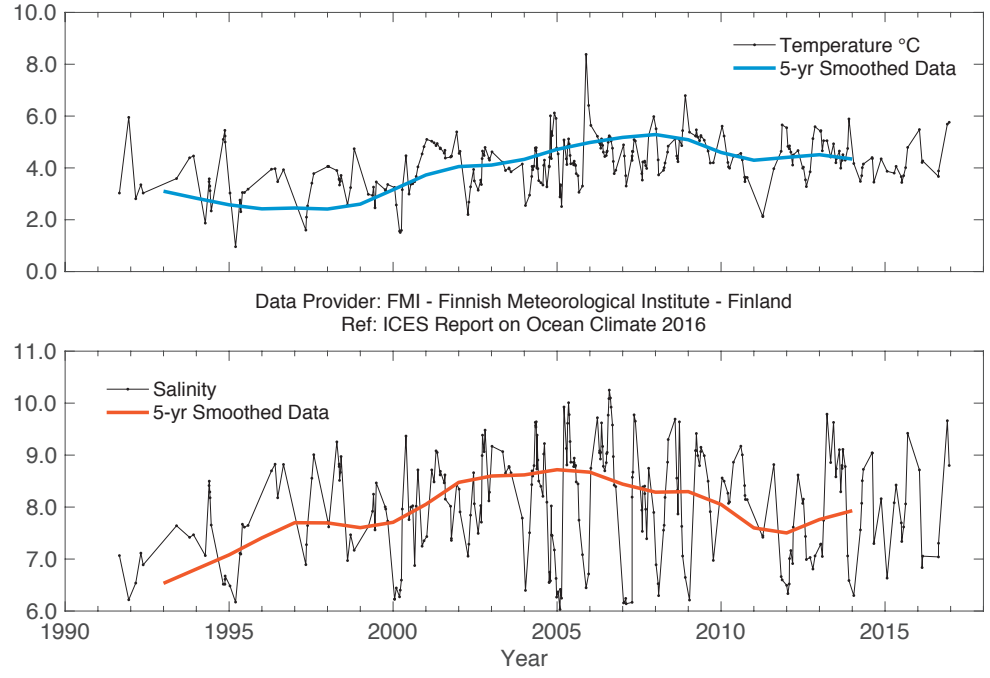

FIGURE 75.
Skagerrak, Kattegat, and the Baltic. Temperature (upper panel) and salinity (lower panel) at Station LL7 in the Gulf of Finland.

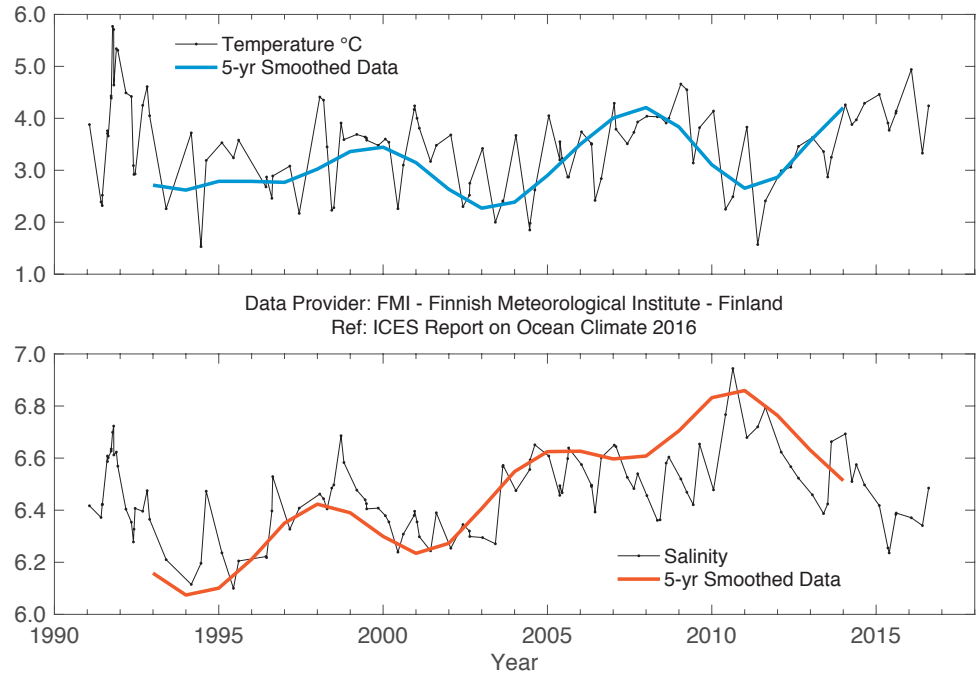

FIGURE 76.
Skagerrak, Kattegat, and the Baltic. Temperature (upper panel) and salinity (lower panel) at Station SR5 in the Bothnian Sea.

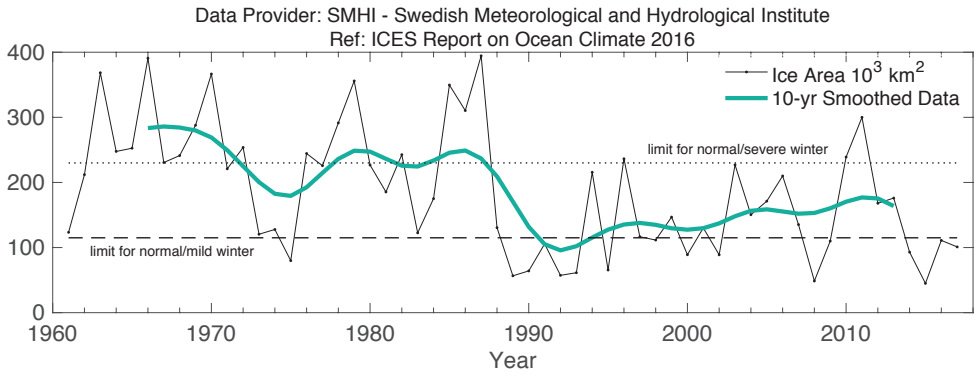

FIGURE 77.
Skagerrak, Kattegat, and the Baltic. The maximum ice extent in the Baltic, starting from 1957.

4.20 NORWEGIAN SEA

The Norwegian Sea is characterized by warm AW on the eastern side and cold Arctic water on the western side, separated by the Arctic front (Figure 78). AW enters the Norwegian Sea through the Faroe-Shetland Channel and between the Faroes and Iceland via the Faroe Front. A smaller branch, the North Icelandic Irminger Current, enters the Nordic seas on the western side of Iceland. AW flows north as the Norwegian Atlantic Current, which splits when it reaches northern Norway; some enters the Barents Sea, whereas the rest continues north into the Arctic Ocean as the West Spitsbergen Current (WSC).

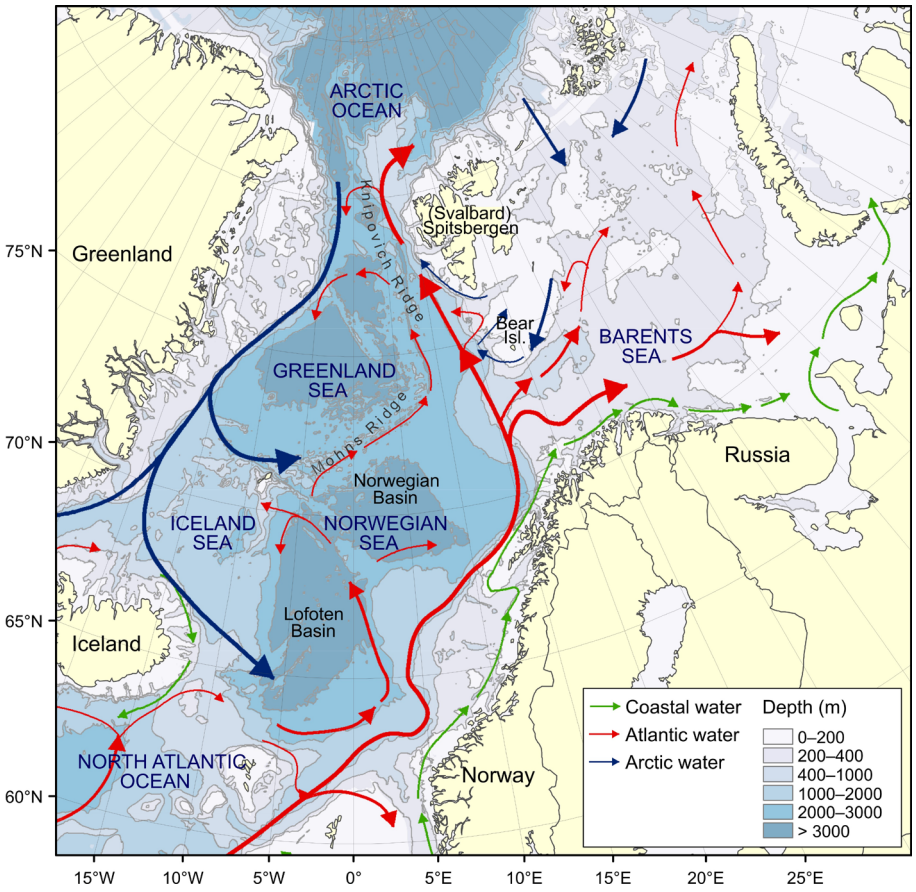

FIGURE 78.
Circulation schematic for the Norwegian Sea, Barents Sea, and Fram Strait. Red lines show the poleward movement of Atlantic water (AW). Blue lines show the circulation of Arctic water. Green lines show the circulation of coastal waters.

Record-high heat content in the Norwegian Sea.

Three sections from south to north in the eastern Norwegian Sea demonstrate the development of temperature and salinity in the core of the AW at Svinøy-NW (Figure 79), Gimsøy-NW (Figure 81), and Sørkapp-W (Figure 82). In general, there has been an increase in temperature and salinity in all three sections since the mid-1990s, except for the most recent years when both temperature and salinity declined. In 2016, salinity decreased to normal values except for the northernmost section where it was still higher than normal. Temperature was still higher than the long-term averages in all three sections. Annual temperature averages in 2016 were 0.3°C above the long-term mean at the Svinøy section, and 0.7°C above the long-term means at both the Gimsøy and Sørkapp sections. Annual salinity averages in 2016 were 0.03 below the long-term mean at the Svinøy section, while it was 0.01 and 0.05 above the long-term means at the Gimsøy and Sørkapp sections, respectively.

Using hydrographic data from spring 1951, the ocean heat and freshwater content of AW describes the climate variability in the Norwegian Sea. Since 2000, the heat content in the Norwegian Sea has been above the long-term mean and was record-high in 2016. The freshwater content increased from 2010 until 2016 when it decreased and remained considerably lower than the long-term mean.

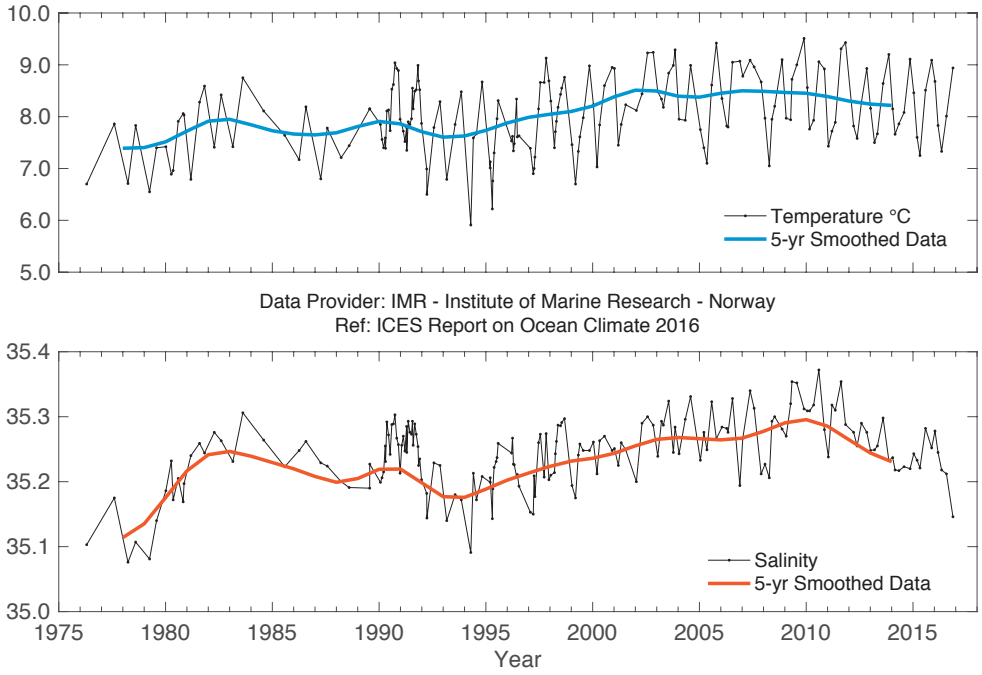

FIGURE 79.
Norwegian Sea. Temperature (upper panel) and salinity (lower panel) above the slope at the Svinøy section (63°N).

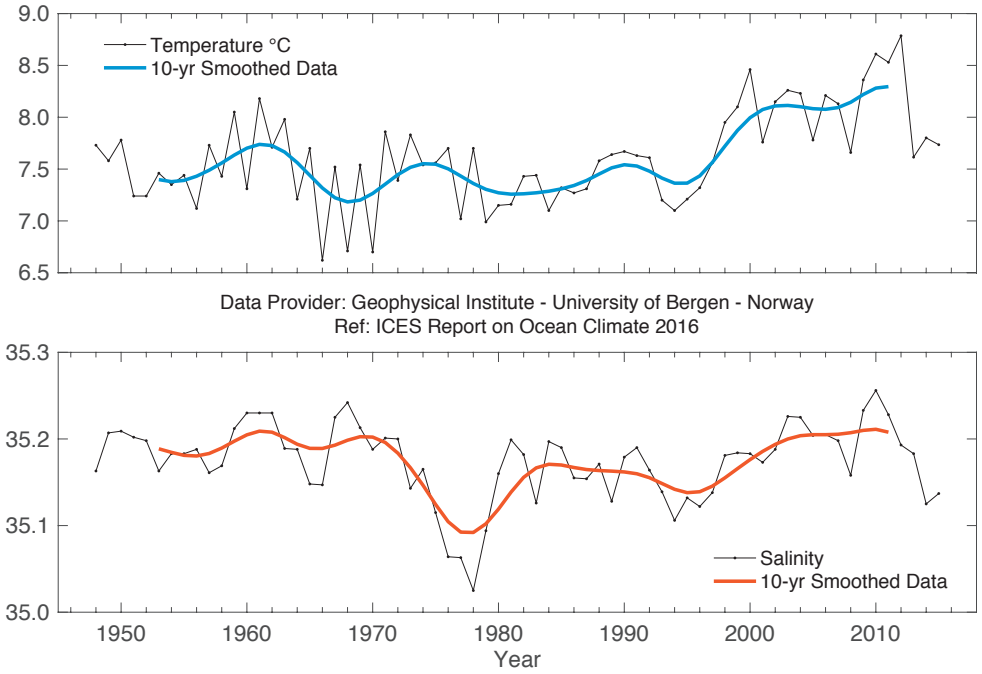

FIGURE 80.
Norwegian Sea: Temperature (upper panel) and salinity (lower panel) at 50 m at Ocean Weather Station M (66°N 2°E). Data until 2015.

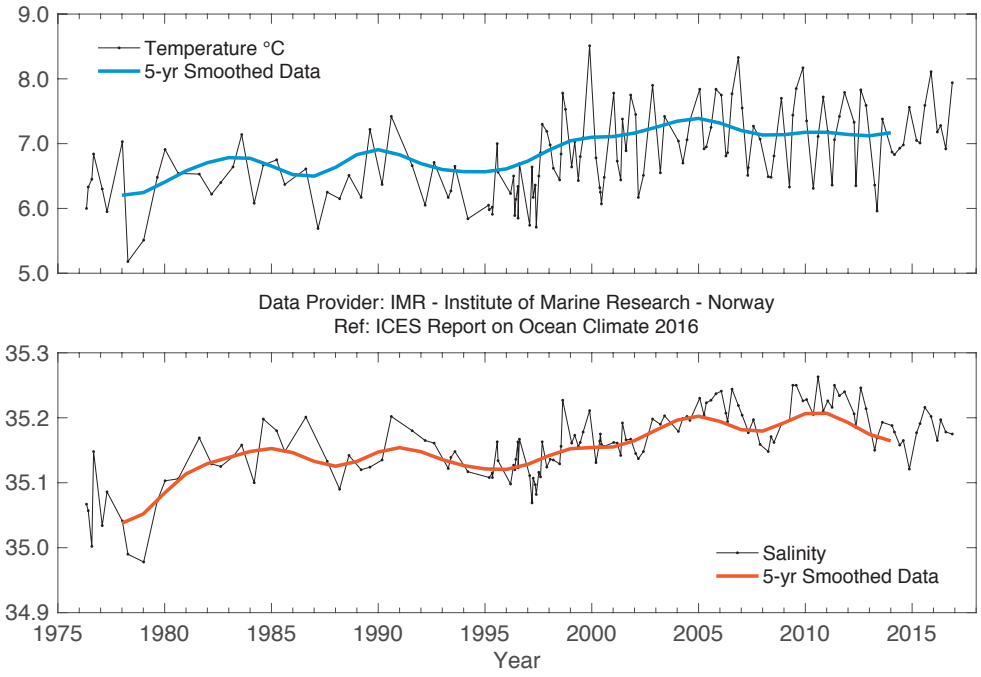

FIGURE 81.
Norwegian Sea. Temperature (upper panel) and salinity (lower panel) above the slope at the Gimsøy section (69°N).

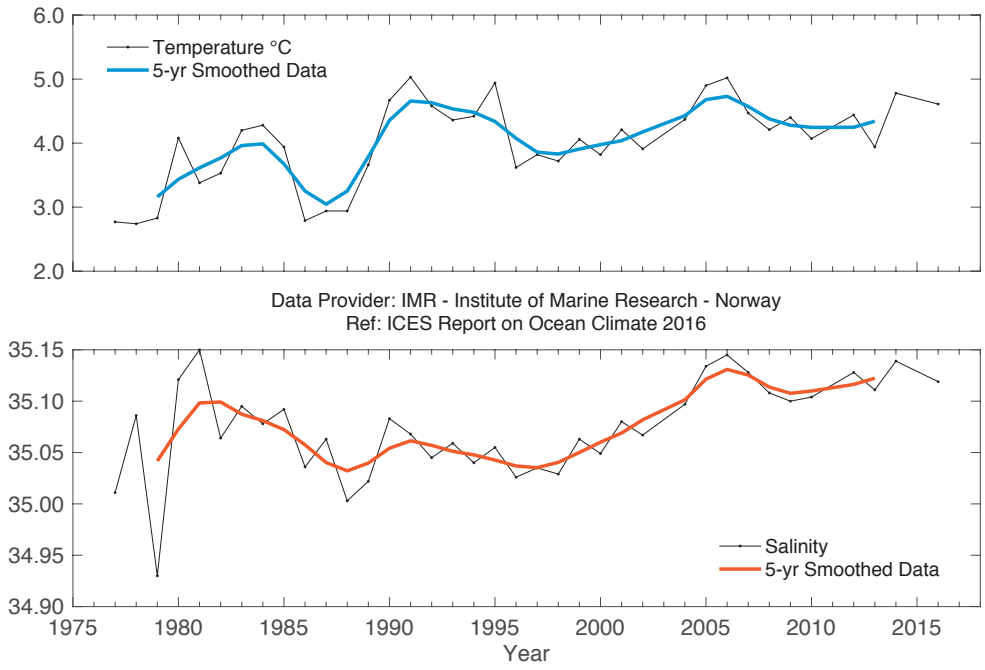

FIGURE 82.
Norwegian Sea. Temperature (upper panel) and salinity (lower panel) above the slope at the Sørkapp section (76°N).

4.21 BARENTS SEA

The Barents Sea is a shelf sea, receiving an inflow of warm AW from the west (Figure 78). The inflow demonstrates considerable seasonal and interannual fluctuations in volume and water mass properties, causing high variability in the heat content and ice coverage of the region.

In 1996 and 1997, after a period with high temperatures in the first half of the 1990s, temperatures in the Barents Sea dropped to values slightly below the long-term average. From March 1998, the temperature in the western Barents Sea increased to just above average, whereas the temperature in the eastern part remained below average during 1998. From the beginning of 1999, there was a rapid temperature increase in the western Barents Sea that also spread to the eastern part. Since then, the temperature has remained above average.

In 2016, air and water temperatures in the Barents Sea were still well above average and typical of anomalously warm years; the anomalies in the eastern part of the sea were larger than in the western one. In the Kola section (Figure 84), from January to May, the coastal and Atlantic waters were warmer than normal (by more than 1°C) and also when compared to 2015 (by up to 0.8°C). In some months, the water masses in the Kola section and air masses over the Barents Sea were the warmest since 1951. As a result, January–May averaged temperature in the Kola section was record-high in the coastal waters and as large as the 2012 record-high value in the Atlantic waters. In January–May 2016, the coastal waters in the Kola section were much fresher than average (by 0.21–0.27) and also when compared to 2015 (by 0.22–0.24). AW salinity in the central part of the section was also below normal, but with smaller anomalies (−0.06 to −0.14) for the first half of 2016, whereas in the outer part of the section, it was close to both the average and salinity in 2015.

From August until September 2016, the surface, deeper, and bottom waters were still much warmer (by 1.8°C, 1.5°C, and 1.6°C, respectively, on average over the surveyed area) than the long-term mean (1931–2010) over the entire Barents Sea. They were also warmer (by on average 1.1°C, 0.5°C, and 0.8°C, respectively) than in 2015 in most of the sea (in more than 70% of the surveyed area). The largest positive anomalies were observed in surface waters in the eastern and southeastern parts of the sea. From August until September, the surface and bottom waters were saltier (by 0.5 and up to 0.1, respectively) than the long-term mean (1931–2010) in most of the Barents Sea, with the largest positive anomalies at the surface in the northern sea and along the Novaya Zemlya Archipelago. In autumn 2016, the area covered by Atlantic waters (> 3°C) was the largest, whereas the areas covered by Arctic and cold bottom waters (< 3°C) were the smallest since 1965. In 2016, the ice coverage of the Barents Sea was still well below both the average (1951–2010) and the coverage in 2015. The 2016 annual mean ice extent and its monthly mean values, from March to July and in November and December, were the lowest since 1951. Furthermore, there was no ice in the Barents Sea from July to September (the first ice-free July since 1951).

Well above-average temperatures and record-low ice coverage in the Barents Sea in 2016.

The volume flux into the Barents Sea varies with periods of several years and was significantly lower from 1997 to 2002 than from 2003 to 2006. In 2006, the volume flux was at a maximum during winter and very low during autumn. After 2006, the inflow was relatively low for several years. The inflow increased during winter 2014/2015, and has been high since. Throughout 2015 and in winter 2015/2016, the inflow was ca. 1 Sv larger than the long-term average. The exception was March 2016, when the volume flux was temporarily smaller than average. The data series presently stops in May 2016; thus, no information about summer, autumn, or early winter 2016/2017 is available yet.

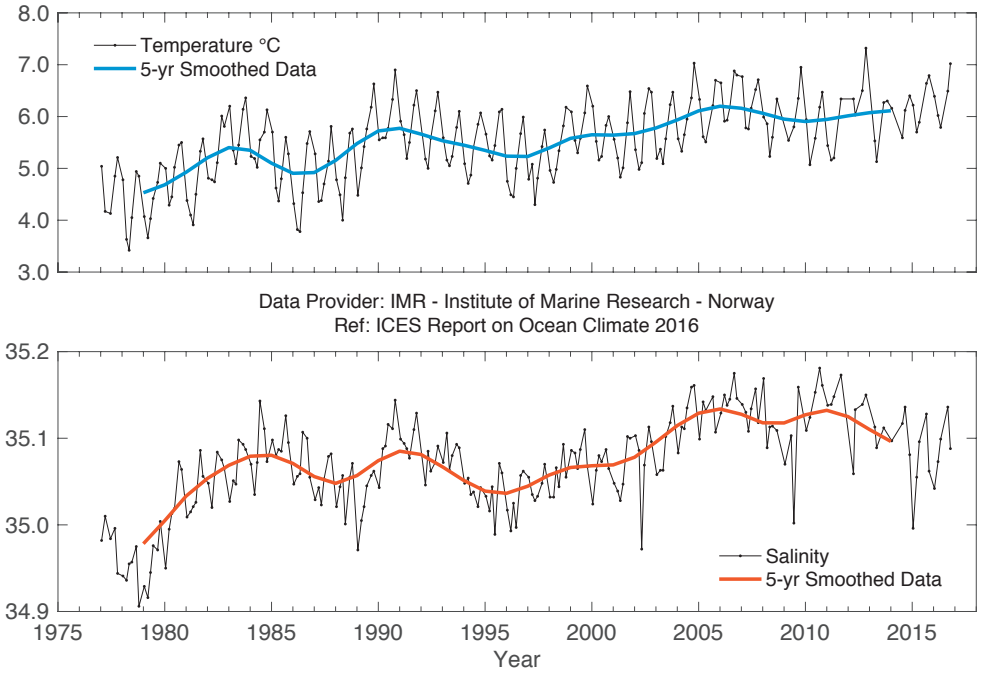

FIGURE 83.
Barents Sea. Temperature (upper panel) and salinity (lower panel) in the Fugløya–Bear Island section.

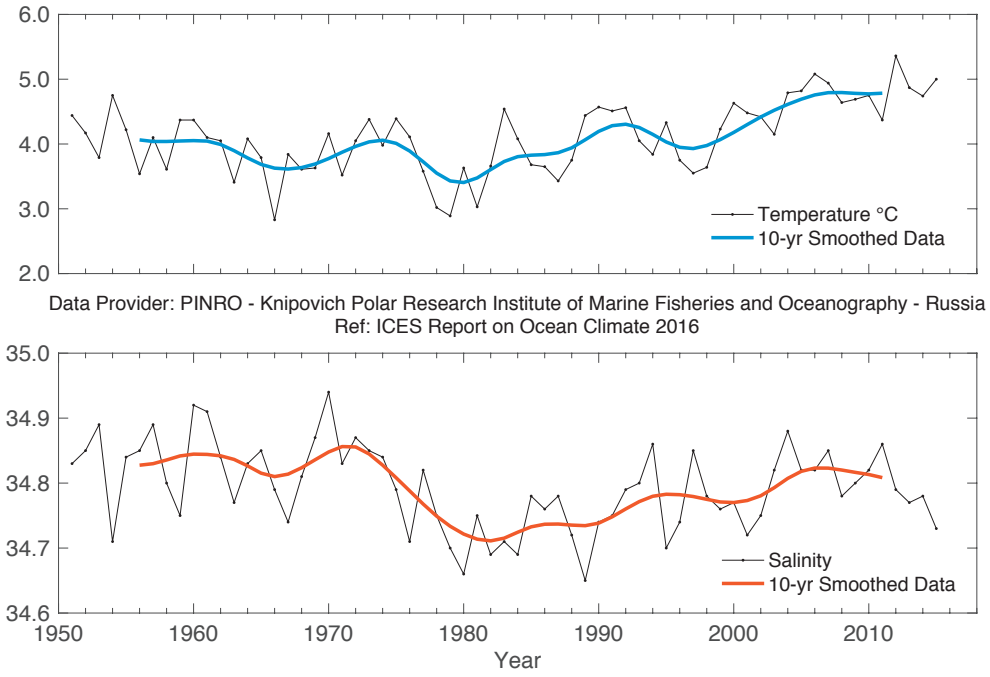

FIGURE 84.
Barents Sea. Temperature (upper panel) and salinity (lower panel) in the Kola section (0–200 m). Data until 2015.

4.22 FRAM STRAIT

The Fram Strait (Figure 78) is the northern border of the Nordic seas, its easternmost side lies within the Barents Sea ecoregion and its westernmost side lies within the Greenland Sea ecoregion. It is the only deep passage connecting the Arctic to the rest of the world ocean and one of the main routes whereby AW enters the Arctic (the other is the Barents Sea). AW is carried polewards by the WSC, and a significant part of the AW recirculates within the Fram Strait and returns southward (Return Atlantic water, RAW). Polar water from the Arctic Ocean flows south in the East Greenland Current (EGC) and affects water masses in the Nordic seas. AW temperature, volume, and heat fluxes exhibit strong seasonal and interannual variations.

The temperature of AW at the eastern rim of the Greenland Sea (along the 75°N section between 10° and 13°E) reached its highest value in 2005–2007, with a peak in 2006. After this period, AW temperature decreased significantly in 2008–2009 and remained below its long-term mean until 2011. In the following three years (2012–2014), the temperature of AW in the eastern Greenland Sea recovered and remained relatively stable, with values slightly exceeding the long-term mean (by 0.3°C). In 2015, the AW temperature increased further and reached 5.09°C (0.55°C warmer than average). A significant increase in the salinity of AW in the eastern Greenland Sea was observed in 2005–2006, with a maximum of 35.16 in 2006 (exceeding the long-term average by 0.07). This peak was followed by a sharp decrease in 2007 and further slow descent until 2009, when AW salinity returned to its long-term average. In 2010, salinity began to rise again and reached its second peak in 2012 (0.06 above its long-term mean). Since then, it has remained relatively steady, with a slight decrease in 2015 (down to 35.12, but still 0.03 above the long-term mean). Since 2004, the salinity of AW in the eastern Greenland Sea has been above its long-term average (except in 2009 when it leveled out). In 2016, both the temperature and salinity of AW in the eastern Greenland Sea were slightly lower than observed in 2015, but remained above their long-term averages (1988–2010).

The western and central part of the Greenland Sea section at 75°N has not been measured since 2010. The temperature of RAW at the western rim of the Greenland Sea reached its maximum in 2006 (2.9°C) and slowly decreased until the end of the observation period (2010). From 2008 until 2010, the temperature of RAW was slightly lower than its long-term average. The temperature maximum in 2006 was accompanied by a very strong peak in RAW salinity (0.13 above the long-term mean, more than threefold larger than the s.d. of RAW salinity). In 2007, the salinity of RAW dropped again and remained slightly higher than its long-term average until 2008. In 2009 and 2010, it decreased farther and was close to the average. Temperature and salinity in the upper layer of the central Greenland Basin, within the Greenland Gyre, were modified by the advection of AW, and by winter convection. The interface with enhanced temperature and salinity gradients has steadily descended (by more than 1000 m) since the beginning of measurements in 1993. After winter 2007/2008, a two-layer structure resulted from a mixed-layer type convection that supplied both salt and heat into the intermediate layers. In winter 2008/2009, almost half of the Greenland Sea had been shielded from convection because of the unusual western location of the Arctic Front (boundary between Atlantic and Greenland Sea waters).

In the southern Fram Strait, at the standard section along 76.50°N (at the level of 200 dbar, spatially averaged between 9° and 12°E), a record-high summer temperature for AW was observed in 2006 (maximum of 4.5°C, exceeding the long-term average by 1.3°C), accompanied by the highest AW salinity (35.13) in the observation period. After that peak, temperature and salinity decreased rapidly in 2007 and 2008 before increasing again in the summers from 2009 until 2012. From 2011 until 2015, the temperature of AW in the southern Fram Strait remained relatively constant (3.7–3.8°C, exceeding its average by ca. 0.6°C), except in summer 2013 when it dropped to 3.22°C and leveled out at its long-term mean value. In 2011, 2012, and 2014, AW salinity in the southern Fram Strait was the same (35.13) as during the 2006 maximum, exceeding its long-term mean by 0.07. Slight drops in salinity were found in 2013 and 2015, but since 2004, the salinity of AW has remained larger than its long-term mean value. In 2016, the temperature of AW increased compared to 2015 and reached its highest value over the last decade. AW salinity recovered in 2016 from its drop in the previous year.

In the northern Fram Strait, at the standard section along 78.83°N, three characteristic areas can be distinguished in relation to the main flows: the WSC between the shelf edge and 5°E, the Return Atlantic

Current (RAC) between 3°W and 5°E, and the polar water in the EGC between 3°W and the Greenland shelf. The spatially averaged mean temperature of the upper 500 m layer in the WSC reached its peak in 2006 (4.54°C) and decreased afterwards, varying from 2007 to 2011 within the range of ±0.4°C from the long-term average. In 2012 and 2013, the temperature in the WSC dropped further, reaching 0.7–0.8°C below its long-term mean. Since 2014, it has been rising again and in 2015 reached the second highest value in the observation period (4.24°C, exceeding the long-term mean by 1.13°C). In 2016, the temperature in the WSC dropped by about 0.7°C, but was still higher than its long-term average. The RAC temperature in 2016 remained close to the previous year and a temperature difference between the AW in the WSC and that recirculating in the RAC was only half of the 2015 value (0.7°C in 2016 compared to 1.5°C). The highest temperature in the RAC was observed in 2005 (3°C) and from 2009 until 2010 (slightly above 2.9°C). From 2011, it remained close to the long-term average of 2.2°C. Since 2013, the RAC temperature has increased slowly and reached 2.8°C in 2016. In the EGC domain, temperature reached its peak in 2007 (1.9°C), decreased significantly to 0.3°C in 2008, and has since remained relatively stable (within ±0.3°C of its long-term mean), with a slight decrease to 0.3°C in 2014 and a return to 1.0°C in 2015. In 2016, the EGC temperature was slightly higher than in the previous year. The highest salinity in the upper 500 m in the WSC was observed in 2006 (35.11), followed by a decrease to the long-term average from 2007 until 2008. Since 2009, the WSC salinity was increasing again until reaching 0.5 above the long-term mean in 2011. After a slight decrease in 2012 and 2013, salinity in the WSC reached its second maximum (35.09) in 2014, followed by slightly lower values in 2015 and 2016. The maximum salinity in the RAC was observed in 2010; in subsequent years (2011, 2012, and 2014), it exceeded its long-term mean by about 0.05, leveled out in 2015, and increased again in 2016. The salinity in the EGC was highest in 2007 (34.90) and dropped afterwards below its long-term average, except for an intermediate peak (34.72) in 2011. In 2008 and 2014, the EGC salinity reached the lowest value during the last decade (34.50 compared to the record-low of 34.45 observed in 2000 and 2002). Since 2014, salinity has steadily increased, and in 2016 was slightly above its long-term mean.

The temperature of the Atlantic inflow in the eastern Greenland Sea and Fram Strait increased from 2012 to 2015 and then decreased slightly in 2016. Over the last decade, it has remained below the 2006 maximum. In 2016, salinity of the Atlantic inflow to the Arctic Ocean slightly decreased compared to 2015, but it has consistently stayed above its long-term average over the last decade. The temperature of recirculating Atlantic water in Fram Strait, flowing westward and ultimately to the south, was rising slowly between 2013 and 2016, while salinity in 2016 recovered from a slight drop in the previous year.

In 2016, the AW at the standard section along 78.83°N occupied the core of the WSC at a much shallower level than in 2015. In 2016, the isotherm of 2°C reached down to 500–600 m in the WSC core located over the upper shelf slope, while one year earlier, it was found at a depth of about 800 m. In the offshore branch of the WSC located over the lower shelf slope, the AW layer was deeper in 2016, with the isotherm of 2°C found at a depth of about 400–500 m compared to about 300 m in 2015. The low salinity surface layer covering the upper 50 m of the WSC in 2015 was absent in 2016.

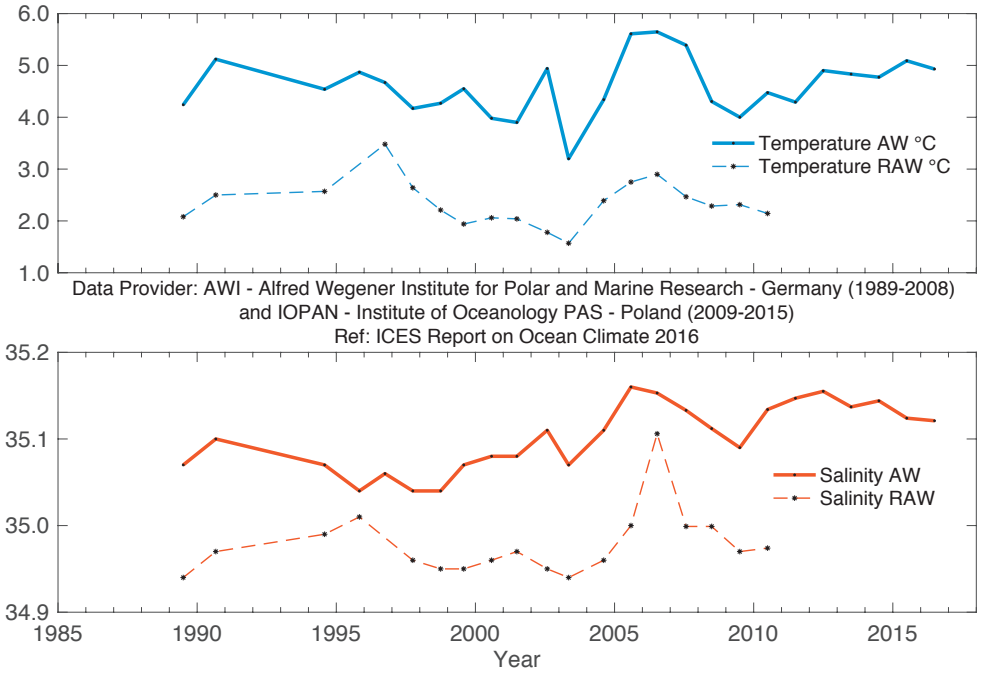

FIGURE 85.
Greenland Sea and Fram Strait. Temperature (upper panel) and salinity (lower panel) of Atlantic water (AW) and Return Atlantic water (RAW) in the Greenland Sea section at 75°N. AW properties are 50–150 m averages at 10–13°E. The RAW is characterized by temperature and salinity maxima below 50 m, averaged over three stations west of 11.5°W.

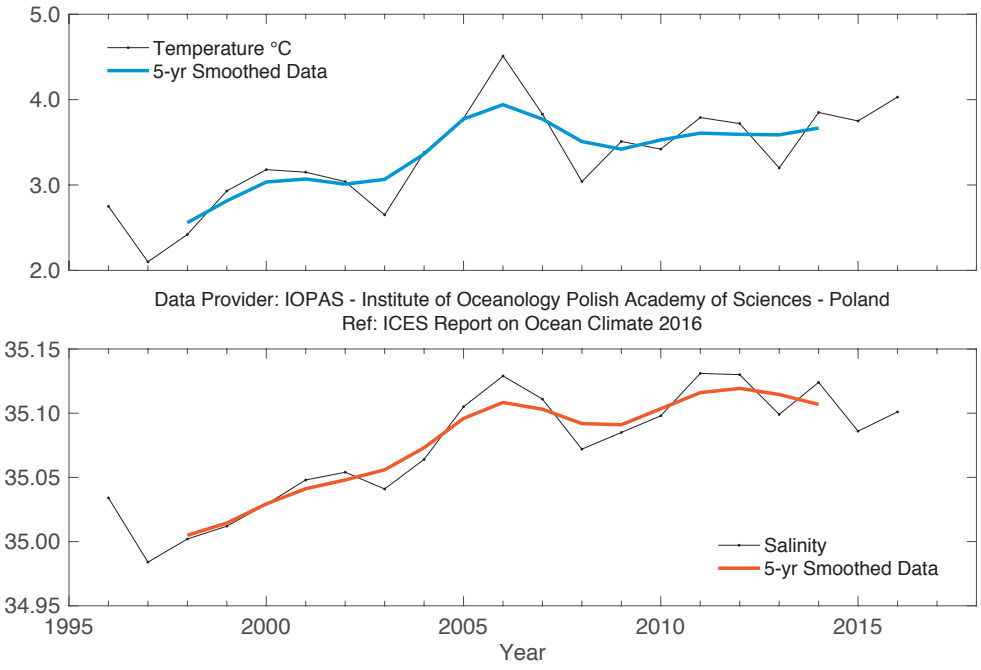

FIGURE 86.
Greenland Sea and Fram Strait. Temperature (upper panel) and salinity (lower panel) at 200 dbar in the southern Spitsbergen section (76.50°N).

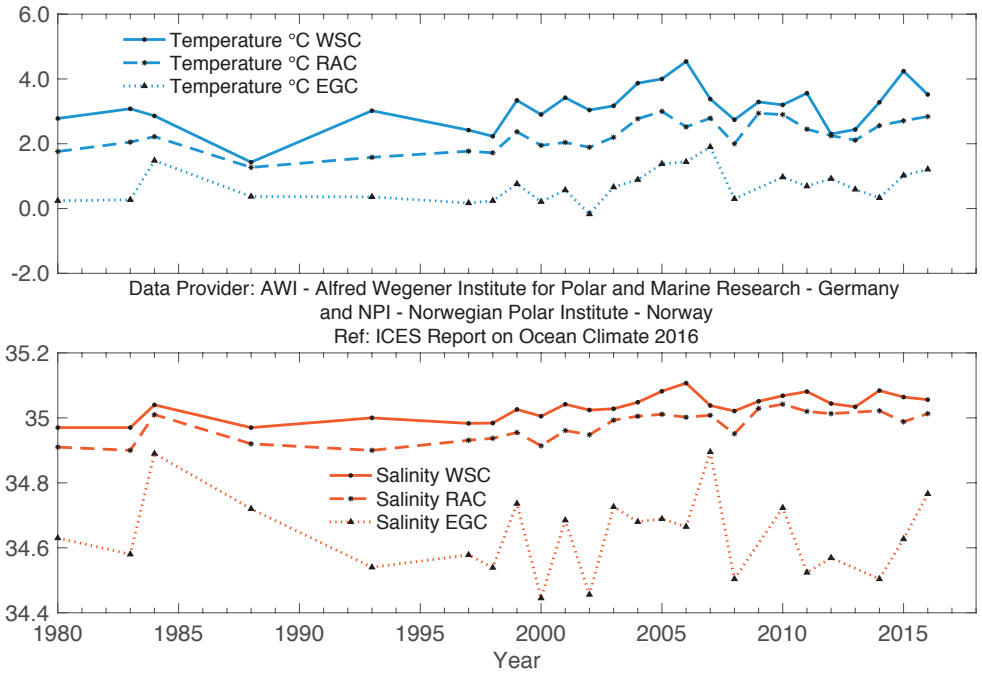

FIGURE 87.
Greenland Sea and Fram Strait. Temperature (upper panel) and salinity (lower panel) in Fram Strait (78.83°N) at 50–500 m: in the Atlantic water (AW) in the West Spitsbergen Current (WSC; between the shelf edge and 5°E), in the Return Atlantic Current (RAC; between 3°W and 5°E), and in the polar water in the East Greenland Current (EGC; between 3°W and the Greenland Shelf).

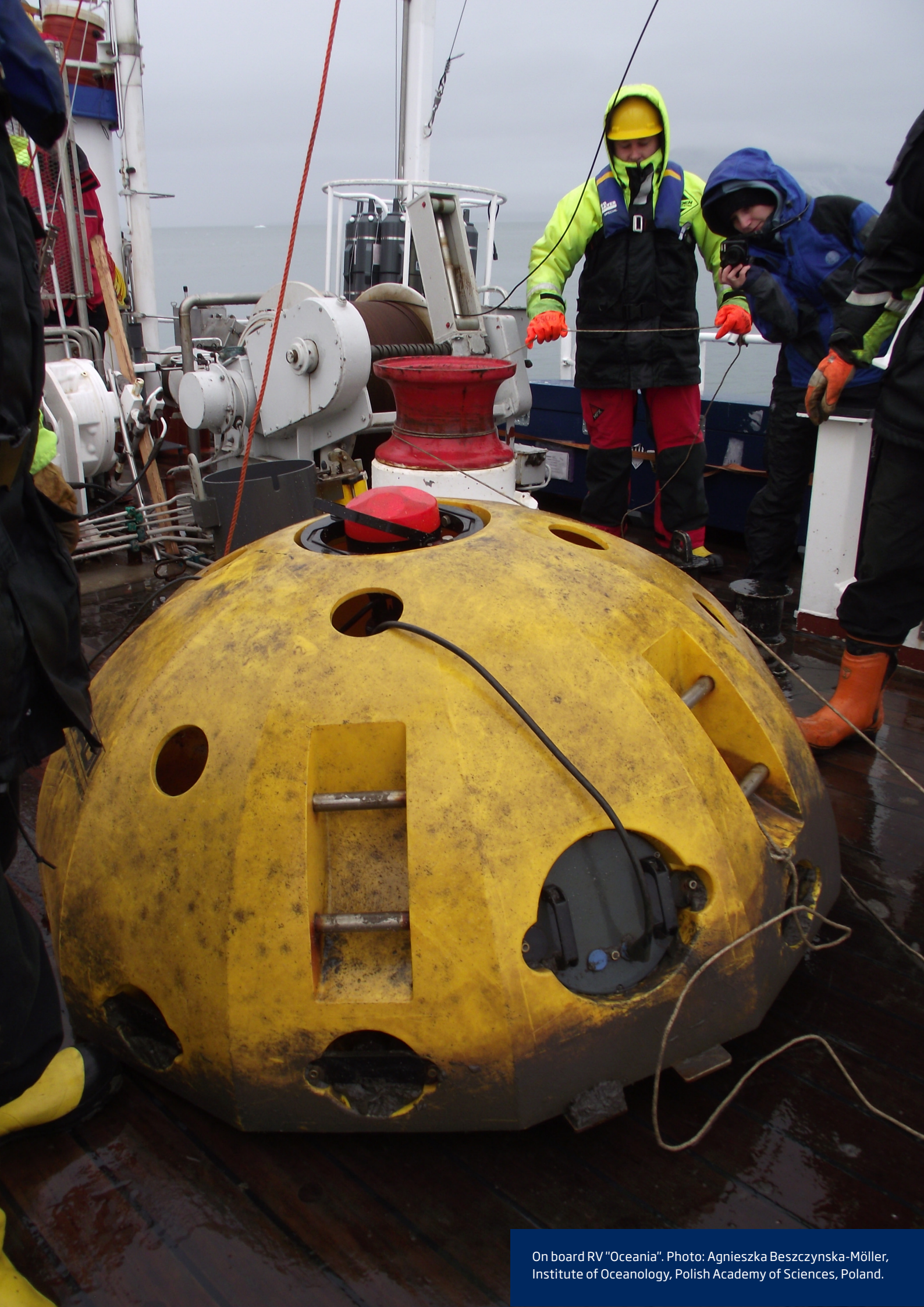

On board RV "Oceania". Photo: Agnieszka Beszczynska-Möller, Institute of Oceanology, Polish Academy of Sciences, Poland.

5. DETAILED AREA DESCRIPTIONS, PART II: DEEP OCEAN

5.1 INTRODUCTION

In this section, we focus on the deeper waters of the Nordic seas and the North Atlantic, typically below 1000 m. The general circulation scheme and dominant water masses are given in Figure 88.

At the northern boundary of our region of interest, the cold and dense outflow from the Arctic Ocean enters Fram Strait along its western side and reaches the Greenland Sea. The outflow is a mixture of Eurasian Basin and Canadian Basin deep waters and upper polar deep water (UPDW). The Eurasian deep water feeds the densest water of all Nordic seas: the Greenland Sea bottom water. The Canadian Basin deep water and UPDW supply the Arctic intermediate water in the Greenland Sea, and the UPDW also includes products of the winter convection. The deep southward outflow from the North Atlantic in the deep western boundary current is fed by the cold and dense overflow waters. The deepest and densest is the Denmark Strait overflow water (DSOW). This water mass originates in the Arctic intermediate water produced in the Greenland and Iceland seas by winter convection and mixing with surrounding water masses. The DSOW sinks to the bottom as it passes over the Denmark Strait sill, vigorously entraining ambient water. Downstream, it is overlain by an intermediate water mass LSW formed by deep winter convection in the Labrador Sea. The middle layer of the deep, cold water export in the deep western boundary current is supplied by the Iceland–Scotland overflow water (ISOW), originating in water masses formed in the Norwegian Sea (Arctic intermediate water and Norwegian Sea deep water). Passing through the Iceland Basin, the ISOW also entrains upper ocean water and LSW. The deep Antarctic bottom water enters the North Atlantic on the western side, but its signature is also present in eastern Atlantic abyssal basins. At intermediate levels, the Mediterranean water (MW) originates from vigorous mixing of Atlantic central waters and Mediterranean outflow waters at the Gulf of Cadiz. This water mass spreads at about 1000 m depth in all directions, with a main vein progressing northward along the European margin. Around the Canaries, the MW encounters the northern limit of AAIW.

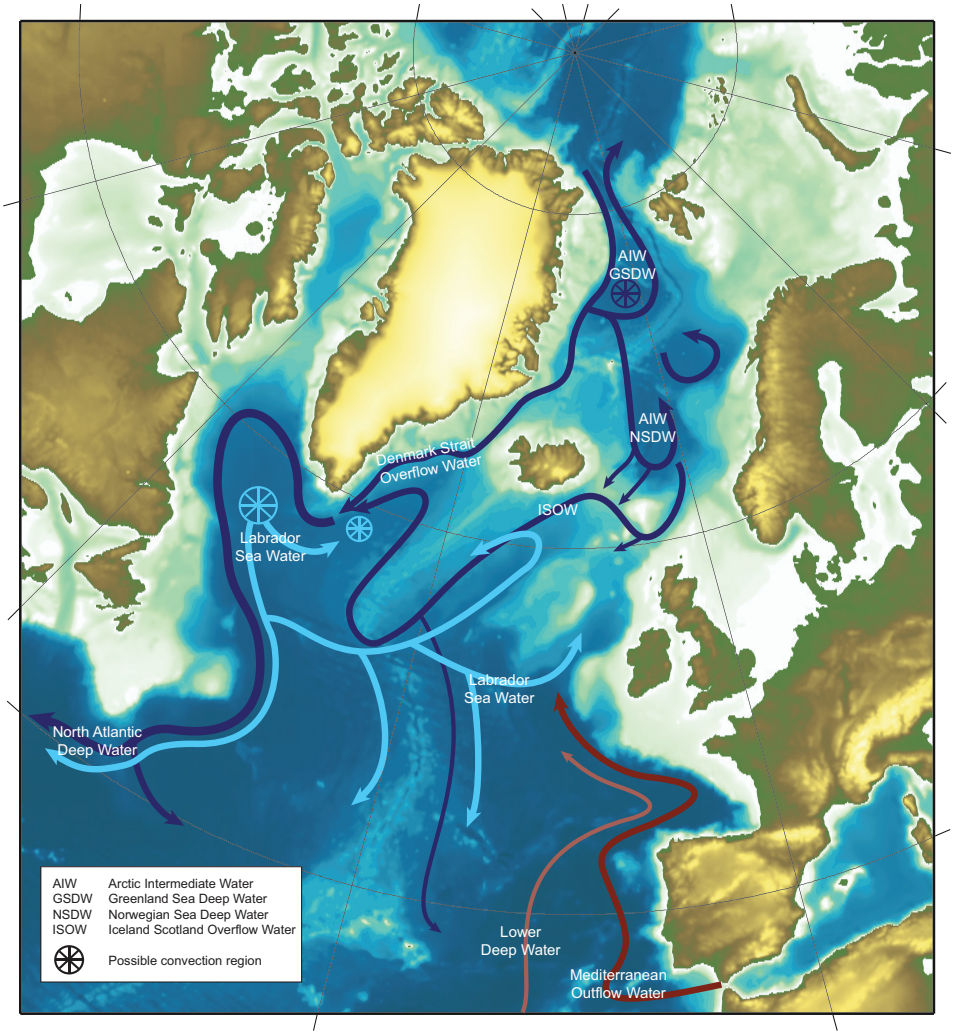

FIGURE 88.
Schematic circulation of the intermediate-to-deep waters in the Nordic seas and North Atlantic.

5.2 NORDIC SEAS DEEP WATERS

The deep waters of the Greenland, Iceland, and Norwegian seas are all warming. The source of the warming is the deep outflow from the Arctic Ocean, a southward flowing current of the Eurasian and Canadian Basin deep waters, and the UPDW found on the western side of Fram Strait at ca. 2000 m depth. The Greenland Sea deep water (GSDW) is warming fastest owing to its direct contact with this Arctic outflow, whereas the Iceland and Norwegian seas are warming more slowly because they are products of the mixing of their own ambient waters with GSDW and Arctic outflow water.

5.2.1 Greenland Sea

Continuous warming has been observed in the Greenland Sea deep layer at 3000 m since the beginning of observations in 1993. A similar rate of warming was found in the centre of the Greenland Sea Gyre (data only until 2010) and in the eastern Greenland Sea at 5°E (data only from 2002), with a long-term mean of 0.012°C year^{-1}. In the Greenland Sea Gyre, the continuous warming was accompanied by a nearly continuous increase in salinity, while in the eastern Greenland Sea, strong interannual variability was superimposed on the long-term positive trend. In 2016, temperature at a depth of 3000 m in the eastern Greenland Sea increased by 0.022°C compared to 2015 and reached −0.89°C, but a small salinity drop was found in 2016 after five years of slow increase and relatively high salinity observed in 2015.

The long-term development of stratification in the Greenland Sea indicates that the doming structure in the Greenland Sea Gyre has been replaced by a two-layered water mass arrangement, after a cessation of deep convection. Since measurements began in 1993, the winter convection depth has varied between 700 and 1600 m and has only been significantly deeper in small-scale convective eddies. In winter 2007/2008, the maximum convection depth was estimated to be 1700 m, similar to the maxima observed during 2001/2002 and 2002/2003. In summer 2009, the usual relatively homogeneous pool, mixed by previous winter convection, was replaced by a bipolar distribution of water masses, with higher salinity in the western part of the gyre and fresher waters in the eastern part. This made it difficult to compose a reliable mean profile for the gyre centre and, consequently, because of the lack of a 2009 mean profile for comparison with the 2010 mean profile, it was not possible to provide

an unambiguous estimate of the convection depth in winter 2009/2010. Therefore, two possible convection depths were obtained, depending on which 2009 mean profile is chosen. Since 2011, no measurements have been collected in the GSDW and development of the convection depth in the Greenland Sea Gyre has not been updated.

The import of warm and saline AW to the Greenland Sea is currently not balanced by an import of cool and fresh polar water from the north. The AW, which dominates changes in the upper ocean, took over the role of former ice production as a source of salt and densification in the context of winter convection. The input of AW tends to prevent ice formation and to vertically homogenize the waters ventilated by convective processes. The GSDW formerly included a small admixture of surface freshwater through the convective process and, therefore, had a lower salinity than the Arctic outflow waters. The observed increase in GSDW salinity may be the result of an adjustment to the Arctic outflow in the continued absence of deep convection and an increased presence of AW in the upper layer.

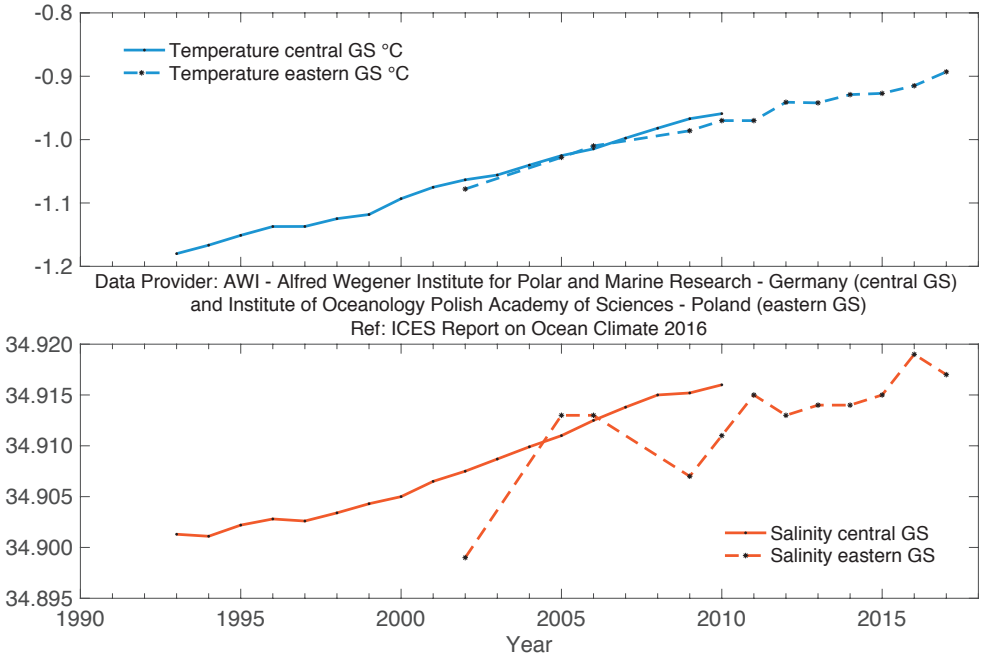

FIGURE 89.
Greenland Sea and Fram Strait. Temperature (upper panel) and salinity (lower panel) at 3000 m in the Greenland Sea Section at 75°N (solid line: in the central Greenland Sea Gyre; dashed line: in the eastern Greenland Sea at 5°E).

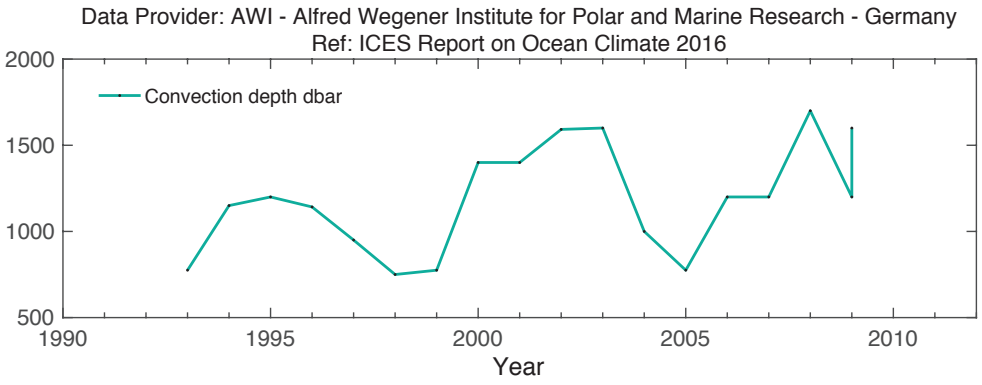

FIGURE 90.
Greenland Sea and Fram Strait. Winter convection depths in the Greenland Sea section at 75°N (data to 2009; note that due to the ambiguous convection depth in winter 2009/2010, two values are provided for this period).

5.2.2 Norwegian Sea

The longest time-series in the Nordic seas is from the Ocean Weather Ship M in the Norwegian Sea. It reveals warming from the mid-1980s; however, a slight decrease in temperature occurred from 2010 to 2011 and again from 2014 to 2015.

In 2016, the temperature at 2000 m increased to −0.78°C, consistent with the warming trend of recent decades. The long-term warming rate for the last decade is 0.08°C, similar to the Iceland Sea, but lower than in the Greenland Sea.

It is unclear whether there has been any corresponding salinity trend in the Norwegian Sea deep waters in recent decades. After a slight decrease in the early 1990s, salinity in Norwegian Sea deep basins has remained relatively stable over the 2000s until 2016, but with a record-low value in 2012.

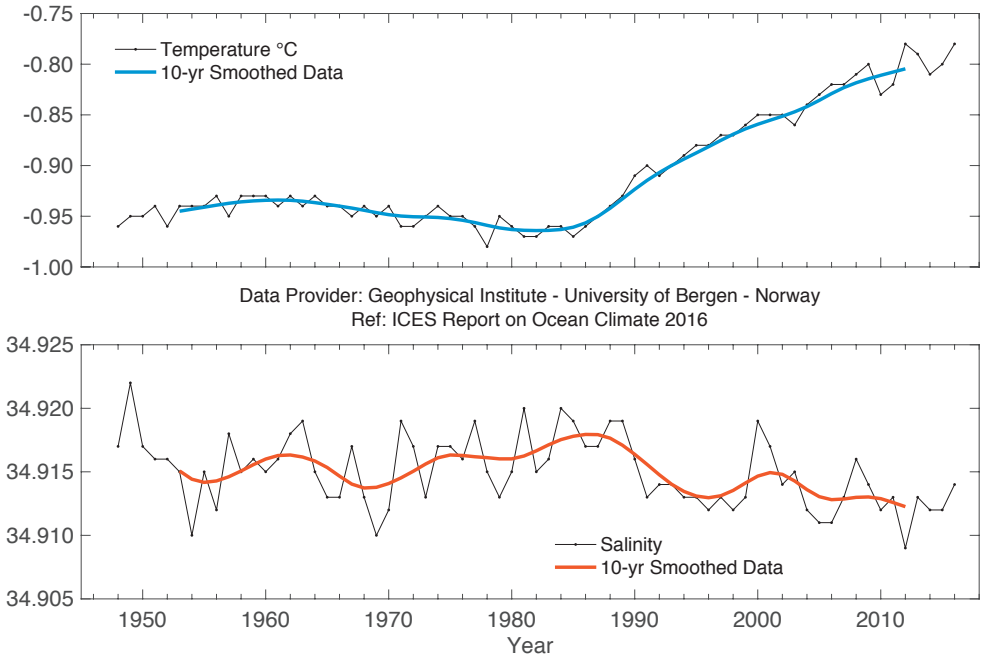

FIGURE 91.
Norwegian Sea. Temperature (upper panel) and salinity (lower panel) at 2000 m at Ocean Weather Station M (66°N 2°E).

5.2.3 Iceland Sea

In the Iceland Sea, an increase in temperature in the depth range 1500–1800 m has been observed since the beginning of the time-series (early 1990s), and the temperature continued to rise slowly until the end of 2016. The long-term warming rate for the last decade is 0.063°C. Salinity has been fairly constant since the late 1990s, but increased slightly in 2016.

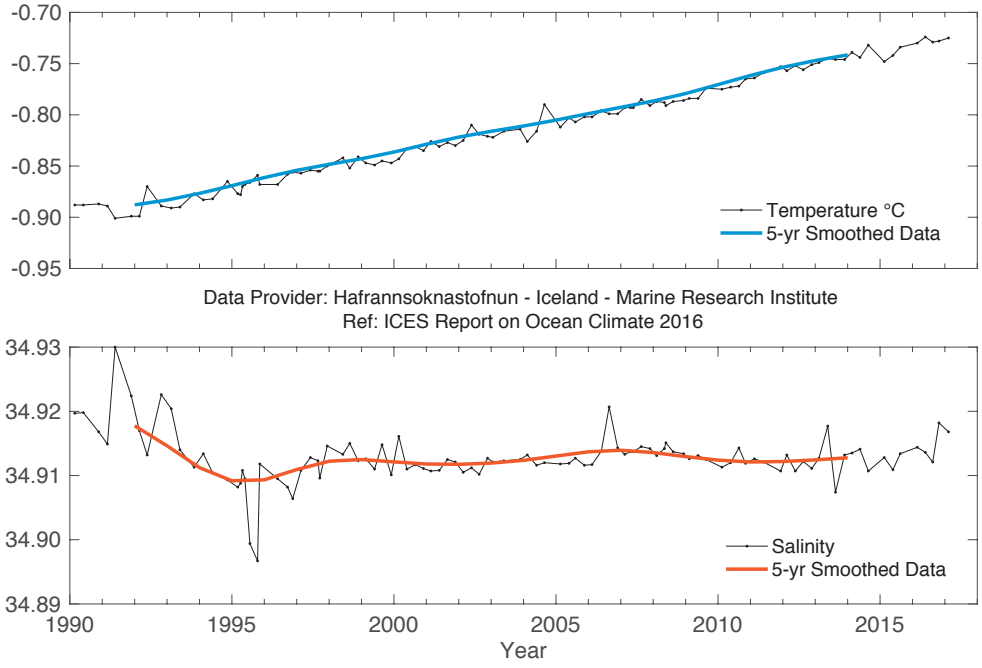

FIGURE 92.
Icelandic waters. Temperature (upper panel) and salinity (lower panel) at 1500–1800 m in the Iceland Sea (68.00°N 12.67°W).

5.3 NORTH ATLANTIC DEEP WATERS

5.3.1 Greenland-Scotland Ridge overflow waters

In the deep layers of the Faroe–Shetland Channel, the properties at 800 m are the same as those of Norwegian Sea deep water as it passes through the Channel back into the North Atlantic.

The temperature at this depth has relatively strong variability, but the overall trend was of decreasing temperature from the 1950s to the 1990s. There has been an increasing trend in temperature since 1995, but it still remains lower than the highest values observed in the 1950s, 1960s, and early 1980s. The relatively stable salinity in the first period of measurements (1950–mid-1970s) was followed by a slow decline. The lowest annual mean salinity values were observed in 1997, after which there has been a slow but gradual increase in salinity.

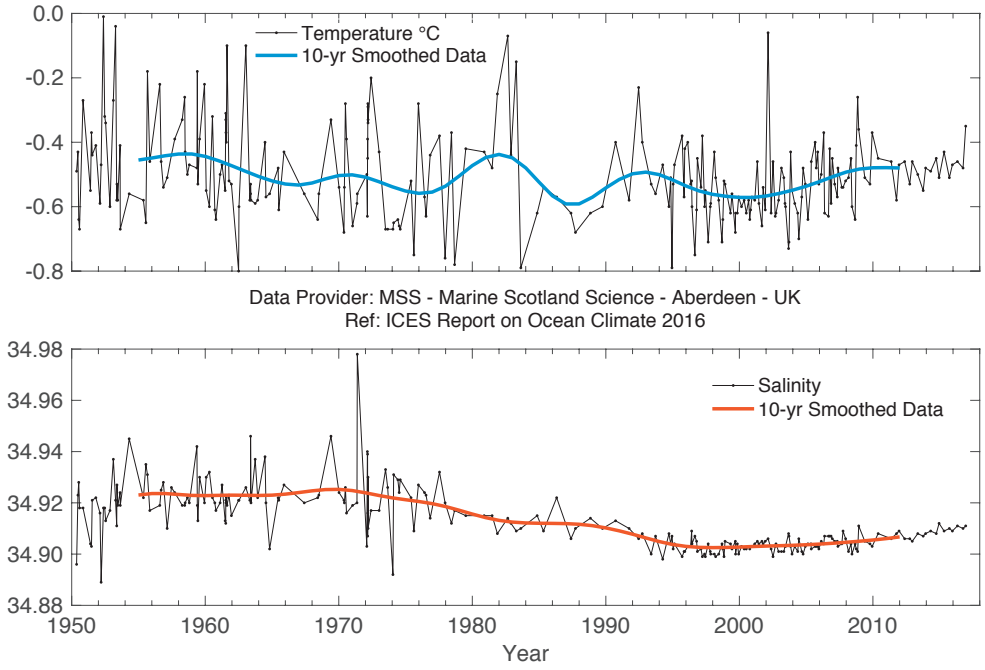

FIGURE 93.
Faroe-Shetland Channel. Temperature (upper panel) and salinity (lower panel) at 800 m.

5.3.2 Iceland Basin

After the Norwegian Sea deep water flows through the Faroe–Shetland Channel and Faroe Bank Channel into the Iceland Basin, it becomes known as the ISOW. The dense water, supplemented by a small amount of additional flow over the sill between Iceland and the Faroes, mixes rapidly with the upper ocean and intermediate water of the Iceland Basin, entraining the lighter water and increasing the volume of the overflow plume. The properties of the ISOW measured at 20°W in the Iceland Basin, therefore, become a product of the properties of the dense water at the sill and the entrained ambient water. The ISOW temperature and salinity vary closely with the LSW and upper ocean water in the Iceland Basin; since 1996, the water has warmed and increased in salinity, though there has been a slight decrease in both since 2011.

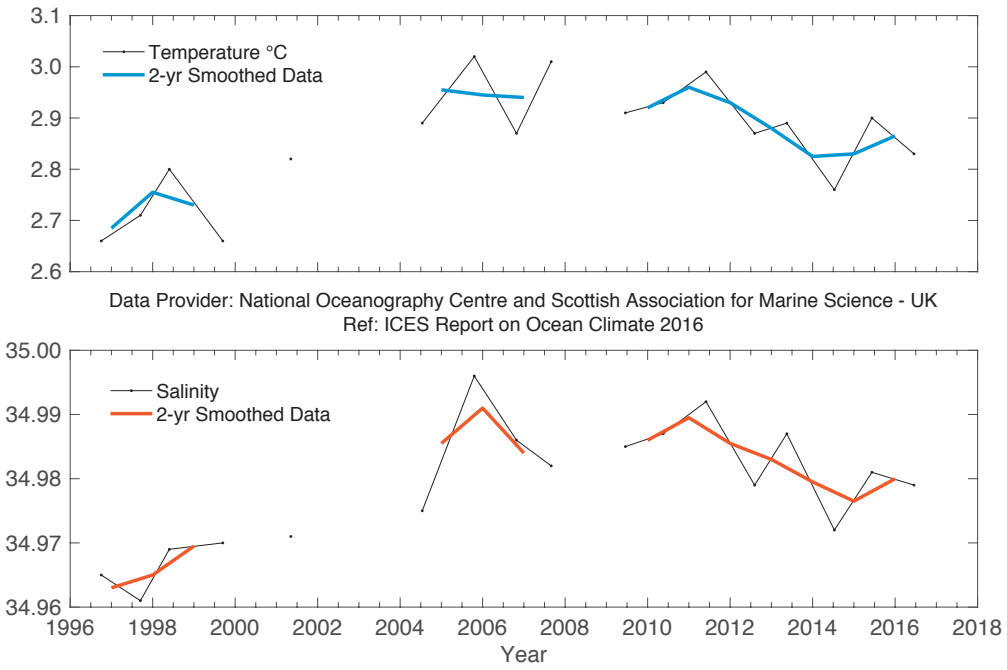

FIGURE 94.
Iceland Basin. Temperature (upper panel) and salinity (lower panel) of Iceland-Scotland Overflow Water (ISOW) (σ_θ > 27.85 kg m^{-3}, ca. 2000–2600 m).

5.3.3 Irminger Basin

Salinity and potential temperature of the DSOW near Cape Farewell showed correlated interannual variations between 1991 and 2007 (correlation = 0.75). However, since 2007, variations in temperature and salinity of the DSOW were less correlated. This continued to be the case in 2016, implying that < 30% of the variance in the salinity can be explained by the variance of the temperature variability. Density of the DSOW hardly changes at long time-scales. Measurements with moored instrumentation have demonstrated that temperature and density mainly vary at an annual time-scale, possibly forced by wind-driven processes near Denmark Strait. In 2016, the temperature of DSOW was 0.049°C below the long-term mean; however, salinity continued to increase and was 0.024 above the mean.

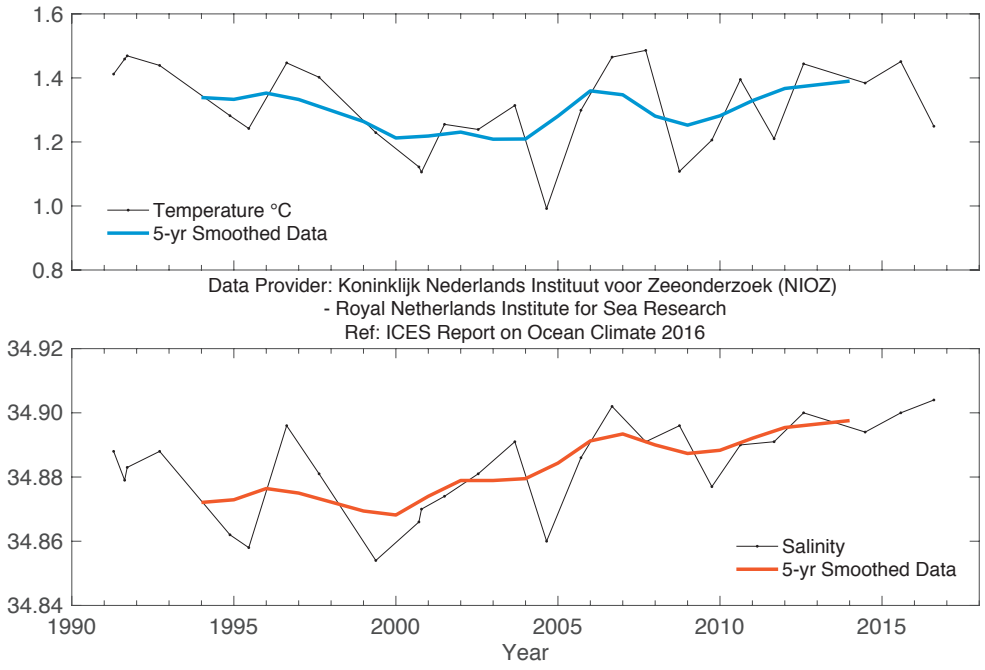

FIGURE 95.
Irminger Sea. Temperature (upper panel) and salinity (lower panel) in Denmark Strait overflow water (DSOW) on the East Greenland slope.

5.3.4 Labrador Basin

The properties of the North Atlantic deep water (NADW) in the deep boundary current west of Greenland are monitored at 2000 m depth at Cape Desolation Station 3. The temperature and salinity of this water mass underwent strong interannual variability during the 1980s. From the beginning of the 1990s, both characteristics were decreasing and reached their minimum values in 1998 and 1997, respectively. After that, the temperature of the NADW revealed a positive trend until 2014, whereas its salinity rather stagnated between 2007 and 2014. In 2016, temperature increased and salinity stagnated and were 0.1°C and 0.02, respectively, above the long-term means.

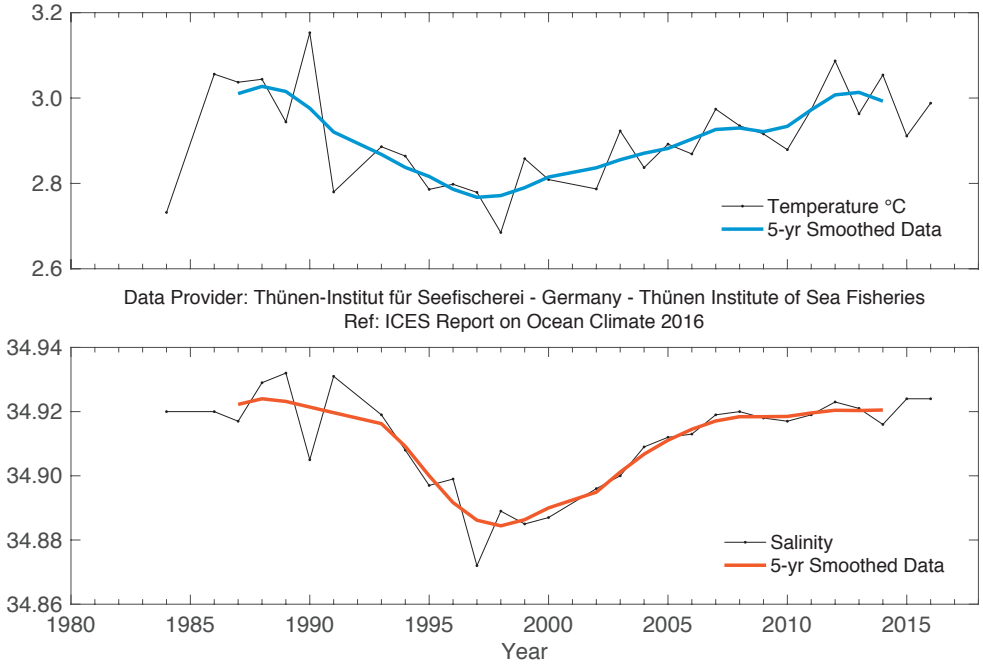

FIGURE 96.
West Greenland. Temperature (upper panel) and salinity (lower panel) at 2000 m water depth at Cape Desolation Station 3 (60.47°N 50.00°W).

5.3.5 Western Iberian margin

Hydrography and biogeochemistry at western Iberia and Biscay has been monitored for the entire water depth (> 5500 m) since 2003 by a repeated section programme that supplements the monthly monitoring of the upper ocean in the area. Cruises were carried out semi-annually from 2003 until 2010 and annually after that. The Finisterre section, ca. 400 km, begins west of the Iberian Peninsula (43.0°N 9.3°W) and reaches the centre of the Iberian Abyssal Plain (43.0°N 15.5°W).

The Finisterre section provides information about upper, intermediate, and deep waters. A depth of 2000 m corresponds to the core of LSW and the base of the permanent thermocline, so this is considered the limit of intermediate waters. The abyssal waters in this basin are NADW (comprised of a mixture of all Arctic water masses) and what is known as lower deep water that presents a signature of waters with Antarctic origin. Interannual variability of these abyssal waters within the monitored period has been weak, with interannual swings below 0.1°C and 0.01 in salinity. No trends have been observed. The 2016 potential temperature was slightly above the long-term average and salinity was slightly below.

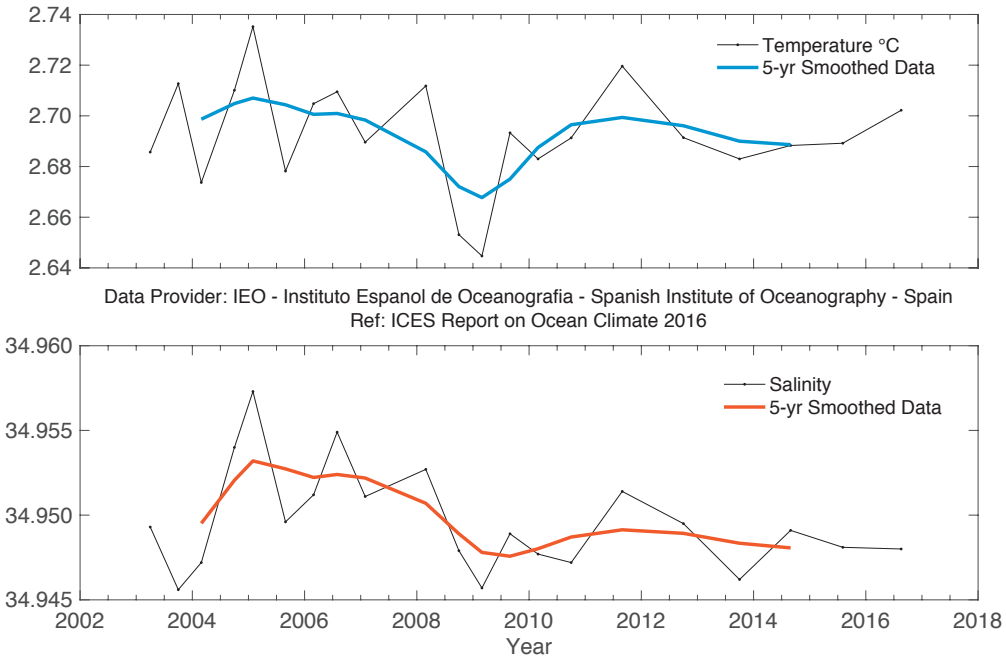

FIGURE 97.
Western Iberian margin. Potential temperature (upper panel) and salinity (lower panel) for the 2000–5500 m layer averaged across the Finisterre section.

5.3.6 Canary Basin

In the layer corresponding to the upper NADW (1700–2600 dbar), there was a weak warming and increase in salinity that is not statistically significantly different from zero. However, in strata corresponding to the NADW (2600–3600 dbar), a marginally statistically significant cooling −0.01 ± 0.01°C decade^{-1} and freshening −0.002 ± 0.002 decade^{-1} has been observed.

The vertical distribution of the trends for the oceanic waters west of Lanzarote corroborate the previous results. The NADW waters show a warming and an increase in salinity that is statistically significantly different from zero. However, the cooling and decrease in salinity and the weak warming and increase in salinity, respectively, for the intermediate waters and the NADW is not statistically significantly different from zero.

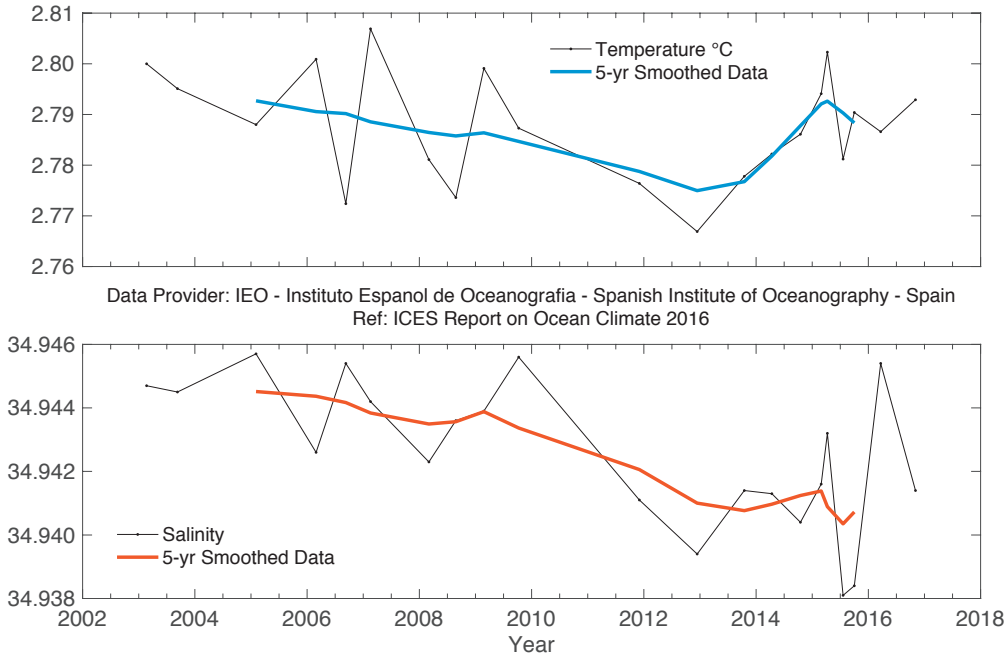

FIGURE 98.
Canary Basin. Potential temperature (upper panel) and salinity (lower panel) for the 2600–3600 m layer averaged across the Canaries section.

5.4 NORTH ATLANTIC INTERMEDIATE WATERS

5.4.1 Iceland Basin

In the Iceland Basin, the dominant water mass below about 1000 m is LSW, evident as a large recirculating body of relatively fresh and low stratified water whose core lies between 1700 and 2000 m (Holliday *et al.*, 2015). In 2016, the LSW was slightly warmer and more saline than in the previous year; temperature and salinity were both slightly higher than their respective 1996–2010 means.

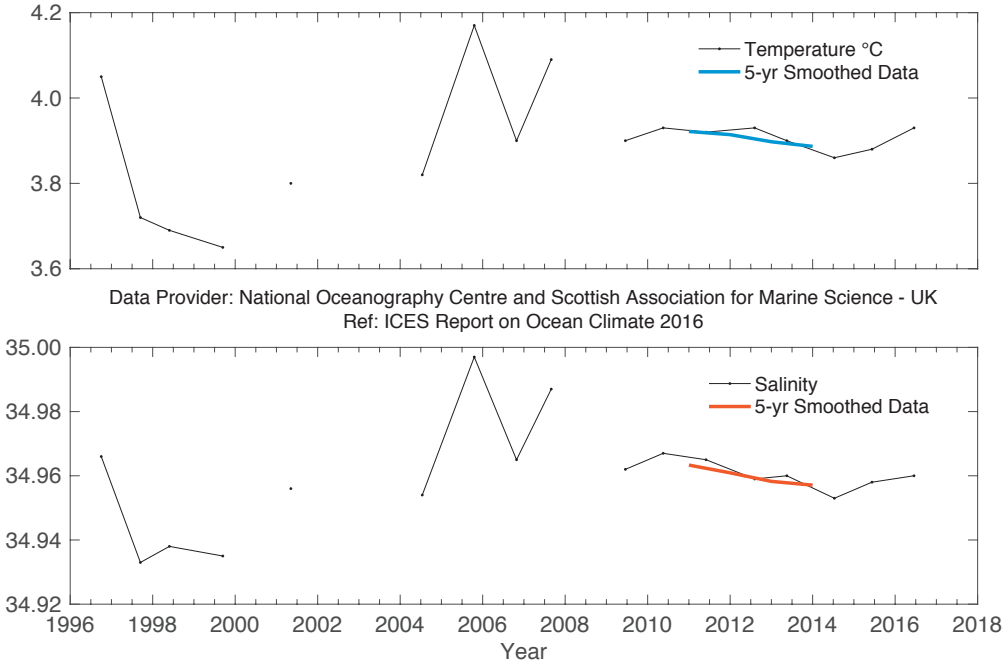

FIGURE 99.
Iceland Basin. Temperature (upper panel) and salinity (lower panel) of Labrador Sea water (LSW; 27.70 ≤ σ_θ ≤ 27.85 kg m^{-3}, ca. 2000–2600 m).

5.4.2 Rockall Trough

In Rockall Trough, the dominant water mass below about 1500 m is LSW, which usually has its maximum concentration between 1700 and 2000 m. East of the Anton Dohrn seamount, this peak tends to be characterized by a minimum in salinity and potential vorticity, although its patchy temporal distribution (possibly due to aliasing of mesoscale eddies) results in a noisy year-on-year signal.

Over the length of the time-series, there is no significant trend. From 1975 to the mid-1990s, there was a cooling and freshening trend, which was followed by gradual warming and increasing salinity. In 2016, the LSW potential temperature and salinity were close to the long-term means.

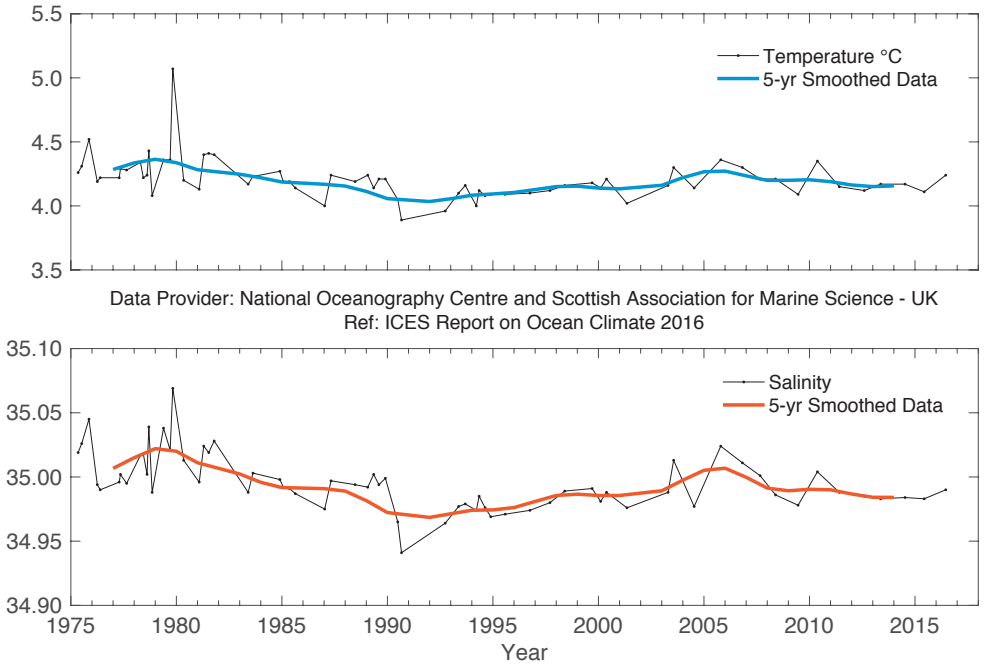

FIGURE 100.
Rockall Trough. Temperature (upper panel) and salinity (lower panel) of Labrador Sea water (LSW, $27.70 \leq \sigma_\theta \leq 27.85$ kg m^{-3}, ca. 1500–2000 m).

5.4.3 Irminger Basin

A cold and low-salinity core was observed between 1600 and 2000 m in the central Irminger Sea during the early 1990s. This was the result of the presence of deep LSW formed in the period 1988–1995. Since summer 1996, this LSW core has generally been increasing in temperature and salinity as it mixes with surrounding water masses. In 2012, temperature and salinity were only slightly below the long-term maximum observed in 2011. In 2014, the temperature of LSW in the Irminger Sea continued to decline relative to 2011. Salinity, however, was higher than in 2011 and actually obtained the highest value ever since 1991. Salinity continued to increase until 2014, but leveled off in 2015 and 2016. The temperature in 2015 was only slightly higher than in 2014. A new maximum record in temperature was set in 2016, 0.314°C above the long-term mean. There has been a clear increasing trend in temperature since 1996 at this depth. Deep convection occurred in the Irminger Sea in the cold winter 2014/2015 and produced a water mass with LSW properties down to 1400 m in the central Irminger Sea; however, this did not impact properties of LSW at depths below 1400 m.

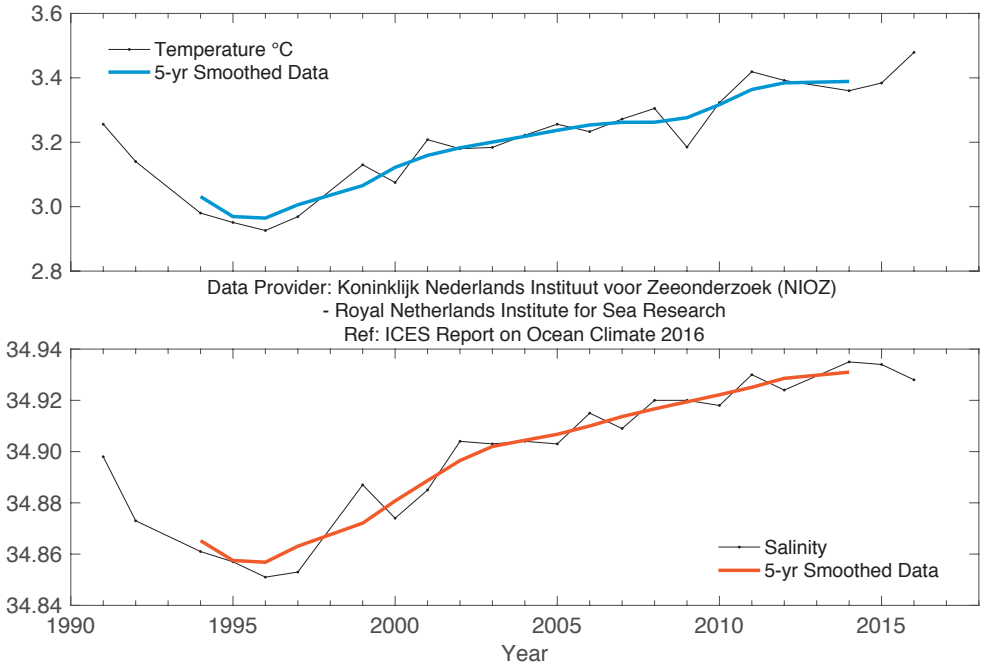

FIGURE 101.
Irminger Sea. Temperature (upper panel) and salinity (lower panel) of Labrador Sea water (LSW, averaged over 1600–2000 m).

5.4.4 Labrador Basin

In the Labrador Sea, the 1000–1800 m depth average temperature and salinity decreased between the beginning of the 1970s and the early 1990s by about 0.9°C and 0.09, respectively. In 2011, less than two decades after reaching its record minimum, temperature was as high as the previous maximum observed in 1970, while salinity was also at its highest since 1971. These trends were interrupted in winter 2011/2012 by strong convection, and both temperature and salinity of the deep intermediate layer (1000–1800 m) continued to decrease from 2013 to 2016.

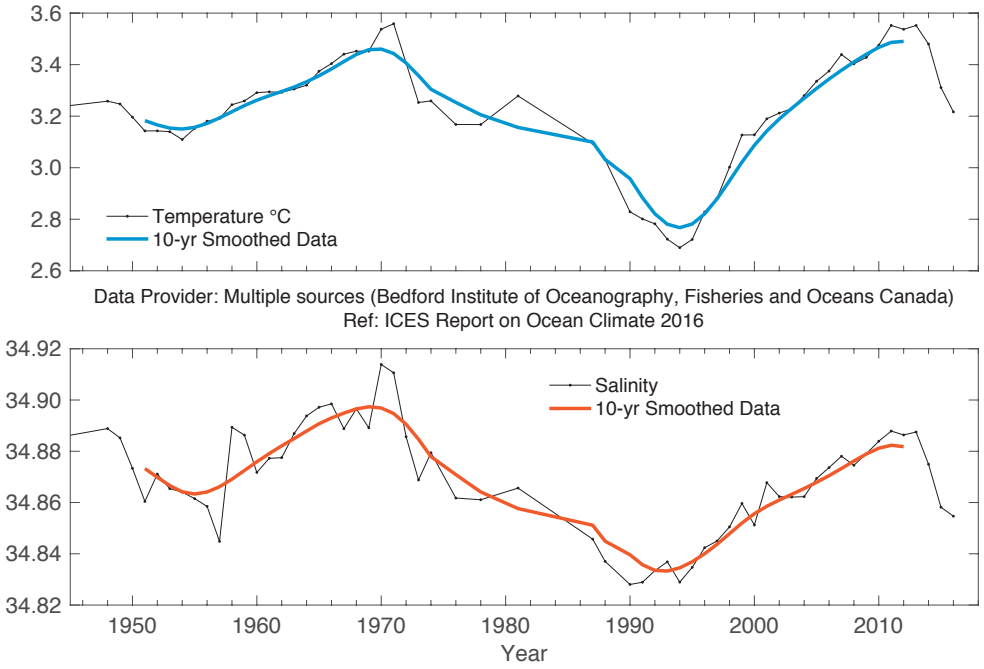

FIGURE 102.
Labrador Sea. Temperature (upper panel) and salinity (lower panel) anomalies of Labrador Sea water (LSW, averaged over 1000-1800 m).

5.4.5 Western Iberian margin

The external stations in Santander have been sampling the entire water column down to 1000 m (core of MW) on a monthly basis since the early 1990s. Overall warming trends for the previous 20 years are evident at most layers, corresponding to the ENACW (300–600 m) and upper MW (600–950 m). Salinity also shows a notable increase along the whole series, but less smooth than temperature.

The development of the water mass has been greatly influenced by a shift in salinity at lower ENACW (ca. 400 m) in 2005 after the occurrence of very strong winter mixing. In 2014, upper central waters underwent freshening for the first time in about a decade. In 2015, salinity values fell continuously during the year, being about 0.05 units lower by the end of 2015 than in mid-2014. During 2016, salinity remained at about the same level as in late 2015, i.e. fresher and colder than in recent years. Deeper at the level of the MW, the water masses were slightly fresher at its core in 2016 (likewise in 2014–2015) after peaking around 2007–2009.

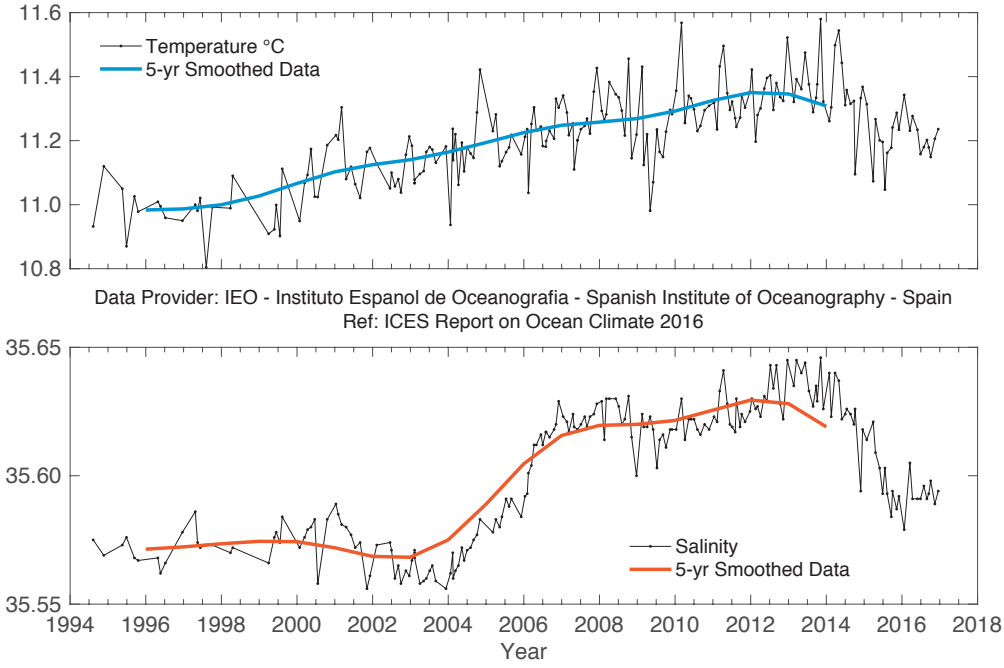

FIGURE 103.
Bay of Biscay. Potential temperature (upper panel) and salinity (lower panel) for the 300-600 m layer at Santander Station 7.

Levels deeper than 1000 m have been monitored in the region and at the western Iberian margin on an annual/semi-annual basis. From the core of MW to the core of LSW (ca. 1900 m) there is a strong gradient and some coherence in variability, indicating the influence of large-scale atmospheric patterns. The main highlight of the series is the passage of a cold and fresh anomaly from 2008 to 2010. After an upward swing in temperature and salinity in 2015, 2016 reversed again becoming colder and fresher, consistent with positive NAO behaviour.

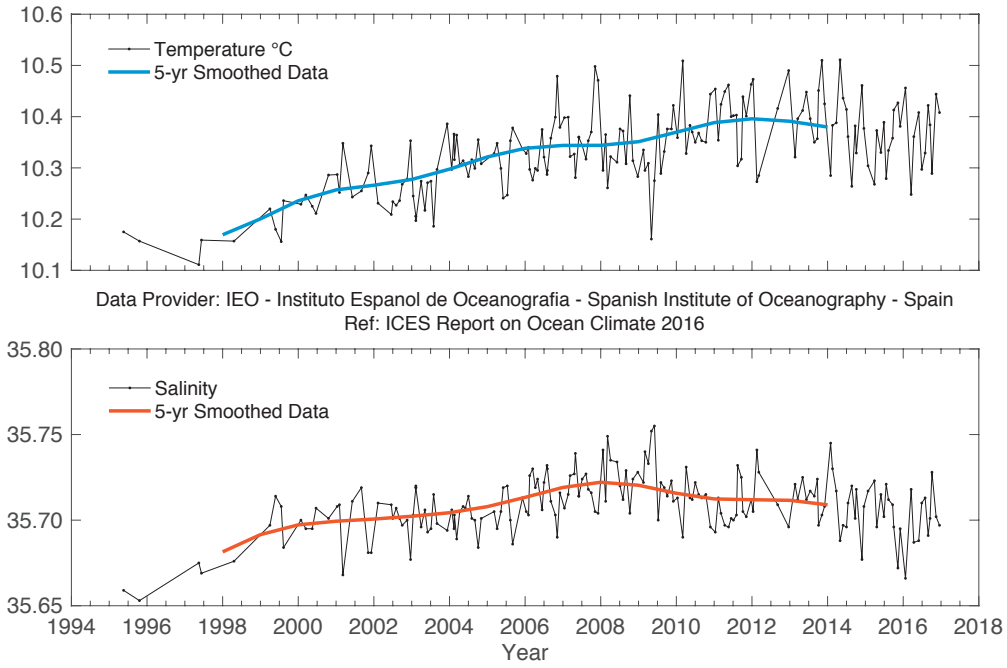

FIGURE 104.
Bay of Biscay. Potential temperature (upper panel) and salinity (lower panel) for the 600–950 m layer at Santander Station 7.

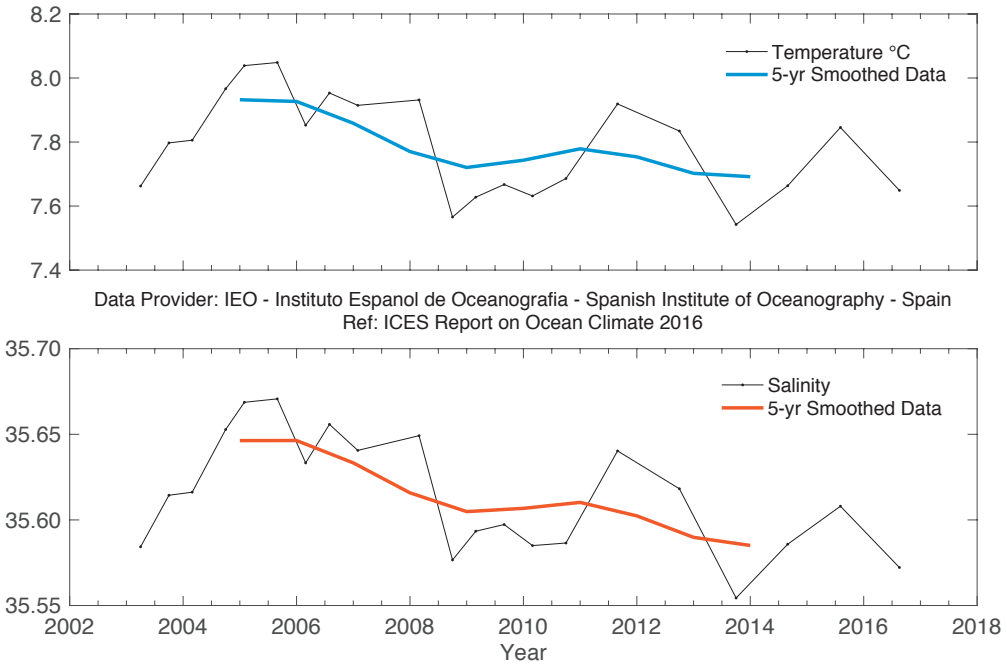

FIGURE 105.
Western Iberian margin. Potential temperature (upper panel) and salinity (lower panel) for the 800–2000 m layer averaged across the Finisterre section.

5.4.6 Canary Basin

In the stratum corresponding to the intermediate waters (800–1400 dbar), there has been a weak cooling and a decrease in salinity that is not statistically significantly different from zero, neither in the oceanic region nor in the CTZ. Both time-series show high variability due to the two very different intermediate water masses present in the region, i.e. the MW and the AAIW.

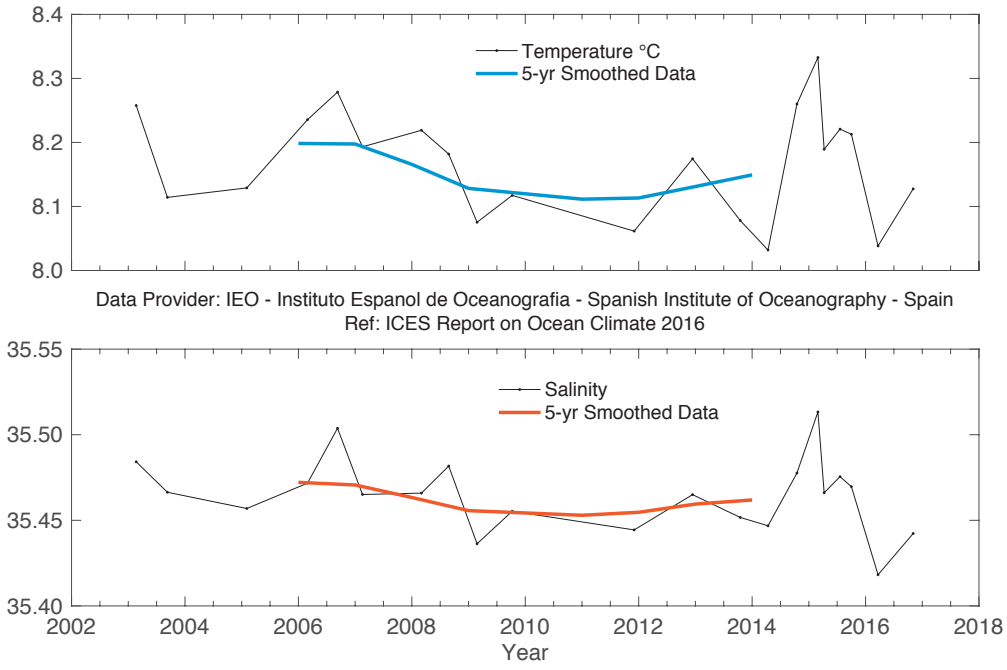

FIGURE 106.
Canary Basin. Potential temperature (upper panel) and salinity (lower panel) for the 800-1400 m layer.

CONTACT INFORMATION

AREA	SECTION	FIGURES	TIME-SERIES	CONTACT	INSTITUTE
West Greenland	4.2	16	Nuuk – air temperature	Boris Cisewski boris.cisewski@thuenen.de	Danish Meteorological Institute, Copenhagen, Denmark
West Greenland	4.2, 5.3.4	17, 18, 96	Fylla section and Cape Desolation section	Boris Cisewski boris.cisewski@thuenen.de	Thünen-Institut für Seefischerei (Thünen Institute of Sea Fisheries), Germany
Northwest Atlantic	4.5	24, 25, 26, 27	Sable Island air temperature, Cabot Strait sea ice, Misaine Bank, Emerald Bank	David Hebert David.Hebert@dfo-mpo.gc.ca	BIO (Bedford Institute of Oceanography), Department of Fisheries and Oceans, Canada
Labrador Sea	4.3, 5.4.4	19, 102	Section AR7W	Igor Yashayaev Igor.Yashayaev@dfo-mpo.gc.ca	BIO (Bedford Institute of Oceanography), Department of Fisheries and Oceans, Canada
Northeast US continental shelf	4.6	30, 31, 32	MAB, Gulf of Maine, Georges Bank, Northeast Channel	Paula Fratantoni paula.fratantoni@noaa.gov	NOAA Fisheries, NEFSC, Oceans and Climate Branch, USA
Icelandic waters	4.7, 5.2.3	38, 39, 40, 41, 92	Reykjavik and Akureyri air temperature, Siglunes Stations 2–4, Stations 2–4, Selvogsbanki Station 5, Langanes Stations 2–6, Faxafloi Station 9, Icelandic deep water (1800 m)	Hedinn Valdimarsson hedinn.valdimarsson@hafogvatn.is	Hafrannsóknastofnun (Marine & Freshwater Research Institute), Iceland
Bay of Biscay	4.8	42, 43	San Sebastian air and water temperature	Almudena Fontán afontan@azti.es	AZTI, Aquarium of San Sebastian (SOG) and Igeldo Meteorological Observatory (INM) in San Sebastian, Spain
Bay of Biscay and western Iberian margin	4.8, 5.3.5, 5.4.5	44, 45, 97, 103, 104, 105	Santander and Finisterre sections	César González-Pola cesar.pola@ieo.es	Instituto Español de Oceanografía (IEO, Spanish Institute of Oceanography), Spain
Gulf of Cadiz	4.9	47	STOCA Station SP6 – Gulf of Cadiz time-series	Ricardo F. Sánchez-Leal rleal@ieo.es	Instituto Español de Oceanografía (IEO, Spanish Institute of Oceanography), Spain
Canary Basin	4.10, 5.3.6, 5.4.6	49, 98, 106	Canary Basin oceanic waters section	Pedro Vélez-Belchí pedro.velez@ieo.es	Instituto Español de Oceanografía (IEO, Spanish Institute of Oceanography), Spain
NW European continental shelf	4.11	50, 51	Astan section, Point 33	Pascal Morin pmorin@sb-roscoff.fr	CNRS–UPMC, Observatoire Oceanologique de Roscoff, France
NW European continental shelf	4.11	52, 53	Western Channel Observatory, Station E1	Tim J. Smyth tjsm@pml.ac.uk	Marine Biological Association and Plymouth Marine Laboratory, UK
NW European continental shelf	4.12	54, 55	Malin Head Weather Station, M3 Weather Buoy	Caroline Cusack Caroline.Cusack@Marine.ie	Marine Institute/Met Eireann, Ireland
Rockall Trough and Iceland Basin	4.13, 4.14, 4.15, 5.3.2, 5.4.1, 5.4.2	56, 57, 58, 94, 99, 100	Ellett Line	N. Penny Holliday nph@noc.soton.ac.uk	National Oceanography Centre, Southampton and Scottish Association for Marine Science, UK
Irminger Sea	4.16	60	Station FX9 (64.33°N 8°W)	Hedinn Valdimarsson hedinn.valdimarsson@hafogvatn.is	Hafrannsóknastofnun (Marine & Freshwater Research Institute), Iceland
Irminger Sea	4.16, 5.3.3, 5.4.3	59, 95, 101	Central Irminger Sea, East Greenland slope	Laura de Steur Laura.de.Steur@nioz.nl	Koninklijk Nederlands, Instituut voor Zeeonderzoek (NIOZ, Royal Netherlands Institute for Sea Research), Netherlands
Faroe Bank Channel	4.17	62, 63, 64	Faroe Bank Channel–West Faroe Islands, Faroe Current – North Faroe Islands, Faroe Shelf	Karin Margretha H. Larsen KarinL@hav.fo	Havstovan (Faroe Marine Research Institute), Faroe Islands
Faroe–Shetland Channel	4.17, 5.3.1	65, 66, 93	Faroe–Shetland Channel, Faroe Shelf and Shetland Shelf, deep waters (800 m)	Sarah Hughes s.hughes@marlab.ac.uk Barbara Berx B.Berx@MARLAB.AC.UK	Marine Scotland Science (MSS, Aberdeen), UK
North Sea	4.18	68	North Sea Utsira, modelled North Sea inflow	Jon Albretsen jon.albretsen@imr.no Solfrid Hjollo solfrids@imr.no	Institute of Marine Research (IMR), Norway
North Sea	4.18	69	Fair Isle Current water	Sarah Hughes s.hughes@marlab.ac.uk	Marine Scotland Science (MSS, Aberdeen), UK
North Sea	4.18	70, 71	Helgoland Roads – coastal waters – German Bight, North Sea	Karen Wiltshire Karen.Wiltshire@awi.de	Alfred Wegener Institute for Polar and Marine Research (AWI)/Biologische Anstalt Helgoland (BAH), Germany
North Sea	4.18	72	Felixstowe–Rotterdam section average (52°N)	Stephen Dye stephen.dye@cefas.co.uk	Centre for Environment, Fisheries and Aquaculture Science (CEFAS), UK
Baltic Sea	4.19	73, 74, 77	Station BY15, Baltic Proper, east of Gotland, and observed ice extent	Johanna Linders johanna.linders@smhi.se	Swedish Meteorological and Hydrological Institute (SMHI), Sweden
Baltic Sea	4.19	75, 76	Stations LL7 and SR5	Pekka Alenius pekka.alenius@fimr.fi	Finnish Institute of Marine Research (FIMR), Finland

AREA	SECTION	FIGURES	TIME-SERIES	CONTACT	INSTITUTE
Norwegian Sea	4.20	79, 81, 82	Svinøy, Gimsøy, and Sørkapp sections	Kjell Arne Mork kjell.arne.mork@imr.no	Institute of Marine Research (IMR), Norway
Norwegian Sea	4.20, 5.2.2	80, 91	Ocean Weather Station Mike (50 and 2000 m)	Svein Østerhus Svein.Osterhus@gfi.uib.no	Geophysical Institute, University of Bergen, Norway
Barents Sea	4.21	83	Fugløya – Bear Island section, Western Barents Sea	Randi Ingvaldsen randi.ingvaldsen@imr.no	Institute of Marine Research (IMR), Norway
Barents Sea	4.21	84	Kola section, Eastern Barents Sea	Oleg V. Titov titov@pinro.ru	Knipovich Polar Research Institute of Marine Fisheries and Oceanography (PINRO), Russian Federation
Greenland Sea and Fram Strait	4.22	87	Greenland Sea section N, west of Spitsbergen (76.5°N)	Waldemar Walczowski walczows@iopan.gda.pl	Institute of Oceanology, Polish Academy of Sciences (IOPAN), Poland
Greenland Sea and Fram Strait	4.22, 5.2.1	85, 89, 90	Greenland Sea section 75°N, Greenland Gyre convection depth and deep waters (3000 m)	Gereon Budeus Gereon.Budeus@awi.de	Alfred Wegener Institute, Helmholtz Centre for Polar and Marine Research (AWI), Germany
Greenland Sea and Fram Strait	4.22	86	Fram Strait (78.83°N), West Spitsbergen Current and East Greenland Current	Wilken-Jon von Appen Wilken-Jon.von.Appen@awi.de	Alfred Wegener Institute, Helmholtz Centre for Polar and Marine Research (AWI), Germany

REFERENCES

Antonov, J. I., Locarnini, R. A., Boyer, T. P., Mishonov, A. V., and Garcia, H. E. 2006. World Ocean Atlas 2005, Volume 2: Salinity. NOAA Atlas NESDIS 62. 182 pp.

Berx, B., and Payne, M. R. 2017a. The Sub-Polar Gyre Index – a community data set for application in fisheries and environment research. Earth System Science Data, 9 (1): 259–266.

Berx, B., and Payne, M. R. 2017b. Marine Scotland Datasets: Sub-Polar Gyre Index. https://doi.org/10.7489/1806-1. Webpage last modified 08 Mar 2017, accessed 28 April 2017 at http://data.marine.gov.scot/dataset/sub-polar-gyre-index

Cappelen, J. 2017. Greenland–DMI historical climate data collection 1784–2016. DMI Report 17–04. 108 pp.

Duchez, A., Frajka-Williams, E., Josey, S. A., Evans, D. G., Grist, J. P., Marsh, R., McCarthy, G. D., *et al.* 2016. Drivers of exceptionally cold North Atlantic Ocean temperatures and their link to the 2015 European heat wave. Environmental Research Letters, 11(7): 074004. https://doi.org/10.1088/1748-9326/11/7/074004

Dunstone, N., Smith, D., Scaife, A., Hermanson, L., Eade, R., Robinson, R., Andrews, M., and Knight, J. 2016. Skilful predictions of the winter North Atlantic Oscillation one year ahead. Nature Geoscience, 9 (11): 809–814. https://doi.org/10.1038/ngeo2824

Gaillard, F. 2012. ISAS-tool Version 6: Method and configuration. Ifremer Rapport LPO-12-02. http://doi.org/10.13155/22583

Häkkinen, S., and Rhines, P. B. 2004. Decline of subpolar North Atlantic circulation during the 1990s. Science, 304 (5670): 555–559.

Hátún, H., Lohmann, K., Matei, D., Jungclaus, J. H., Pacariz, S., Bersch, M., Gislason, A., *et al*. 2016. An inflated subpolar gyre blows life toward the northeastern Atlantic. Progress in Oceanography, 147: 49–66.

Holliday, N. P., Cunningham, S. A., Johnson, C., Gary, S. F., Griffiths, C., Read, J. F., and Sherwin, T. 2015. Multidecadal variability of potential temperature, salinity, and transport in the eastern subpolar North Atlantic. Journal of Geophysical Research: Oceans, 120 (9): 5945–5967. https://doi.org/10.1002/2015jc010762

Holliday, N. P., Hughes, S. L., Bacon, S., Beszczynska-Möller, A.,Hansen, B., Lavín, A., Loeng, H., *et al.* 2008. Reversal of the 1960s to 1990s freshening trend in the northeast North Atlantic and Nordic Seas. Geophysical Research Letters, 35 (3): L03614. https://doi.org/10.1029/2007gl032675

Hurrell, J. W., and Deser, C. 2010. North Atlantic climate variability: the role of the North Atlantic Oscillation. Journal of Marine Systems, 79(3): 231–244. https://doi.org/10.1016/j.jmarsys.2009.11.002

Hurrell, J. W., Kushnir, Y., Ottersen, G., and Visbeck, M. 2003. An overview of the North Atlantic oscillation. Wiley Online Library. https://doi.org/10.1029/134GM01

Hurrell, J., and National Center for Atmospheric Research Staff (Eds). 2017. Climate Data Guide: Hurrell North Atlantic Oscillation (NAO) Index (station-based). Webpage last modified 7 July 2017, accessed 25 September 2017 at https://climatedataguide.ucar.edu/climate-data/hurrell-north-atlantic-oscillation-nao-index-station-based

Kalnay, E., Kanamitsu, M., Kistler, R., Collins, W., Deaven, D., Gandin, L., Iredell, M., *et al.* 1996. The NCEP/NCAR 40-Year Reanalysis Project. Bulletin of the American Meteorological Society, 77 (3): 437–471. https://doi.org/10.1175/1520-0477(1996)077<0437>tnyrp)2.0.co;2

Loncarnini, R., Mishonov, V., Antonov, J., Boyer, T., and Garcia, H. 2006. World Ocean Atlas 2005, Volume 1: Temperature. NOAA Atlas NESDIS 61. 182 pp.

Mountain, D. 2012. Labrador Slope Water entering the Gulf of Maine in response to the North Atlantic Oscillation. Continental Shelf Research, 47: 150–155. https://doi.org/10.1016/j.csr.2012.07.008

Scaife, A. A., Arribas, A., Blockley, E., Brookshaw, A., Clark, R. T., Dunstone, N., Eade, R., *et al.* 2014. Skillful long-range prediction of European and North American winters. Geophysical Research Letters, 41(7): 2514–2519. https://doi.org/10.1002/2014gl059637

Scaife, A. A., Karpechko, A. Y., Baldwin, M. P., Brookshaw, A., Butler, A. H., Eade, R., Gordon, M., *et al.* 2015. Seasonal winter forecasts and the stratosphere. Atmospheric Science Letters, 17(1): 51–56. https://doi.org/10.1002/asl.598

Yashayaev, I., and Loder, J. W. 2017. Further intensification of deep convection in the Labrador Sea in 2016. Geophysical Research Letters, 44(3): 1429–1438. https://doi.org/10.1002/2016gl071668

ABBREVIATIONS AND ACRONYMS

AAIW	Antarctic intermediate waters
Argo	Not an acronym, but the name of a type of instrument used to collect data. The name Argo is a reference to Greek mythology.
AW	Atlantic water
AZOMP	Atlantic Zone Off-Shelf Monitoring Program
BSH	Bundesamt für Seeschifffahrt und Hydrographie (German Federal Maritime and Hydrographic Agency)
CCLME	Canary Current Large Marine Ecosystem
CIL	cold intermediate layer
CIRES	Cooperative Institute for Research in Environmental Sciences (USA)
CTD	conductivity, temperature, and depth profiles
CTZ	coastal transition zone
DJF(M)	December, January, February (March)
DSOW	Denmark Strait overflow water
EGC	East Greenland Current
ENAW	eastern North Atlantic water
ENACW	eastern North Atlantic central water
ERSST	Extended Reynolds sea surface temperature
GSDW	Greenland Sea deep water
IFREMER	Institut Francais de Recherche pour l'Exploitation de la MER (French Institute for Ocean Research)
IROC	ICES Report on Ocean Climate
ISAS	*In Situ* Analysis System
ISOW	Iceland–Scotland overflow water
JJA	June, July, and August
LME	Large Marine Ecosystem
LSW	Labrador Sea water
MAM	March, April, and May
MNAW	modified North Atlantic water
MW	Mediterranean water
NAC	North Atlantic Current
NACW	North Atlantic central waters
NADW	North Atlantic deep water
NAO	North Atlantic Oscillation
NL	Newfoundland–Labrador
NOAA	National Oceanic and Atmospheric Administration (USA)
OISST.v2	Optimum Interpolation SST dataset version 2
PW	polar water
RAC	Return Atlantic Current
RAW	return Atlantic water
RP	reference period
SLP	sea level pressure
SON	September, October, and November
SPMW	subpolar-mode water
SST	sea surface temperature
STOCA	Series Temporales de datos Oceanográficos en el golfo de CAdiz
UPDW	upper polar deep water
WGC	West Greenland Current
WGOH	Working Group on Oceanic Hydrography
WGWIDE	Working Group on Widely Distributed Stocks
WOA5	World Ocean Atlas 05
WSC	West Spitsbergen Current